ABSTRACT

Title of dissertation: BRIDGING QUANTUM, CLASSICAL AND STOCHASTIC SHORTCUTS TO ADIABATICITY.

Ayoti Patra, Doctor of Philosophy, 2017

Dissertation directed by: Professor Christopher Jarzynski
Department of Chemistry and Biochemistry;
Institute for Physical Science and Technology;
Department of Physics.

Adiabatic invariants – quantities that are preserved under the slow driving of a system's external parameters – are important in classical mechanics, quantum mechanics and thermodynamics. Adiabatic processes allow a system to be guided to evolve to a desired final state. However, the slow driving of a quantum system makes it vulnerable to environmental decoherence, and for both quantum and classical systems, it is often desirable and time-efficient to speed up a process. *Shortcuts to adiabaticity* are strategies for preserving adiabatic invariants under rapid driving, typically by means of an auxiliary field that suppresses excitations, otherwise generated during rapid driving. Several theoretical approaches have been developed to construct such shortcuts. In this dissertation we focus on two different approaches, namely *counterdiabatic* driving and *fast-forward* driving, which were originally developed for quantum systems. The counterdiabatic approach introduced independently by Dermirplak and Rice [*J. Phys. Chem. A*, 107:9937, 2003], and Berry [*J. Phys.*

A: Math. Theor., 42:365303, 2009] formally provides an exact expression for the auxiliary Hamiltonian, which however is abstract and difficult to translate into an experimentally implementable form. By contrast, the fast-forward approach developed by Masuda and Nakamura [*Proc. R. Soc. A*, 466(2116):1135, 2010] provides an auxiliary potential that may be experimentally implementable but generally applies only to ground states.

The central theme of this dissertation is that classical shortcuts to adiabaticity can provide useful physical insights and lead to experimentally implementable shortcuts for analogous quantum systems. We start by studying a model system of a tilted piston to provide a proof of principle that quantum shortcuts can successfully be constructed from their classical counterparts. In the remainder of the dissertation, we develop a general approach based on *flow-fields* which produces simple expressions for auxiliary terms required for both counterdiabatic and fast-forward driving. We demonstrate the applicability of this approach for classical, quantum as well as stochastic systems. We establish strong connections between counterdiabatic and fast-forward approaches, and also between shortcut protocols required for classical, quantum and stochastic systems. In particular, we show how the fast-forward approach can be extended to highly excited states of quantum systems.

BRIDGING QUANTUM, CLASSICAL AND STOCHASTIC SHORTCUTS TO ADIABATICITY

by

Ayoti Patra

Dissertation submitted to the Faculty of the Graduate School of the
University of Maryland, College Park in partial fulfillment
of the requirements for the degree of
Doctor of Philosophy
2017

Advisory Committee:
Professor Christopher Jarzynski, Chair/Advisor
Dr. Alexey V. Gorshkov
Professor Perinkulam S. Krishnaprasad, Dean's Representative
Professor Rajarshi Roy
Professor Victor M. Yakovenko

Dedication

To my *father,*

who envisoned a future scientist the first time he saw his infant daughter.

Acknowledgments

First and foremost I'd like to thank my advisor, Prof. Christopher Jarzynski for giving me an invaluable opportunity to work with him. Chris is an exemplary scientist and an extremely humble person. Through his patient guidance and encouragement over the years, I have developed my scientific self, and learnt to persevere through the challenges of research. He has shown me the importance of clarity in research. His approach to solve difficult problems starting from simple text book problems has left a deep impact on me. I will forever be grateful to Chris and will strive to achieve the standards that he has set.

Next, I want to thank my first research advisor, Prof. Amit Dutta of IIT Kanpur. I was not only fortunate to attend his courses during my entire time at IIT, but also was priviledged to work with him for a year post M.Sc. My foundation as a researcher was laid under the influence of his infectious enthusiasm for science. I thank him for igniting my excitement and dedication for research. I also thank him for introducing me to my life partner.

I thank all my physics teachers from UMD, IIT Kanpur and St. Stephen's college for building a strong foundation through rigourous training. I would specially like to thank Dr. Paulo Bedaque and Dr. Zacharia Chacko from UMD, and Dr. Bikram Phookun and Dr. Abhinav Gupta from St. Stephen's. Late Dr. Swaminathan played a pivotal role in starting my journey as a physicist and I am extremely thankful to him for the chat we had during my initial days at St. Stephen's.

My PhD experience has been enriched by the current and former members of

the Jarzynski group. Thank you Sebastian, Yigit, Oren, Marcus, Shaon, Zhiyue, Jeff and Andrew. A special thanks to Dibyendu for not only introducing me to the group but also for all the scientific and moral support I got from him.

I thank the organizers of the annual workshops at Telluride, which have been a rich hub for exchanging scientific ideas. I thank Prof. Krishnaprasad for the stimulating discussions we had. I thank him and the other dissertation committee members for volunteering their time and effort to help me improve this dissertation.

The past few years of my life would not have been as colorful and memorable without my friends at College Park. I thank Wrick, Chana da (Anirban), Amit, Swarnav, Manjistha, Sumalika, Mahashweta, Santanu, Arka, Apara, Jonathan, Ranchu, Kim and my ex-roommates Shweta, Srimoyee, Vidya, Meera and Arthita for all the good times we shared.

My deepest gratitude is reserved for my family – Patras and Dhabals – for the myriad ways in which they have supported me. I consider myself extremely fortunate to have a father and a husband who understand the technicalities of my work, and therefore have supported me professionally as well as personally. Thank you *Baba* for making science fun since an early age and for continuing to do so, and *Ma* for always believing in my potential. Thanks Arnab for sharing your life with me, and for making mine so grand as a result. Without you all, none of this would have been possible.

Finally, I thank the U.S. Army Research Office (Grant number W911NF-13-1-0390) and the University of Maryland for financial support.

Table of Contents

List of Tables

List of Figures

Chapter 1: Introduction

1.1 Background

1.1.1 Overview

In the last few decades, experimental advancements in quantum optics have led to a surge of research in quantum information and computation. As a result, the need to create and manipulate quantum states with high speed and accuracy has become increasingly important. However, the quantum adiabatic theorem due to Max Born and Vladimir Fock, which states that "a physical system remains in its instantaneous eigenstate if a given perturbation is acting on it slowly enough and if there is a gap between the eigenvalue and the rest of the Hamiltonian's spectrum" [1,2], comes as a hindrance. Adiabatic processes make a system robust against systematic errors and various kinds of noise by enabling it to adapt its configuration and retain its initial character. However, the requirement for slow driving is not only inefficient, but also makes the system vulnerable to environmental decoherence thereby leading to loss of important quantum mechanical features. *Shortcuts to adiabaticity* – a term coined in 2010 by Chen et. al [3] – are strategies for achieving adiabatic results with fast driving protocols. Shortcuts to adiabaticity have been applied to many

fields including adiabatic quantum computing [4–6], cold atom transport [3, 7, 8], many-body state engineering [9–12], quantum sensing and metrology [13] quantum simulation [14, 15] and quantum thermodynamics [16–18].

Shortcut protocols achieve the desired evolution by means of an auxiliary Hamiltonian which supresses the excitations arising due to fast driving [19]. A variety of shortcut protocols have been developed including invariant-based inverse engineering [20, 21], transitionless counterdiabatic driving [22–25], fast-forward methods [11, 26–30] and methods based on unitary [31–35] or gauge [36] transformations. Shortcuts to adiabaticity have been extended to non-Hermitian Hamiltonians [37, 38], open quantum systems [39, 40] and Dirac-dynamics [41–43]. They have been demonstrated experimentally [14, 44–48], and their relationship with quantum speed limits has been clarified [49, 50].

Adiabatic processes are significant also for classical systems. They preserve quantities known as adiabatic invariants. While the *quantum number* of an initial energy eigenstate is the quantum adiabatic invariant, the *classical action* of a system, equivalently the volume of phase space enclosed by a surface of constant energy, is the classical adiabatic invariant in one degree of freedom [51]. Studies on shortcuts to adiabaticity for classical dynamics, which aim at preserving the classical action of a rapidly driven system, has also gained attention recently [25, 34, 52–56]. Analogous problems for stochastic dynamics have also been studied [57–60].

1.1.2 Methods

In this dissertation, we focus on developing general methods to construct shortcuts to adiabaticity whilst its direct applications on physical systems are not discussed in detail. Here, we review the *transitionless quantum driving* protocol, developed independently by Dermirplak and Rice [22, 23], and Berry [24]; and the *fast-forward* method developed by Masuda and Nakamura [26], which are of particular relevance to this work. We use the terms 'counterdiabatic driving' and 'transitionless driving' synonymously to indicate that during these processes, the system tracks the adiabatic path at every instant, as shown in Fig. 1.1(a). In contrast, fast-forward driving refers to those processes where the system starts from a given state and ends up at the desired state at the final time, but need not follow the adiabatic trajectory at intermediate times, see Fig. 1.1(b).

Consider a system initialized in the n'th energy eigenstate and evolving under a time-dependent Hamiltonian $\hat{H}_0(t)$. In the counterdiabatic approach, an auxiliary Hamiltonian $\hat{H}_{CD}(t)$ is constructed, such that when the system evolves under

$$\hat{H}(t) = \hat{H}_0(t) + \hat{H}_{CD}(t), \tag{1.1}$$

it follows the adiabatic trajectory of $\hat{H}_0(t)$ at every instant even for rapid driving, see Fig. 1.1(a). The auxiliary term $\hat{H}_{CD}(t)$ ensures that the excitations to other eigenstates are supressed at every instant [22, 24]. The exact expression for $\hat{H}_{CD}(t)$ was derived by Berry [24] using reverse engineering. Berry's derivation is straight-

forward and simple, and is presented below. An energy eigenstate $|n(t)\rangle$ of $\hat{H}_0(t)$ satisfies the eigenvalue equation

$$\hat{H}_0(t)|n(t)\rangle = E_n(t)|n(t)\rangle, \tag{1.2}$$

and the corresponding adiabatic path is given by [1]

$$|\psi_n(t)\rangle = \exp\left[-\frac{i}{\hbar}\int_0^t dt' E_n(t') - \int_0^t dt' \langle n(t')|\partial_{t'} n(t')\rangle\right]|n(t)\rangle. \tag{1.3}$$

The first term in the phase is dynamically generated while the second term arises due to a geometric contribution where the integrand $\langle n(t')|\partial_{t'} n(t')\rangle$ acts as an effective vector potential. In the reverse engineering approach, a Hamiltonian $\hat{H}(t)$ needs to be determined for which $|\psi_n(t)\rangle$ is an exact solution of the time-dependent Schrödinger equation

$$i\hbar\partial_t|\psi_n(t)\rangle = \hat{H}(t)|\psi_n(t)\rangle. \tag{1.4}$$

It can be verified that any time-dependent unitary operator $\hat{U}(t)$ satisfies

$$i\hbar\partial_t\hat{U}(t) = \hat{H}(t)\hat{U}(t), \tag{1.5}$$

where

$$\hat{H}(t) = i\hbar(\partial_t\hat{U}(t))\hat{U}^\dagger(t). \tag{1.6}$$

By choosing

$$\begin{aligned}\hat{U}(t) &= \sum_n |\psi_n(t)\rangle\langle n(0)| \\ &= \sum_n \exp\left[-\frac{i}{\hbar}\int_0^t dt' E_n(t') - \int_0^t dt' \langle n(t')|\partial_{t'} n(t')\rangle\right] |n(t)\rangle\langle n(0)|, \quad (1.7)\end{aligned}$$

and upon using Eq. 1.6, Berry [24] showed that the Hamiltonian driving the eigenstates $|n(t)\rangle$ according to Eq. 1.4 is

$$\hat{H}(t) = \sum_n |n(t)\rangle E_n(t)\langle n(t)| + i\hbar \sum_n \big(|\partial_t n\rangle\langle n| - \langle n|\partial_t n\rangle |n\rangle\langle n|\big) = \hat{H}_0(t) + \hat{H}_{CD}(t). \quad (1.8)$$

Therefore the counterdiabatic Hamiltonian is given by

$$\hat{H}_{CD}(t) = i\hbar \sum_n \big(|\partial_t n\rangle\langle n| - \langle n|\partial_t n\rangle |n\rangle\langle n|\big), \quad (1.9)$$

where $|n\rangle = |n(t)\rangle$ denotes the instantaneous n'th eigenstate of $\hat{H}_0(t)$, and $|\partial_t n\rangle \equiv \partial_t |n(t)\rangle$. If a wavefunction evolves under $\hat{H}_0 + \hat{H}_{CD}$ from an initial state $|n(0)\rangle$, then the quantum number n is preserved at every instant during the evolution. Note that $\hat{H}_{CD}(t)$ in Eq. 1.9 does not depend on the choice of n. Transitionless quantum driving is derived from basic principles of unitary evolution and is consequently quite general: it applies both to spatially continuous systems such as a particle in a time-dependent potential, and to discrete-state, e.g. spin, systems.

It was shown for a harmonic oscillator and a particle in a box by Chen, et al. [20] and del Campo et al. [61] respectively, that Eq 1.9 can be recast in terms of position

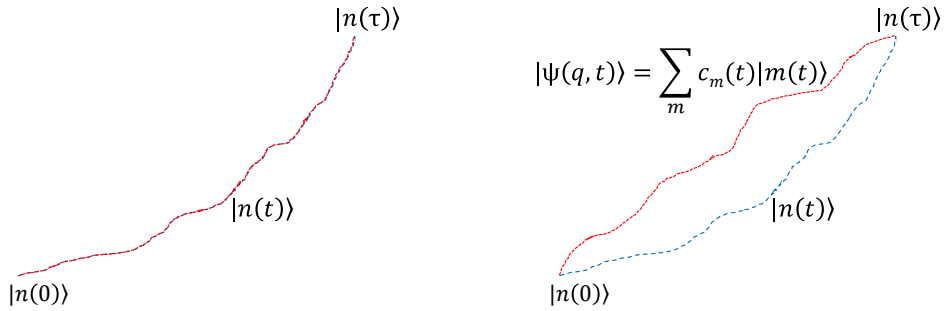

(a) Counterdiabatic driving

(b) Fast-forward driving

Figure 1.1: This figure shows a schematic representation of the adiabatic path (blue dashed curve) and the path traversed by the system during Hamiltonian evolution (red dotted curve). For counterdiabatic or transitionless driving, the red and the blue curves coincide as the system follows the adiabatic path at every instant. On the other hand, for fast-forward driving, the system starts from a given state and ends on the desired state at the final time τ, however at intermediate times it is in general in a linear superposition of the instantaneous eigenstates and does not follow the adiabatic path.

and momentum operators to yield

$$\hat{H}_{CD} \propto \hat{p}\hat{q} + \hat{q}\hat{p}. \tag{1.10}$$

Rewriting $\hat{H}_{CD}$ in terms of operators corresponding to physical observables provide physical insight into the underlying process and pave the way for experimental implementation. Also, the knowledge of the entire eigenspectrum at every instant will not be required if a systematic procedure is developed to obtain $\hat{H}_{CD}$ in terms of operators like $\hat{p}$ and $\hat{q}$.

In Ref. [25], Jarzynski has shown that the original Hamiltonian written as a function of time-dependent parameters $\boldsymbol{\lambda}$ leads to an auxiliary Hamiltonian $\hat{H}_{CD}(t)$

which can be cast in the form:

$$\begin{aligned}\hat{H}(t) &= \hat{H}_0(\boldsymbol{\lambda}(t)) + \hat{H}_{CD}(t) \\ &= \hat{H}_0(\boldsymbol{\lambda}(t)) + \dot{\boldsymbol{\lambda}} \cdot \hat{\boldsymbol{\xi}}(\boldsymbol{\lambda}(t)).\end{aligned} \tag{1.11}$$

Here, $\hat{\boldsymbol{\xi}}(\boldsymbol{\lambda})$ is a vector of Hermitian operators: [24]

$$\hat{\boldsymbol{\xi}}(\boldsymbol{\lambda}(t)) = i\hbar \sum_m \Big(|\partial_{\boldsymbol{\lambda}} m\rangle\langle m| - \langle m|\partial_{\boldsymbol{\lambda}} m\rangle |m\rangle\langle m| \Big), \tag{1.12}$$

where the sum is taken over eigenstates $|m(\boldsymbol{\lambda})\rangle$ of $\hat{H}_0(\boldsymbol{\lambda})$, and $|\partial_{\boldsymbol{\lambda}} m\rangle \equiv \partial_{\boldsymbol{\lambda}} |m(\boldsymbol{\lambda})\rangle$. The vector $\hat{\boldsymbol{\xi}}(\boldsymbol{\lambda})$ can be viewed as a generator of adiabatic transformations which associates infinitesimal displacements in parameter space, $\boldsymbol{\lambda} \to \boldsymbol{\lambda} + \delta\boldsymbol{\lambda}$, with displacements in Hilbert space, $|\psi\rangle \to |\psi\rangle + |\delta\psi\rangle$, according to the rule

$$i\hbar |\delta\psi\rangle = \Big[\delta\boldsymbol{\lambda} \cdot \hat{\boldsymbol{\xi}}(\boldsymbol{\lambda}) \Big] |\psi\rangle. \tag{1.13}$$

For an eigenstate $|n(\boldsymbol{\lambda})\rangle$, up to first order in $\delta\boldsymbol{\lambda}$, Eq. 1.13 leads to the following displacement in the Hilbert space [25]:

$$|n(\boldsymbol{\lambda})\rangle \to \left(1 + \frac{1}{i\hbar} \delta\boldsymbol{\lambda} \cdot \hat{\boldsymbol{\xi}} \right) |n(\boldsymbol{\lambda})\rangle = \exp\left[-\delta\boldsymbol{\lambda} \cdot \langle n|\nabla n\rangle \right] |n(\boldsymbol{\lambda} + \delta\boldsymbol{\lambda})\rangle \tag{1.14}$$

When Eq. 1.13 is applied stepwise along a curve $\boldsymbol{\lambda}_s$ in parameter space, the wavefunction gets transported along $e^{i\varphi_s} |n(\boldsymbol{\lambda}_s)\rangle$, where the phase is the line integral of $i\langle n|\nabla n\rangle$. Thus the system is escorted along the eigenstates of $\hat{H}_0(\boldsymbol{\lambda})$ as a result of

the unitary flow in Hilbert space generated by the operator $\hat{\boldsymbol{\xi}}$.

Alternatively, it can be stated that a small displacement in time, $t \to t + \delta t$ leads to the following displacement in the Hilbert space:

$$e^{-i\delta t\, \hat{H}_{CD}(t)/\hbar}|n(t)\rangle = |n(t+\delta t)\rangle\,, \tag{1.15}$$

aside from an overall phase. Eq. 1.15 clarifies why adding $\hat{H}_{CD}(t)$ to $\hat{H}_0$ produces transitionless driving [25]: for each time step δt, the evolution operator under $\hat{H}_0 + \hat{H}_{CD}(t)$ is $e^{-i\delta t\, \hat{H}_0/\hbar}\, e^{-i\delta t\, \hat{H}_{CD}/\hbar}$, which first evolves the state $|n(t)\rangle$ to $|n(t+\delta t)\rangle$, and then contributes an increment in the dynamical phase, $e^{-i\delta t\, E_n/\hbar}$. Here, δt is taken to be infinitesimal, and $\mathcal{O}(\delta t^2)$ corrections have been ignored.

The generator $\hat{\boldsymbol{\xi}}$ can alternatively be specified by the conditions: [25]

$$\left[\hat{\boldsymbol{\xi}}, \hat{H}_0\right] = i\hbar\left(\boldsymbol{\nabla}\hat{H}_0 - \mathrm{diag}(\boldsymbol{\nabla}\hat{H}_0)\right) \tag{1.16a}$$

$$\langle n|\boldsymbol{\xi}|n\rangle = 0, \tag{1.16b}$$

where $\mathrm{diag}(\boldsymbol{\nabla}\hat{H}_0) = \sum_m |m\rangle\langle m|\boldsymbol{\nabla}\hat{H}_0|m\rangle\langle m|$. Eq. 1.16a determines the off-diagonal elements of $\boldsymbol{\xi}$, while Eq. 1.16b sets the diagonal elements. The identity $\langle m|\boldsymbol{\nabla}n\rangle = \langle m|\boldsymbol{\nabla}\hat{H}_0|n\rangle/(E_n - E_m)$ [24] establishes the equivalence of the two definitions of $\hat{\boldsymbol{\xi}}$ (Eqs. 1.12 and 1.16).

Eqs. 1.16 have a classical counterpart described in Eqs. 1.18. This observation leads to the following question: Can a classical generator $\boldsymbol{\xi}(\boldsymbol{\lambda}(t))$ solve a problem on *dissipationless classical driving* – the classical analogue of transitionless quantum

driving? In one degree of freedom, the classical adiabatic invariant is the action $I_0(q,p;\boldsymbol{\lambda}) = \oint p'\,\mathrm{d}q'$, equivalently the volume of phase space enclosed by a surface of constant energy [51]. The problem of dissipationless classical driving is formulated as follows: For a classical time-dependent Hamiltonian $H_0(q,p;\boldsymbol{\lambda}(t))$, find the counterdiabatic term $H_{CD}(q,p,t) = \dot{\boldsymbol{\lambda}}\cdot\boldsymbol{\xi}(q,p;\boldsymbol{\lambda}(t))$ such that the action $I_0(q,p;\boldsymbol{\lambda}(t))$ (defined with respect to H_0) remains constant along any trajectory evolving under the Hamiltonian

$$H(t) = H_0(\boldsymbol{\lambda}(t)) + \dot{\boldsymbol{\lambda}}\cdot\boldsymbol{\xi}(\boldsymbol{\lambda}(t)). \tag{1.17}$$

It was shown in by Jarzynski in Ref. [25] that the classical generator $\boldsymbol{\xi}(\boldsymbol{\lambda}(t))$ can be determined by the following equations [62]:

$$\{\boldsymbol{\xi}, H_0\} = \boldsymbol{\nabla}H_0 - \langle\boldsymbol{\nabla}H_0\rangle_{H_0,\boldsymbol{\lambda}} \equiv \boldsymbol{\nabla}\tilde{H}_0 \tag{1.18a}$$

$$\langle\boldsymbol{\xi}\rangle_{E,\boldsymbol{\lambda}} = 0, \tag{1.18b}$$

where $\{\cdot,\cdot\}$ denotes the Poisson bracket. Note that Eqs. 1.18 are the classical analogues of Eqs. 1.16.

A natural question then arises: if we solve for the classical generator $\boldsymbol{\xi}(q,p;\boldsymbol{\lambda})$ and then quantize it to obtain an operator $\hat{\boldsymbol{\xi}}(\boldsymbol{\lambda}) \equiv \boldsymbol{\xi}(\hat{q},\hat{p};\boldsymbol{\lambda})$, will the term $\dot{\boldsymbol{\lambda}}\cdot\hat{\boldsymbol{\xi}}(\boldsymbol{\lambda}(t))$ suppress non-adiabatic transitions under quantum evolution? In other words, can we construct $\hat{H}_{CD}$ – either exactly or approximately – by first obtaining its classical counterpart and then quantizing it? In Ref. [25], it was shown that for even-power-law potentials in one degree of freedom, the classical H_{CD} obtained in terms of

position and momentum, upon quantization produces the correct quantum auxiliary term $\hat{H}_{CD}$. Deffner et al. extended the idea of solving for transitionless quantum driving using an analogous problem on dissipationless classical driving for the general class of *scale-invariant* dynamical processes which describe expansion and transport [34]. In this dissertation, we investigate the example of a time-dependent tilted piston, which does not follow scale invariance, and explore whether the aproach from Ref. [25] is applicable to a more general system.

The fast-forward approach, due to Masuda et al. [26], solves for an auxiliary potential $U_{FF}(\hat{\mathbf{q}}, t)$ for a system evolving under a kinetic plus potential Hamiltonian of the form $\hat{H}_0(t) = \hat{\mathbf{p}}^2/2m + U_0(\hat{\mathbf{q}}, t)$. This is in contrast with the counterdiabatic approach which solves for a general auxiliary Hamiltonian $\hat{H}_{CD}(t)$. As shown in Fig. 1.1(b), the system need not follow the adiabatic path but the goal is to make the system end in the desired state at the final time. The system may choose any path from the initial to the final state and one such path is accessible by a potential $\hat{U}_{FF}(t)$. The experimental implementation of a fast-forward shortcut is more feasible as compared to that of a CD shortcut. The derivation of $U_{FF}(\hat{\mathbf{q}}, t)$ derived in Refs. [26, 28] is straightforward and briefly shown below.

It is assumed that an ansatz of the form

$$\begin{aligned} \bar{\psi}_n(\mathbf{q}, t) &= \psi_n(\mathbf{q}, t) \exp\left[i\frac{S(\mathbf{q}, t)}{\hbar}\right] \\ &= \phi_n(\mathbf{q}, t) \exp\left[-\frac{i}{\hbar}\int_0^t E_n(t')dt'\right] \exp\left[i\frac{S(\mathbf{q}, t)}{\hbar}\right] \end{aligned} \tag{1.19}$$

describes the state of the system during its evolution, where $\psi_n(\mathbf{q}, t)$ is the position

space representation of the adiabatic path described in Eq. 1.3, $\phi_n(\mathbf{q},t) = \langle \mathbf{q}|n\rangle$ and $E_n(t)$ are the corresponding instantaneous energy eigenfunction and eigenvalue respectively. The ansatz $\bar{\psi}_n(\mathbf{q},t)$ therefore must satisfy the time-dependent Schrödinger equation

$$i\hbar\dot{\bar{\psi}}_n(\mathbf{q},t) = (\hat{H}_0 + U_{FF}(\hat{\mathbf{q}},t))\bar{\psi}_n(\mathbf{q},t). \tag{1.20}$$

We have introduced two unknowns $S(\mathbf{q},t)$ and $U_{FF}(\mathbf{q},t)$ which can be solved by substituting Eq. 1.19 in Eq. 1.20. For a one-dimensional system, separating the imaginary and real parts of the resulting equation gives rise to the following two differential equations respectively [28]:

$$\partial_t\phi_n + \frac{1}{m}\partial_q\phi_n\partial_q S + \frac{1}{2m}\phi_n\partial_q^2 S = 0, \tag{1.21a}$$

$$\frac{1}{2m}\phi_n(\partial_q S)^2 + U_{FF}\phi_n = -\phi_n\partial_t S. \tag{1.21b}$$

Solving Eq. 1.21a determines the function $S(q,t)$, which can then be substituted in Eq. 1.21b to obtain $U_{FF}(q,t)$. These results can be easily generalized for three dimensional systems as well.

The main differences between counterdiabatic and fast-forward driving is listed below. The auxiliary fast-forward potential $U_{FF}(\hat{\mathbf{q}},t)$ in general depends on the initial state, i.e., on the initial quantum number n unlike the auxiliary counterdiabatic Hamiltonian $\hat{H}_{CD}(t)$ which is independent of n. Therefore, $U_{FF}(\hat{\mathbf{q}},t)$ is different for every energy level while a single $\hat{H}_{CD}(t)$ is valid for the entire eigenspectrum. Also

note that Eq. 1.21a can be recast as a continuity equation of the probability density:

$$\partial_t \phi_n^2 + \partial_q (v \phi_n^2) = 0, \tag{1.22}$$

where $v(q,t) = \partial_q S/m$. It can be seen that in general, the velocity diverges at nodes of ϕ_n. Therefore, $S(q,t)$ and consequently $U_{FF}(q,t)$ can in general be solved only for the ground state where nodes are absent. Since the fast-forward potential typically (though not always) becomes singular at nodes of the instantaneous eigenstate, the applicability of the fast-forward method becomes restricted to the ground state only. Such singularities do not occur in $\hat{H}_{CD}(t)$. As pointed out earlier, $U_{FF}(\hat{\mathbf{q}},t)$ is easier to implement experimentally compared to $\hat{H}_{CD}(t)$.

A scale-invariant process is an exception for which $U_{FF}(\hat{\mathbf{q}},t)$ in independent of n and does not suffer from singularities. This will be shown in Sec. 3.6. The auxiliary potential $U_{FF}(\hat{\mathbf{q}},t)$ for a scale invariant process was obtained by Deffner et al. in Ref. [34]. A canonical transformation was performed on the classical CD term, $H_{CD}(t)$, required for dissipationless classical driving to obtain an auxiliary classical potential $U_{FF}(\mathbf{q},\mathbf{t})$. The classical $U_{FF}(\mathbf{q},\mathbf{t})$ was then quantized to obtain $U_{FF}(\hat{\mathbf{q}},t)$. In this dissertation, we reformulate Eqs. 1.21 by introducing '*flow-fields*'. We extend the fast-forward method to classical systems evolving more generally, i.e., not following scale invariance, and use the classical solutions to solve for approximate $U_{FF}(\hat{\mathbf{q}},t)$ beyond the ground state.

1.2 Scope of this work

The motivation behind this thesis comes from the need to obtain experimentally implementable quantum shortcut protocols for generic systems which are subjected to an arbitrary driving protocol. We study beyond the simple scale invariant or *self-similar* driving which preserves the topology of a system and only accounts for expansion and translation. In an attempt to solve for quantum shortcuts, we often solve for the analogous classical problem first and gain useful physical insights. We focus on obtaining auxiliary counterdiabatic and fast-forward terms which can be applied to a generic system and are robust against the limitations specified in the previous section. In the rest of the thesis, we study one-dimensional systems unless mentioned otherwise. The thesis is structured as follows:

- In the second chapter, we investigate the example of a *tilted piston* subjected to non-scale-invariant driving. We solve exactly for the classical CD Hamiltonian $H_{CD}(q,p,t)$ following the method introduced in Ref. [25]. $H_{CD}(q,p,t)$ is then quantized to obtain a Hermitian operator $\hat{H}_{CD}(t)$. Using numerical simulations, we find that $\hat{H}_{CD}$ effectively suppresses non-adiabatic excitations under rapid driving. This chapter offers a proof of principle – beyond the special case of scale-invariant driving – that quantum shortcuts to adiabaticity can successfully be constructed from their classical counterparts. However, even for such a simple example, the expression for $H_{CD}(q,p,t)$ is very complicated when the system is driven in a non scale invariant fashion as compared

to the $H_{CD}(q,p,t)$ required for scale invariant driving. We therefore follow a different approach to shortcuts in the subsequent chapters.

- In chapter three, we introduce a general framework for constructing shortcuts to adiabaticity from *flow-fields* that describe the desired adiabatic evolution. This approach provides surprisingly compact expressions for both counterdiabatic Hamiltonians and fast-forward potentials. We illustrate our method with numerical simulations of a model system, and we compare our shortcuts with previously obtained results. Our method, like the fast-forward approach developed previously [26], is susceptible to singularities when applied to excited states of quantum systems; we propose a simple, intuitive criterion for determining whether these singularities will arise, for a given excited state.

- We extend the flow-fields based framework to classical systems in chapter four, and construct approximate counterdiabatic Hamiltonian and fast-forward potential which preserves the classical action under non-adiabatic conditions. We show that the fast-forward potential guides all trajectories with an initial action I_0 to end with the same value of action. We also construct a local dynamical invariant $J(q,p,t)$ whose value remains constant along these trajectories. We illustrate our results with numerical simulations of a model double-well system. We sketch how these classical results may be used to design approximate quantum shortcuts to adiabaticity.

- In chapter five, we demonstrate how to construct counterdiabatic Hamiltonian and fast-forward potential for quantum excited states subjected to an

arbitrary driving protocol. In order to construct the shortcut, we will use semiclassical analysis of a quantum wavefunction along with classical tools for obtaining shortcuts. We illustrate our results using the quantum analogous model double-well system from chapter four. We also carry out a semiclassical analysis of the final distribution of trajectories on a classical energy shell to quantitatively predict the accuracy of the quantal shortcut.

- In chapter six, we demonstrate the universality of the flow-fields based method by extending it to solve analogous shortcut protocols for stochastic systems. We solve the counterdiabatic potential for a system of overdamped Browninan particles subjected to a rapidly changing trapping potential. This counterdiabatic potential enables the system to track its instantaneous equilibrium state at every instant. We compare our method with previous theoretical and experimental work on swift equilibration [59] of Brownian particles.

This dissertation has elaborated the results presented by the author and collaborators in the following papers. Chap. 2 presents the contents from Ref. [54], Chaps. 3 and 6 present contents from Ref. [63], and Chap. 4 presents content from Ref. [56]. The contents of Chap. 5 are under preparation for submission to a journal.

Chapter 2: Shortcuts for a tilted piston

2.1 Overview

In this chapter, we study if Jarzynski's method from Ref. [25] can be extended to more general systems subjected to an arbitrary driving protocol. We study a test case: a particle in a box with infinite walls and a slanted base, i.e. a *tilted piston*. Recasting the counterdiabatic Hamiltonian $\hat{H}_{CD}(t)$ (Eq. 1.9) in terms of position and momentum operators may provide physical insights and pave way for experimental implementation. As discussed in Chap. 1, for a harmonic oscillator with a time-dependent stiffness $k(t)$, Eq. 1.9 reduces to: [20]

$$\hat{H}_{CD} = -\frac{\dot{k}}{8k}(\hat{p}\hat{q} + \hat{q}\hat{p}). \tag{2.1}$$

Similar expressions hold for a particle in a box [61], for attractive power law potentials [25], and more generally for arbitrary potentials undergoing *scale invariant driving* (see Eq. 2.10), characterized by simple expansion, contraction or translation of the potential [32, 34]. However, for general $\hat{H}_0(t)$ it is not clear how to rewrite Eq. 1.9 in terms of operators such as $\hat{q}$ and $\hat{p}$.

In Ref. [25] it was proposed that a problem on transitionless quantum driving

can usefully be approached by studying dissipationless classical driving – the classical counterpart of transitionless quantum driving. Consider a Hamiltonian $\hat{H}_0(\boldsymbol{\lambda})$, where $\boldsymbol{\lambda}$ denotes a vector of externally controlled parameters that are varied with time according to a protocol $\boldsymbol{\lambda}(t)$. In the transitionless quantum driving approach, the counterdiabatic Hamiltonian $\hat{H}_{CD}(t)$ of Eq. 1.9 ensures that when the system evolves under the full Hamiltonian $\hat{H}(t)$ given by Eq. 1.1, it follows the adiabatic trajectory of $\hat{H}_0(\boldsymbol{\lambda}(t))$ even for rapid driving, i.e. the term $\hat{H}_{CD}(t)$ suppresses non-adiabatic excitations. The counterdiabatic Hamiltonian can be expressed as [25]

$$\hat{H}_{CD}(t) = \dot{\boldsymbol{\lambda}} \cdot \hat{\boldsymbol{\xi}}(\boldsymbol{\lambda}(t)). \tag{2.2}$$

From Eq. 2.2, it is clear that the more rapidly the parameters $\boldsymbol{\lambda}$ are varied, the greater the magnitude of the term $\hat{H}_{CD} = \dot{\boldsymbol{\lambda}} \cdot \hat{\boldsymbol{\xi}}$ needed to suppress excitations [10,64].

It was shown in Ref. [25] that the proposed strategy for constructing $\hat{H}_{CD}$ yields correct result for attractive power law potentials, including the harmonic oscillator and the particle in a box as limiting cases. This encouraging result was generalized to arbitrary potentials undergoing scale-invariant driving (Eq. 2.10) [32, 34]. In all these cases the classical counterdiabatic term takes the form $H_{CD} = g(t)p + h(t)qp$, and its quantized counterpart

$$\hat{H}_{CD} = g(t)\hat{p} + \frac{h(t)}{2}\left(\hat{p}\hat{q} + \hat{q}\hat{p}\right) \tag{2.3}$$

can be shown to be equivalent to Eq. 1.9.

In this chapter, we investigate whether this strategy succeeds for *non*-scale-invariant driving protocols. In Sec. 2.2, we briefly review dissipationless classical driving, and we specify the tilted piston Hamiltonian and the driving protocols that will be studied. We solve exactly for $H_{CD}(q,p,t)$ in Sec. 2.3, and we quantize it semi-classically in Sec. 2.4. Finally we study numerically whether the resulting quantum operator $\hat{H}_{CD}(t)$ produces the desired transitionless quantum driving. Details of the numerical approach are described in Sec. 2.5, and the results are presented in Sec. 2.6. We summarize the results from this chapter in Sec. 2.7.

2.2 Classical Dissipationless driving and the system under study

Let $z = (p,q)$ denote a point in the system's two-dimensional phase space. The counterdiabatic Hamiltonian $H_{CD}(z;t) = \dot{\boldsymbol{\lambda}} \cdot \boldsymbol{\xi}(z;\boldsymbol{\lambda}(t))$, when added to the unperturbed Hamiltonian $H_0(z;\boldsymbol{\lambda}(t))$, ensures that the classical system follows an adiabatic trajectory – along which the action I_0 is constant – even when the driving is rapid. Below we briefly summarize how $\boldsymbol{\xi}(z;\boldsymbol{\lambda})$ is constructed [25].

Let the microcanonical average of a quantity be denoted by

$$\langle \ldots \rangle_{E,\boldsymbol{\lambda}} \equiv \frac{1}{\partial_E \Omega} \int dz \delta(E - H_0) \ldots , \tag{2.4}$$

and the volume of phase space enclosed by an energy shell E be denoted by

$$\Omega(E,\boldsymbol{\lambda}) \equiv \int dz \theta \left[E - H_0(z;\boldsymbol{\lambda})\right] . \tag{2.5}$$

Then the desired classical generator $\boldsymbol{\xi}$ satisfies [25]:

$$\boldsymbol{\xi}(z_b;\boldsymbol{\lambda}) - \boldsymbol{\xi}(z_a;\boldsymbol{\lambda}) = \int_a^b dt \boldsymbol{\nabla}\tilde{H}_0(z(t);\boldsymbol{\lambda}), \tag{2.6}$$

where z_a and z_b are two points on the energy shell E, $z(t)$ is a trajectory that evolves from z_a to z_b under $H_0(z;\boldsymbol{\lambda})$ (with $\boldsymbol{\lambda}$ fixed), and the integrand is defined as $\boldsymbol{\nabla}\tilde{H}_0 \equiv \boldsymbol{\nabla}H_0 - \langle\boldsymbol{\nabla}H_0\rangle_{E,\boldsymbol{\lambda}}$, with $\boldsymbol{\nabla} \equiv \partial/\partial\boldsymbol{\lambda}$. By convention the microcanonical average of $\boldsymbol{\xi}$ is set to zero,

$$\langle\boldsymbol{\xi}\rangle_{E,\boldsymbol{\lambda}} = 0. \tag{2.7}$$

Eqs. 2.6 and 2.7 uniquely specify the generator $\boldsymbol{\xi}(z;\boldsymbol{\lambda})$.

For a system with one degree of freedom, the time average and the microcanonical average of a quantity are equivalent, therefore we can compute $\langle\boldsymbol{\nabla}H_0\rangle_{E,\boldsymbol{\lambda}}$ by evaluating the time average of $\boldsymbol{\nabla}H_0$ along a periodic trajectory of energy E. Alternatively, this microcanonical average can be determined by defining the inverse function $E(\Omega,\boldsymbol{\lambda})$ from $\Omega(E,\boldsymbol{\lambda})$, and by using the cyclic identity of partial derivatives:

$$\boldsymbol{\nabla}E(\Omega,\boldsymbol{\lambda}) = -\frac{\boldsymbol{\nabla}\Omega(E,\boldsymbol{\lambda})}{\partial_E\Omega(E,\boldsymbol{\lambda})} = \langle\boldsymbol{\nabla}H_0\rangle_{E,\boldsymbol{\lambda}}. \tag{2.8}$$

For a harmonic oscillator with a time-dependent stiffness $k(t)$, the procedure described above leads to the classical counterdiabatic Hamiltonian

$$H_{CD}(z,t) = -\frac{\dot{k}}{4k}qp. \tag{2.9}$$

Upon quantization, this result agrees with the quantum counterdiabatic Hamiltonian for the harmonic oscillator, Eq. 2.1, which was originally obtained by direct evaluation of the Demirplak-Rice-Berry formula, Eq. 1.9 in Ref. [20]. More generally, a time-dependent potential of the form

$$V(q; f, \gamma) = \frac{1}{\gamma^2} V_0 \left(\frac{q - f}{\gamma} \right) \tag{2.10}$$

where $f = f(t)$ and $\gamma = \gamma(t)$, is said to undergo *scale-invariant driving*. For scale-invariant driving, Eqs. 2.6 and 2.7 lead to a simple expression for $H_{CD}(z;t)$ that, upon quantization, give the exact quantum counterdiabatic Hamiltonian $\hat{H}_{CD}(t)$ [34], in the form given by Eq. 2.3.

To investigate how well these results extend to systems that are driven in non-scale-invariant fashion, we will study a *tilted piston*: a particle of mass m confined in a one-dimensional box with infinite walls and a slanted base. In terms of the length of the box L and slope of its base s, the classical Hamiltonian is given by

$$H_0\left(q, p; s, L\right) = \frac{p^2}{2m} + sq + \Theta(q; 0, L), \tag{2.11}$$

where the function

$$\Theta(q; q_L, q_R) = \begin{cases} 0, & q_L < q < q_R \\ \infty & \text{otherwise} \end{cases} \tag{2.12}$$

describes hard walls at $q = q_L$ and $q = q_R$.

We subject the system to two different driving protocols. In case (a), the slope s is changed while the length L is held fixed, whereas in case (b), s is held fixed and the box length is changed by moving the wall at $q = L$. Without loss of generality, we will assume that the slope is positive, $s > 0$, and that the wall at $q = 0$ remains fixed. Although the protocols (a) and (b) are both non-scale-invariant, when s and L are varied simultaneously while holding sL^3 fixed, the system undergoes scale-invariant driving, as verified directly from Eqs. 2.10 and 2.11.

2.3 Classical counterdiabatic terms

Fig.2.1 illustrates the classical energy shells of the Hamiltonian $H_0(q, p; s, L)$ defined by Eq. 2.11. There is a critial value of energy, $E_c = sL$, below which a classical particle interacts only with the wall at $q = 0$, and above which the particle interacts with both walls. When $E \leq E_c$, the energy shell is a single curve that is symmetric about the q-axis and has a discontinuity at $q = 0$, whereas when $E > E_c$, the energy shell is a pair of curves symmetric about the q-axis with discontinuities at $q = 0$ and $q = L$. The expression for the classical counterdiabatic generator $\boldsymbol{\xi}(z, \boldsymbol{\lambda}(t))$ depends on E_c.

Let $\Omega_<$ denote the volume enclosed by an energy shell of energy $E < E_c$ and $\Omega_>$ denote the volume enclosed when $E > E_c$. From Eq. 2.11 using $p = \sqrt{2m(E - sq)}$

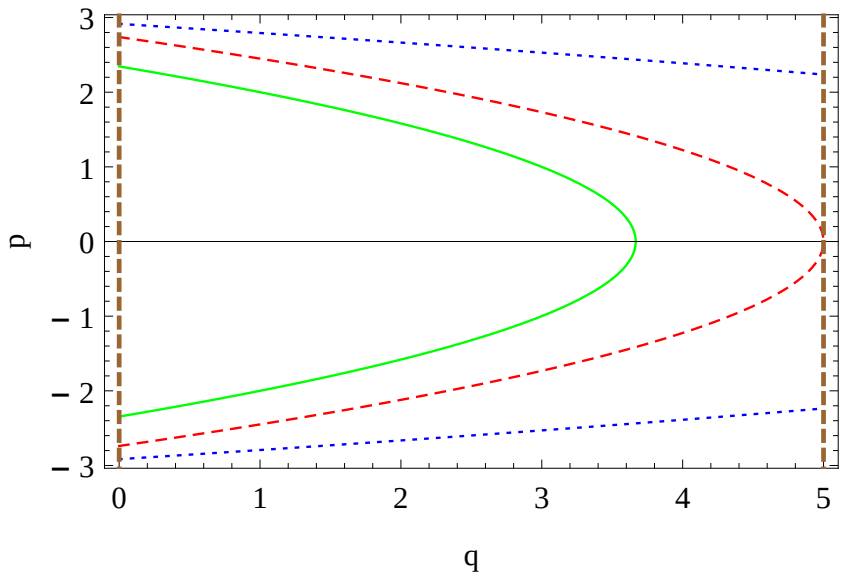

Figure 2.1: Three energy shells of H_0 (Eq. 2.11) are shown for mass $m = 1/2$, length $L = 5$ and slope $s = 1.5$. The green solid, red dashed and the blue dotted curves correspond to $E = 5.5(< sL)$, $E = 7.5(= sL)$ and $E = 8.5(> sL)$ respectively. The brown dashed lines at $q = 0$ and $q = 5$ denote the hard walls.

we obtain

$$\Omega_<(E,s,L) = 2\int_0^{E/s} p\,dq = \frac{4\sqrt{2m}E^{\frac{3}{2}}}{3s}, \tag{2.13a}$$

$$\Omega_>(E,s,L) = 2\int_0^{L} p\,dq = \frac{4\sqrt{2m}}{3s}\left[E^{\frac{3}{2}} - (E-sL)^{\frac{3}{2}}\right]. \tag{2.13b}$$

We now solve explicitly for the classical generator $\xi(z;\boldsymbol{\lambda})$ specified by Eqs. 2.6 and 2.7. We analyze separately the two protocols (a) and (b) mentioned above.

2.3.1 Case (a): time-dependent slope at fixed length

The time-dependent parameter $\boldsymbol{\lambda}$ is the slope s in this case. Let us first solve for ξ when $E \leq E_c$. Using Eqs. 2.8 and 2.13a

$$\langle \partial_s H_0 \rangle_{E,s} = -\frac{\partial_s \Omega_<(E,s,L)}{\partial_E \Omega_<(E,s,L)} = \frac{2E}{3s}, \tag{2.14}$$

and from Eq. 2.11

$$\nabla H_0 = \partial_s H_0 = q. \tag{2.15}$$

Hence, from Eq. 2.6, upon using $dt = m\,dq/\sqrt{2m(E-sq)}$, we arrive at

$$\xi(z_b;s) - \xi(z_a;s) = \int_a^b dt \nabla \tilde{H}_0(z(t);s) = -\frac{qp}{3s}\bigg|_a^b. \tag{2.16}$$

Together with the condition $\langle \xi \rangle_{E,s} = 0$, this result gives us, for $E < sL$,

$$\xi_C^<(q,p;s) = -\frac{qp}{3s}, \tag{2.17}$$

where the subscript C stands for classical. This simple form for Eq. 2.17 reflects the fact that when $E < sL$, varying the slope of the base at fixed box length is tantamount to scale invariant driving.

We now construct the generator $\xi_C^>(q,p;s)$, for $E \geq E_c$. For the upper and the lower branches of the energy shell, let $\xi(0,p(0);s) = \xi_0$, and $\xi(L,p(L);s) = \xi_1$

denote two constants to be determined later. Eqs. 2.8 and 2.13b yield

$$\langle \partial_s H_0 \rangle_{E,s} = \frac{E + sL - \sqrt{E(E-sL)}}{3s}. \tag{2.18}$$

Using Eqs. 2.6, 2.15 and 2.18, we obtain the following two equations for the upper and the lower branches respectively:

$$\begin{aligned} \xi(z;s) - \xi_0 &= -\frac{p}{3s^2}\left[E - sL + \sqrt{E(E-sL)}\right] - \frac{pq}{3s} \\ &+ \frac{\sqrt{2mE}}{3s^2}\left[E - sL + \sqrt{E(E-sL)}\right], \end{aligned} \tag{2.19a}$$

$$\begin{aligned} \xi(z;s) - \xi_1 &= -\frac{p}{3s^2}\left[E - sL + \sqrt{E(E-sL)}\right] - \frac{pq}{3s} \\ &- \frac{\sqrt{2m(E-sL)}}{3s^2}\left[E + \sqrt{E(E-sL)}\right]. \end{aligned} \tag{2.19b}$$

The constants ξ_0 and ξ_1 are now determined by demanding continuity of ξ at $q = 0$ and $q = L$, along with the condition that $\langle \xi \rangle_{E,s} = 0$. A series of simple calculations yield $\xi_0 = 0 = \xi_1$. Eqs. 2.19 can be rearranged to obtain the general expression for the classical generator when $E > sL$

$$\begin{aligned} \xi_C^{>}(q,p;s) &= -\frac{p}{3s^2}\left[E - sL + \sqrt{E(E-sL)}\right] - \frac{pq}{3s} \\ &+ \text{sign}(p) \cdot \frac{\sqrt{2m}}{3s^2}\left[E\sqrt{E-sL} + \sqrt{E}(E-sL)\right], \end{aligned} \tag{2.20}$$

where $\text{sign}(p) = +1$ for the upper branch and -1 for the lower branch. As a consistency check, we note that at the critical energy $E = E_c = sL$, Eq. 2.20 reduces to Eq. 2.17.

2.3.2 Case (b): time-dependent length at fixed slope

In this case, the length L plays the role of the parameter $\boldsymbol{\lambda}$. A particle with energy $E \leq E_c$ is not influenced by the motion of the wall at $q = L$. Hence we expect

$$\xi_C^<(q, p; L) = 0. \tag{2.21}$$

This is mathematically verified by noting that $\partial_L H_0 = 0$ for $q < L$, and $\langle \partial_L H_0 \rangle_{E,L} = 0$ (from Eqs. 2.8 and 2.13a), therefore Eq. 2.6 gives us $\xi_C^< = 0$. When $E > E_c$, Eqs. 2.8 and 2.13b yield $\langle \partial_L H_0 \rangle_{E,L} = -\left[E - sL + \sqrt{E(E - sL)}\right]/L$. Hence at all points except at $q = L$,

$$\partial_L \tilde{H}_0(z(t); L) = \frac{E - sL + \sqrt{E(E - sL)}}{L}. \tag{2.22}$$

Analogous to case (a), to-be-determined constants $\xi(0, p(0); L) = \xi_0'$ and $\xi(L, p(L); L) = \xi_1'$ are introduced for the upper and lower branches respectively. Using Eqs. 2.6 and 2.22 we obtain, for the upper and the lower branches respectively:

$$\xi(z; L) - \xi_0' = \frac{E - sL + \sqrt{E(E - sL)}}{sL}\left[\sqrt{2mE} - p\right], \tag{2.23a}$$

$$\xi(z; L) - \xi_1' = \frac{E - sL + \sqrt{E(E - sL)}}{sL} \times \left[-\sqrt{2m(E - SL)} - p\right]. \tag{2.23b}$$

Setting $\langle \xi \rangle_{E,L} = 0$ and demanding continuity of ξ at $q = 0$ and $q = L$, we get $\xi'_0 = 0$ and

$$\xi'_1 = \frac{E - sL + \sqrt{E(E-sL)}}{sL} \times \left[\sqrt{2m(E - SL)} - \sqrt{2mE} \right]. \tag{2.24}$$

Eqs. 2.23 and 2.24 can be combined to give the classical generator for $E > E_c$:

$$\begin{aligned} \xi^{>}_C(q,p;L) &= -\frac{p}{sL}\left[E - sL + \sqrt{E(E-sL)}\right] \\ &+ \text{sign}(p) \cdot \frac{\sqrt{2m}}{sL}\left[E\sqrt{E-sL} + \sqrt{E}(E-sL)\right], \end{aligned} \tag{2.25}$$

which is consistent with Eq. 2.21 at $E = E_c$.

Eqs. 2.17 and 2.21 provide explicit expression for ξ at energies $E < E_c$, and Eqs. 2.20 and 2.25 give ξ for $E \geq E_c$. As mentioned earlier, below the critical energy the system is effectively driven in a scale-invariant manner. We will focus our attention on energies above the critical energy, where the driving is non-scale-invariant.

Comparing Eqs. 2.17 and 2.20 with Eqs. 2.21 and 2.25 respectively, we note that the classical generators for cases (a) and (b) are related to each other by the following relation:

$$\xi_C(q,p;s) + \frac{pq}{3s} = \xi_C(q,p;L) \cdot \frac{L}{3s}. \tag{2.26}$$

2.4 Semiclassical counterdiabatic terms

Having obtained exact classical expressions for the generator $\xi(z;\boldsymbol{\lambda})$, we now wish to utilize these results to construct its quantum counterpart $\hat{\xi}(\boldsymbol{\lambda})$, in terms of position and momentum operators $\hat{q}$ and $\hat{p}$. In later sections we will study, numerically, the extent to which the operator constructed in this manner produces transitionless quantum driving for the quantum tilted piston.

We seek a semiclassical approximation for the quantum generator, denoted by $\hat{\xi}_{SC}$. In cases (a) and (b) described above, $\hat{H}_{CD}(t)$ is given by $\dot{s}\cdot\hat{\xi}_{SC}(q,p;s)$ and $\dot{L}\cdot\hat{\xi}_{SC}(q,p;L)$ respectively, where $\hat{\xi}_{SC}$ is Hermitian. As the operators $\hat{q}$ and $\hat{p}$ do not commute, merely putting 'hats' on the observables in Eqs. 2.17, 2.20 and 2.25 will not ensure Hermiticity. Rather, the terms in ξ_C must be symmetrized. Complete symmetrization as prescribed in Ref. [65] becomes unfeasible as ξ_C contains terms with non-integer powers of q and p. We therefore implement the following procedure to symmetrize the expressions.

Any term in ξ_C of the form $f(p)\cdot g(E)$, where f and g are arbitrary functions, is symmetrized as

$$\frac{f(\hat{p})\cdot g(\hat{H}_0)+g(\hat{H}_0)\cdot f(\hat{p})}{2}, \tag{2.27}$$

where $\hat{H}_0$ is the quantized version of Eq. 2.11. The semiclassical operators for

$E \leq sL$ are given by

$$\hat{\xi}^{<}_{SC}(\hat{q},\hat{p};s) = -\frac{1}{6s}(\hat{q}\hat{p}+\hat{p}\hat{q}), \tag{2.28a}$$

$$\hat{\xi}^{<}_{SC}(\hat{q},\hat{p};L) = 0, \tag{2.28b}$$

where Eqs. 2.17 and 2.21 have been used. Let $\hat{\eta}$ be the semiclassical operator for sign(p) (to be determined later). For $E > sL$, from Eq. 2.20 and 2.25, we obtain

$$\hat{\xi}^{>}_{SC}(\hat{q},\hat{p};s) = -\frac{1}{3s^2}\hat{\xi}_1 - \frac{1}{3s}\hat{\xi}_2 + \frac{1}{3s^2}\hat{\xi}_3, \tag{2.29a}$$

$$\hat{\xi}^{>}_{SC}(\hat{q},\hat{p};L) = -\frac{1}{sL}\hat{\xi}_1 + \frac{1}{sL}\hat{\xi}_3, \tag{2.29b}$$

where

$$\hat{\xi}_1 = \frac{\hat{p}\cdot f(\hat{H}_0) + f(\hat{H}_0)\cdot\hat{p}}{2} \tag{2.29c}$$

$$\hat{\xi}_2 = \frac{\hat{q}\hat{p}+\hat{p}\hat{q}}{2} \tag{2.29d}$$

$$\hat{\xi}_3 = \frac{\hat{\eta}\cdot g(\hat{H}_0) + g(\hat{H}_0)\cdot\hat{\eta}}{2} \tag{2.29e}$$

$$f(\hat{H}_0) = \hat{H}_0 - sL + \sqrt{\hat{H}_0(\hat{H}_0 - sL)} \tag{2.29f}$$

$$g(\hat{H}_0) = \sqrt{2m}\left[\hat{H}_0\sqrt{\hat{H}_0 - sL} + \sqrt{\hat{H}_0}(\hat{H}_0 - sL)\right] \tag{2.29g}$$

The generators $\hat{\xi}_{SC}(\hat{q},\hat{p};s)$ and $\hat{\xi}_{SC}(\hat{q},\hat{p};L)$ defined by Eqs. 2.28-2.29 satisfy

$$\hat{\xi}_{SC}(\hat{q},\hat{p};s) + \frac{1}{3s}\cdot\frac{\hat{q}\hat{p}+\hat{p}\hat{q}}{2} = \hat{\xi}_{SC}(\hat{q},\hat{p};L)\cdot\frac{L}{3s}, \tag{2.30}$$

which is the semiclassical counterpart of Eq. 2.26.

2.5 Solving the time-dependent Schrödinger Equation

In the previous section, we obtained semiclassical expressions for the generators $\hat{\xi}_{SC}(\hat{q},\hat{p};\boldsymbol{\lambda})$, where $\boldsymbol{\lambda} = s$ for case (a) and $\boldsymbol{\lambda} = L$ for case (b). We now aim to simulate the evolution of the system under the time dependent Schrödinger equation, to establish how well these generators produce transitionless quantum driving.

Let the wavefunction

$$u_n(q,\boldsymbol{\lambda}) = \langle q|n(\boldsymbol{\lambda})\rangle \tag{2.31}$$

denote the n^{th} eigenstate of the unperturbed Hamiltonian $\hat{H}_0(\boldsymbol{\lambda})$, in the position representation. For a given protocol $\boldsymbol{\lambda}(t)$, we will evolve a wavefunction $\psi(q,t)$ under the time dependent Schrödinger equation, $\mathcal{H}\psi = i\hbar\,\partial\psi/\partial t$, using the Hamiltonian

$$\hat{\mathcal{H}}(t) = \hat{H}_0(\boldsymbol{\lambda}(t)) + \dot{\boldsymbol{\lambda}}\cdot\hat{\xi}_{SC}(\hat{q},\hat{p};\boldsymbol{\lambda}(t)), \tag{2.32}$$

with initial condition $\psi(q,0) = u_n(q,\boldsymbol{\lambda}(0))$. We will compare the evolving wavefunction $\psi(q,t)$ with the instantaneous n^{th} energy eigenstate by evaluating the *fidelity*:

$$\mathcal{F}(t) = |\langle n(\boldsymbol{\lambda}(t))|\psi(t)\rangle| = \left|\int dq\, u_n^*(q,\boldsymbol{\lambda}(t))\psi(q,t)\right|. \tag{2.33}$$

The fidelity provides a direct measure, between 0 and 1, of the degree to which the term $\dot{\boldsymbol{\lambda}}\cdot\hat{\xi}_{SC}$ appearing in Eq. (2.32) suppresses transitions out of the n^{th} energy eigenstate.

In this section we describe our approach to solving the time dependent Schrödinger equation numerically, and we develop the tools required to implement this procedure. We expand the time-dependent wave function as

$$\psi(q,t) = \sum_n a_n(t) u_n(q, \boldsymbol{\lambda}(t)) \exp\left[-\frac{i}{\hbar}\int_0^t E_n(t')dt'\right], \tag{2.34}$$

where $E_n(t)$ is the n^{th} eigenvalue of $\hat{H}_0(\boldsymbol{\lambda}(t))$, and the expansion coefficients satisfy $\sum_n |a_n(t)|^2 = 1$. Upon substituting Eq. 2.34 in the time dependent Schrödinger equation, using the Hamiltonian $\hat{\mathcal{H}}(t)$ given by Eq. 2.32, we obtain

$$\dot{a}_m = \sum_n N_{mn} a_n, \tag{2.35}$$

where

$$N_{mn} = \dot{\boldsymbol{\lambda}} \exp\left[-\frac{i}{\hbar}\int_0^t (E_n(t') - E_m(t'))dt'\right] M_{mn}, \tag{2.36}$$

and

$$\begin{aligned} M_{mn} &= -\langle m|\boldsymbol{\nabla} n\rangle + \frac{1}{i\hbar}\langle m|\hat{\xi}_{SC}|n\rangle \\ &= M^0_{mn} + M^{CD}_{mn}. \end{aligned} \tag{2.37}$$

The term $M^0_{mn} \equiv -\langle m|\boldsymbol{\nabla} n\rangle$ arises from the term $\hat{H}_0$ in Eq. 2.32, while $M^{CD}_{mn} \equiv (i\hbar)^{-1}\langle m|\hat{\xi}_{SC}|n\rangle$ is the contribution from the semiclassical counterdiabatic generator, $\dot{\boldsymbol{\lambda}} \cdot \hat{\xi}_{SC}$. Solving the Schrödinger equation is equivalent to solving the first order matrix differential equation Eq. 2.35 for the expansion coefficients $a_n(t)$.

In order to obtain explicit expressions for the matrices M^0 and M^{CD} appearing in Eq. 2.37, it is convenient to make use of two different time-dependent basis sets in Hilbert space. The first is the *energy basis*, $\{|n(\boldsymbol{\lambda})\rangle\}$, consisting of the eigenstates of $\hat{H}_0(\boldsymbol{\lambda})$. The second is the *sine basis*, $\{|\alpha(L)\rangle\}$, by which we mean the orthogonal sinusoidal functions of length L:

$$\langle q|\alpha(L)\rangle = \sqrt{\frac{2}{L}}\sin\left(\frac{\alpha\pi q}{L}\right) \quad , \quad \alpha \geq 1 \tag{2.38}$$

where $L = L(t)$. We will use Latin and Greek letters, respectively, to denote energy and sine basis states. Given a Hermitian operator $\hat{O}$, its representation in the energy and sine bases will be denoted by the matrices

$$\bar{O}_{mn} = \langle m|\hat{O}|n\rangle \tag{2.39a}$$

$$\tilde{O}_{\alpha\beta} = \langle \alpha|\hat{O}|\beta\rangle \tag{2.39b}$$

The operators $f(\hat{H}_0)$ and $g(\hat{H}_0)$, defined by Eqs. 2.29f and 2.29g, are conveniently represented in the energy basis, in which they become diagonal matrices with entries

$$\bar{f}_{mm} = E_m - sL + \sqrt{E_m(E_m - sL)} \tag{2.40}$$

$$\bar{g}_{mm} = \sqrt{2m}\left[E_m\sqrt{E_m - sL} + \sqrt{E_m}(E_m - sL)\right] \tag{2.41}$$

The operators $\hat{p}$, $\hat{\xi}_2$ and $\hat{\eta}$ are more conveniently represented in the sine basis.

Using Eq. 2.38, we obtain

$$\tilde{p}_{\alpha\beta} = \begin{cases} 0 & \alpha - \beta = even \\ \frac{4i\hbar\alpha\beta}{L(\beta^2-\alpha^2)} & \alpha - \beta = odd \end{cases}, \tag{2.42}$$

and

$$(\tilde{\xi}_2)_{\alpha\beta} = \begin{cases} 0 & \alpha = \beta \\ -\frac{2i\hbar\alpha\beta}{\beta^2-\alpha^2} & \alpha - \beta = even\,,\ \alpha \neq \beta \\ \frac{2i\hbar\alpha\beta}{\beta^2-\alpha^2} & \alpha - \beta = odd \end{cases} \tag{2.43}$$

A representation of $\hat{\eta}$ in the sine basis is obtained by semiclassical means in Appendix A, yielding the result:

$$\tilde{\eta}_{\alpha\beta} = \begin{cases} 0 & \alpha - \beta = even \\ \frac{2i}{(\beta-\alpha)\pi} & \alpha - \beta = odd \end{cases}. \tag{2.44}$$

In order to use Eqs. 2.40-2.44 to construct the matrix elements M^{CD}_{mn}, we required the similarity transformation

$$\bar{O}_{mn} = \sum_{\alpha\beta} Z^{\dagger}_{m\alpha} \tilde{O}_{\alpha\beta} Z_{\beta n}, \tag{2.45}$$

where $Z_{\beta n} = \langle \beta | n \rangle$. Z is the matrix that diagonalizes $\tilde{H}_0$ – the sine basis represen-

tation of $\hat{H}_0$ – which can be evaluated explicitly:

$$(\tilde{H}_0)_{\alpha\beta} = \begin{cases} 0 & \alpha - \beta = even\,,\ \alpha \neq \beta \\ -\frac{8\alpha\beta sL}{(\alpha^2-\beta^2)^2\pi^2} & \alpha - \beta = odd \\ \frac{(\alpha\pi\hbar)^2}{2mL^2} + \frac{sL}{2} & \alpha = \beta \end{cases} . \tag{2.46}$$

We obtained Z from $\tilde{H}_0$ numerically, and we used the result to transform $\tilde{p}$, $\tilde{\xi}_2$ and $\tilde{\eta}$ (Eqs. 2.42 - 2.44) into $\bar{p}$, $\bar{\xi}_2$ and $\bar{\eta}$ via Eq. 2.45. We then combined these expressions with $\bar{f}$ and $\bar{g}$ (Eqs. 2.40, 2.41) to construct $\bar{\xi}_1$, $\bar{\xi}_2$ and $\bar{\xi}_3$ (see Sec. 2.4). Finally, from these we obtained $\bar{\xi}_{SC}$ and therefore M^{CD}_{mn} (Eq. 2.37).

In addition to M^{CD}_{mn}, Eq. 2.37 contains the term

$$M^0_{mn} = -\langle m|\nabla n\rangle = -\frac{\langle m|\nabla \hat{H}_0|n\rangle}{E_n - E_m} \tag{2.47}$$

For case (a), $\nabla\hat{H}_0 = \partial_s\hat{H}_0 = \hat{q}$. The elements of $\hat{q}$ in the sine basis are

$$\tilde{Q}_{\alpha\beta} = \begin{cases} 0 & \alpha - \beta = even\,,\ \alpha \neq \beta \\ -\frac{8\alpha\beta L}{(\alpha^2-\beta^2)^2\pi^2} & \alpha - \beta = odd \\ \frac{L}{2} & \alpha = \beta \end{cases} . \tag{2.48}$$

After obtaining $\bar{Q} = Z^T\tilde{Q}Z$, we have

$$-\langle m|\partial_s n\rangle = \begin{cases} -\frac{\bar{Q}_{mn}}{E_n - E_m} & m \neq n \\ 0 & m = n \end{cases} . \tag{2.49}$$

For case (b) we have $\nabla \hat{H}_0 = \partial_L \hat{H}_0$, whose classical counterpart $\partial_L H_0$ is singular at $q = L(t)$. We will determine $\langle m|\partial_L n\rangle$ by relating it to $\langle m|\partial_s n\rangle$ using scale invariance.

The potential $V(q; s, L) = sq + \Theta(q; 0, L)$ that appears in our Hamiltonian, Eq. 2.11, depends parametrically on both the slope s and the length L. If these two parameters are constrained to satisfy

$$s(L)L^3 = constant \tag{2.50}$$

(treating the slope s as a function of the length L) then the potential function satisfies

$$V(q; s(L), L) = \frac{1}{L^2} V\left(\frac{q}{L}; s(1), 1\right) \tag{2.51}$$

which is the condition for scale invariance. In this situation the n^{th} energy eigenfunction satisfies [34]

$$u_m(q; s(L), L) = \frac{1}{\sqrt{L}} u_m\left(\frac{q}{L}; s(1), 1\right). \tag{2.52}$$

Differentiating both sides of Eq. 2.52 with respect to L and equating the results, we get

$$\frac{\partial u_m}{\partial L} = \frac{3s}{L}\frac{\partial u_m}{\partial s} - \frac{u_m}{2L} - \frac{q}{L}\frac{\partial u_m}{\partial q}. \tag{2.53}$$

Since the entire parameter space can be filled by a set of non-intersecting curves defined by Eq. 2.50, Eq. 2.53 is valid for any slope s and any positive length L.

Now consider the expressions

$$\begin{aligned}\langle n|\partial_L m\rangle &= \int_0^L dq\ u_n^* \frac{\partial u_m(q)}{\partial L} \\ &= \frac{3s}{L}\langle n|\partial_s m\rangle - \frac{1}{2L}\delta_{mn} - \frac{1}{L}\int_0^L dq\ u_n^*\ q\frac{\partial u_m(q)}{\partial q} \end{aligned} \tag{2.54}$$

and

$$\begin{aligned}\frac{1}{i\hbar}\langle n|\frac{\hat{q}\hat{p}+\hat{p}\hat{q}}{2}|m\rangle &= -\frac{1}{2}\int_0^L dq\ u_n^*\ q\frac{\partial u_m(q)}{\partial q} - \frac{1}{2}\int_0^L dq\ u_n^*\ \frac{\partial(q\ u_m(q))}{\partial q} \\ &= -\int_0^L dq\ u_n^*\ q\frac{\partial u_m(q)}{\partial q} - \frac{\delta_{mn}}{2} \end{aligned} \tag{2.55}$$

Substituting Eq. 2.55 into Eq. 2.54, we arrive at

$$\langle n|\partial_L m\rangle = \frac{3s}{L}\langle n|\partial_s m\rangle + \frac{1}{L}\frac{1}{i\hbar}\langle n|\frac{\hat{q}\hat{p}+\hat{p}\hat{q}}{2}|m\rangle, \tag{2.56}$$

which can alternatively be obtained from Eq. 2.30. We can therefore compute the matrix representation of $\langle n|\partial_L m\rangle$ as we have already determined both the terms on the right side of Eq. 2.56: Eq. 2.49 gives the first term while the second is obtained after performing a similarity transformation on the matrix given in Eq. 2.43.

2.6 Numerical Results

Having determined the matrices M^0 and M^{CD} (Eq. 2.37), we solved the time dependent Schrödinger equation by numerically integrating Eq. 2.35 using the (fourth-order) Runge-Kutta-Gill method [66]. In each simulation the system was initialized

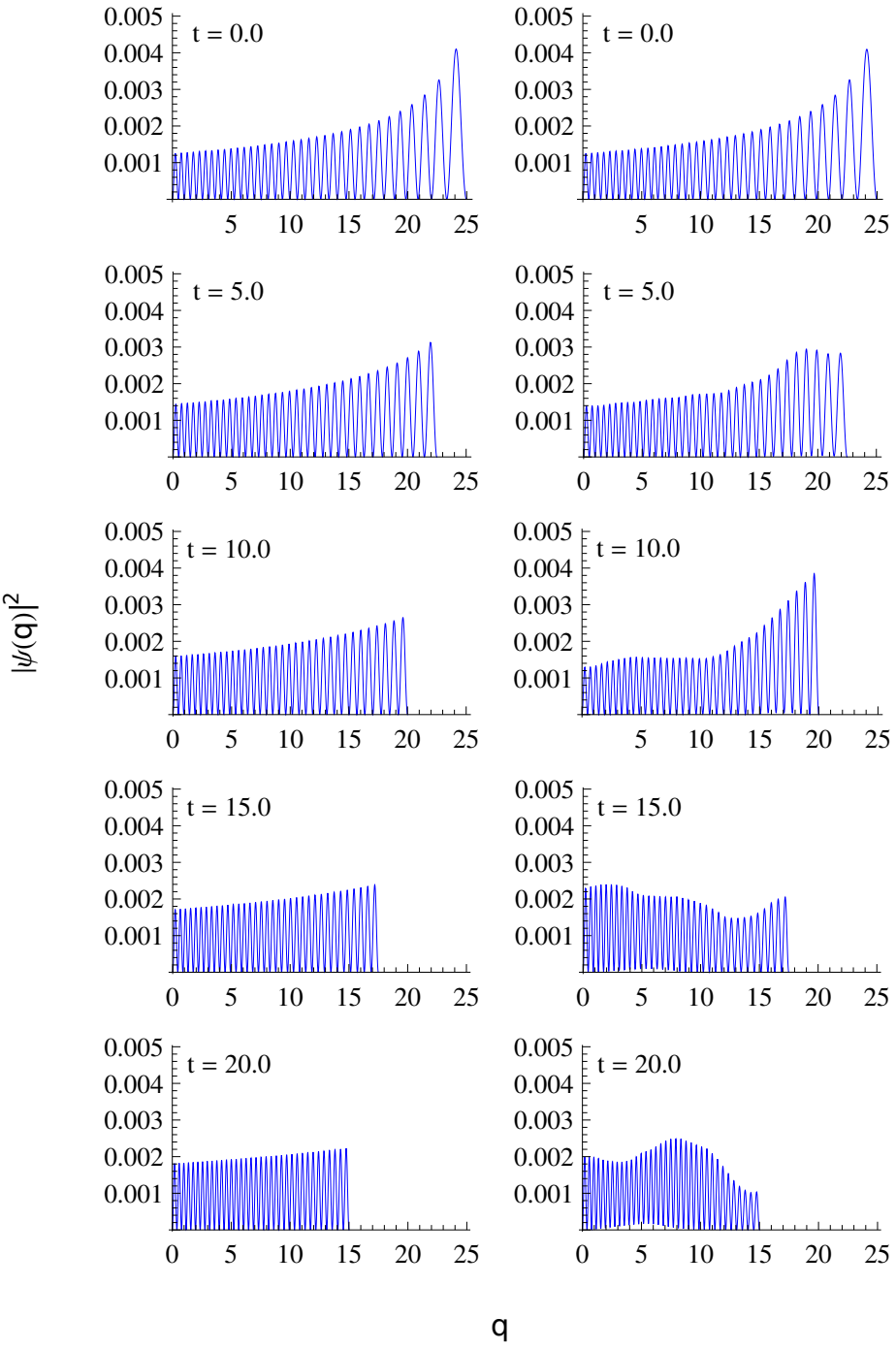

Figure 2.2: Evolution of the probability density $|\psi(q,t)|^2$ for a particle of mass $m = 1.0$ in a box whose slope is fixed at $s = 3.0$ and whose length is decreased from $L = 25.0$ to 15.0 at a rate $\dot{L} = -0.5$. Snapshots of the wavefunction are taken at times t=0, 5.0, 10.0, 15.0 and 20.0. The plots on the left depict evolution under the full Hamiltonian $\hat{\mathcal{H}}(t) = \hat{H}_0(t) + \dot{\boldsymbol{\lambda}} \cdot \hat{\xi}_{SC}(\boldsymbol{\lambda}(t))$, while those on the right depict evolution under $\hat{H}_0(t)$.

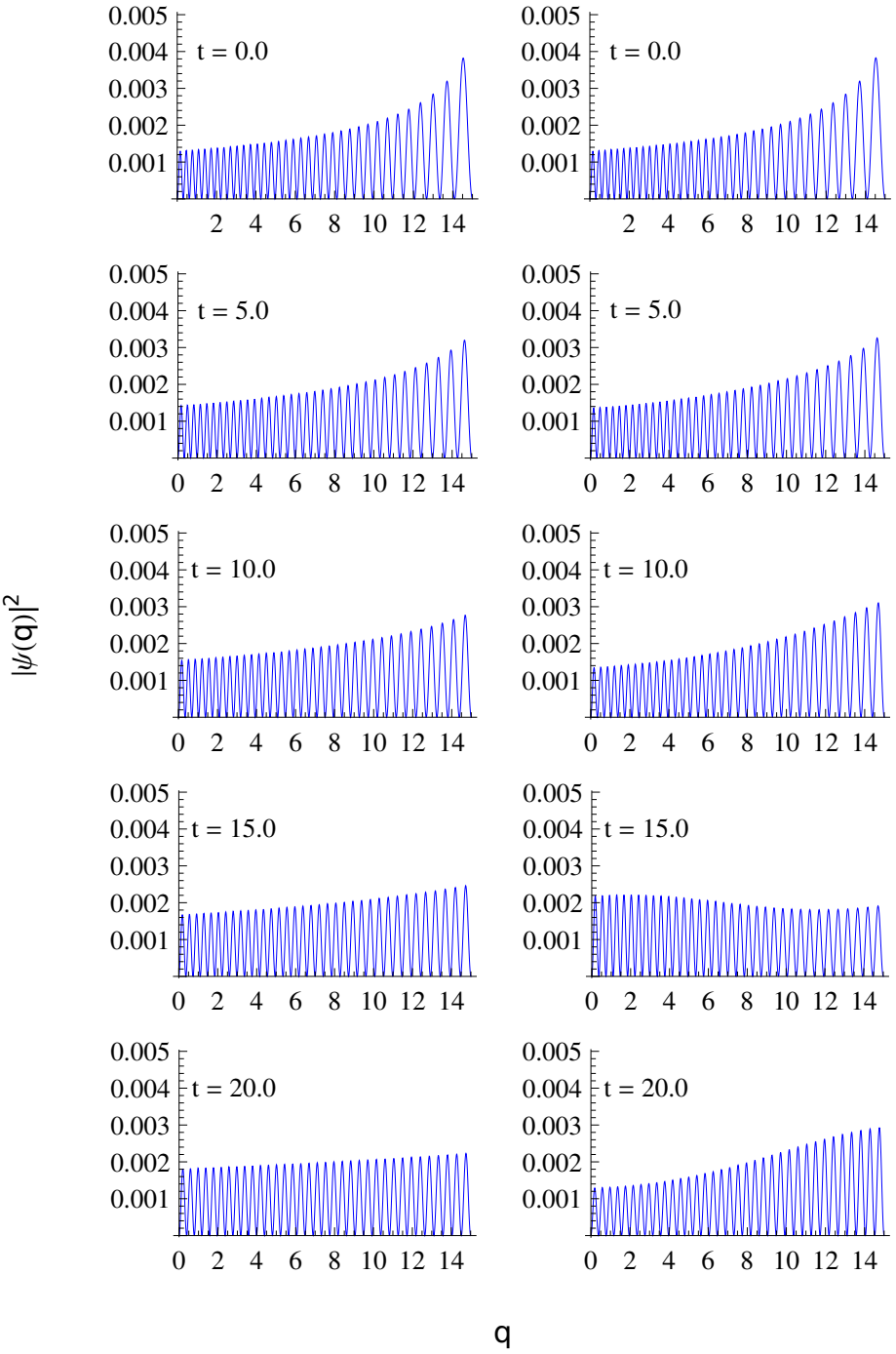

Figure 2.3: Same as Fig.2.2 except that the length of the box is fixed at $L = 15.0$, while the slope is decreased from $s = 13.0$ to 3.0 at a rate $\dot{s} = -0.5$.

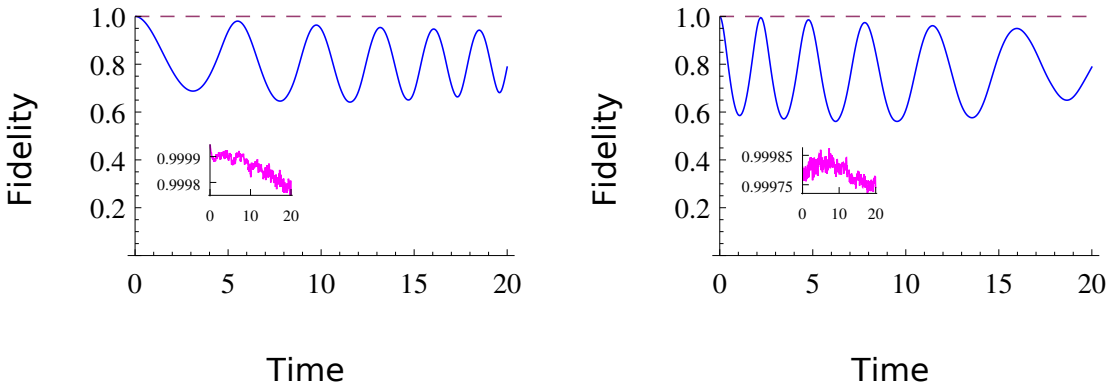

Figure 2.4: Evolution of the fidelity $\mathcal{F}(t)$. The plot on the left is for the case shown in Fig.2.2, whereas the plot on the right is for the same system but subjected to the reverse process: the box length increases from $L = 15.0$ to 25.0 at $\dot{L} = 0.5$. The dashed magenta curve depicts the fidelity for evolution under $\hat{\mathcal{H}} = \hat{H}_0 + \dot{\boldsymbol{\lambda}} \cdot \hat{\xi}_{SC}$, while the blue curve is the fidelity upon evolution under $\hat{H}_0$. The inset is a magnified view of the dashed magenta curve.

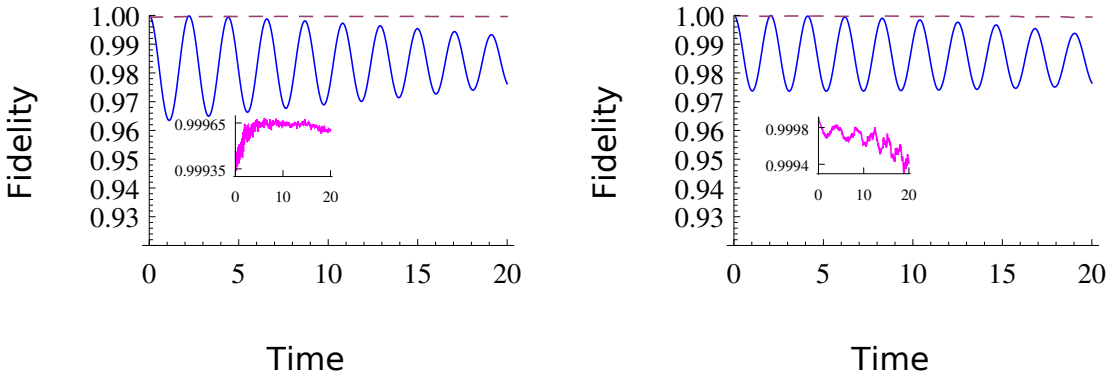

Figure 2.5: Similar to Fig.2.4. The left plot is for the case shown in Fig.2.3, whereas in the right plot the same system is subjected to the reverse process: the slope s increases from $s = 3.0$ to 13.0 at $\dot{s} = 0.5$.

in the n^{th} energy eigenstate, $a_k(0) = \delta_{kn}$, then it was evolved in time as either the slope s was varied at fixed length L (case (a)), or else the length was varied at constant slope (case (b)). The rate of change, $\dot{s}$ or $\dot{L}$, was set to a constant value sufficiently large to produce non-adiabatic evolution in the absence of the counterdiabatic term.

Simulations were performed both under the original Hamiltonian $\hat{H}_0(t)$, describing the time-dependent tilted piston (Eq. 2.11), and under the composite Hamiltonian

$$\hat{\mathcal{H}}(t) = \hat{H}_0(t) + \dot{\boldsymbol{\lambda}} \cdot \hat{\xi}_{SC}(\boldsymbol{\lambda}(t)) \tag{2.57}$$

that includes the counterdiabatic term. In both cases the fidelity $\mathcal{F}(t) = |\langle n(\boldsymbol{\lambda}(t))|\psi(t)\rangle|$ was computed. In these simulations the particle mass was set to $m = 1$ and Planck's reduced constant to $\hbar = 2$, and the system was initialized in the quantum number $n = 35$. The results, Figs. 2.2 - 2.5, are discussed in the following paragraphs.

Fig. 2.2 shows the evolving probability distribution $|\psi(q,t)|^2$ as the length of the tilted piston is reduced from $L = 25.0$ to 15.0, at a rate $\dot{L} = -0.5$ and fixed slope $s = 3.0$. The left column shows snapshots of $|\psi|^2$ at five instants in time, for evolution under the Hamiltonian $\hat{\mathcal{H}}(t)$. The right column shows evolution under $\hat{H}_0(t)$. In these simulations the initial energy is $E_n = 79.52$. The plots on the left are visually indistinguishable from the probability distribution of the adiabatic energy eigenstate, $|u_n(q, \boldsymbol{\lambda}(t))|^2$, with $n = 35$. By contrast, in the plots on the right the probability distribution develops noticeable shock waves, due to the rapid

compression of the piston length. Thus, with the addition of the counterdiabatic term the system faithfully follows a fixed eigenstate of $\hat{H}_0(t)$ (left plots), while in the absence of this term it is unable to keep pace with the rapidly changing Hamiltonian (right plots).

Fig.2.3 presents evolution in a tilted piston of fixed length $L = 15.0$, with a slope that decreases from $s = 13.0$ to 3.0 at a rate $\dot{s} = -0.5$. As in Fig. 2.2, the plots in the left and right columns depict evolution with and without the counterdiabatic term $\dot{\boldsymbol{\lambda}} \cdot \hat{\xi}_{SC}$. Once again, the plots on the left are indistinguishable from the instantaneous energy eigenstate $|u_n(q, \boldsymbol{\lambda}(t))|^2$, while those on the right reveal (mild) shock waves that are evidence of non-adiabatic evolution. The counterdiabatic term again successfully guides the wavefunction along the desired adiabatic trajectory.

These claims are supported by analyses of the fidelity $\mathcal{F}(t)$. Fig.2.4 shows fidelity plots for a tilted piston undergoing compression (left plot) and expansion (right plot). The former corresponds to the evolution shown in Fig.2.2, while the latter depicts the reverse process, in which the length *increases* from $L = 15.0$ to 25.0 at $\dot{L} = 0.5$. Similarly, Fig.2.5 shows a fidelity plot for the evolution depicted in Fig.2.3 (left plot), and for the reverse process in which the slope is varied from $s = 3.0$ to 13.0 at $\dot{s} = 0.5$ (right plot). In these figures, the solid blue curves depict the fidelity for evolution under $\hat{H}_0(t)$, while the dashed magenta curves correspond to evolution under $\hat{\mathcal{H}}(t)$. In all four plots the blue curves deviate significantly, while the dashed magenta curves remain very close to unity, confirming that our semiclassically obtained counterdiabatic term has the desired effect of enforcing adiabatic evolution, with high accuracy.

As a side comment we observe that, in Fig.2.4, the oscillations in $\mathcal{F}(t)$ become more rapid in time when the tilted piston is compressed (left plot), and less rapid as it expands (right plot). These oscillations reflect the shock waves propagating between the two walls of the box, hence it makes sense that the period of oscillation diminishes or grows as the length L decreases or increases.

Because the counterdiabatic term $\dot{\boldsymbol{\lambda}}\cdot\hat{\xi}_{SC}$ was obtained semiclassically, we expect its efficacy to degrade as we approach the deep quantum regime. To test this hypothesis, we performed simulations at fixed slope $s = 3.0$, with piston length decreasing from $L = 25.0$ to 15.0 at $\dot{L} = -0.5$, and with particle mass $m = 1$, as in Fig.2.2. We carried out seven such simulations, with the value of $\hbar$ ranging from 1.0 to 7.0, choosing the initial state n so that the particle starts with energy $E_n \approx 80$ in each simulation. Thus Planck's constant was varied while the classical parameters remained essentially fixed. As before, the system was subjected to evolution under both $\hat{H}_0(t)$ and $\hat{\mathcal{H}}(t)$, and the fidelity $\mathcal{F}(t)$ was computed. Table 2.1 lists $\mathcal{F}_{min}^{wcd}$, which is the minimum fidelity (over the duration of the process) when the system evolves under $\hat{\mathcal{H}}(t)$, and $\mathcal{F}_{min}^{wocd}$, the minimum fidelity when the system evolves under $\hat{H}_0(t)$. We see that as $\hbar$ increases and n decreases – that is, as we go deeper into the quantum regime – $\mathcal{F}_{min}^{wcd}$ deviates further from unity. As expected, the semiclassical counterdiabatic term $\dot{\boldsymbol{\lambda}}\cdot\hat{\xi}_{SC}$ works best in the semiclassical limit of small $\hbar$ / large n.

Interestingly, Table 2.1 reveals that $\mathcal{F}_{min}^{wocd}$ *increases* with $\hbar$: in the absence of the counterdiabatic term, the fidelity improves as we go deeper into the quantum regime. We attribute this behavior to the fact that the spacing between adjacent

$\hbar$	n	$\mathcal{F}_{min}^{wcd}$	$\mathcal{F}_{min}^{wocd}$
1.0	70	0.999	0.092
2.0	35	0.999	0.641
3.0	23	0.999	0.842
4.0	17	0.997	0.917
5.0	14	0.992	0.939
6.0	12	0.979	0.953
7.0	10	0.943	0.970

Table 2.1: The dependence of fidelity on the value of the reduced Planck's constant $\hbar$, keeping classical parameters fixed. The initial quantum number n is chosen such that the initial energy is $E_n \approx 80$. Each simulation is performed at fixed $s = 3.0$, while the box length is varied from $L = 25.0$ to $L = 15.0$ at $\dot{L} = -0.5$. $\mathcal{F}_{min}^{wcd}$ is the minimum fidelity when the system evolves under $\hat{\mathcal{H}}(t)$, and $\mathcal{F}_{min}^{wocd}$ is the minimum fidelity when the system evolves under $\hat{H}_0(t)$.

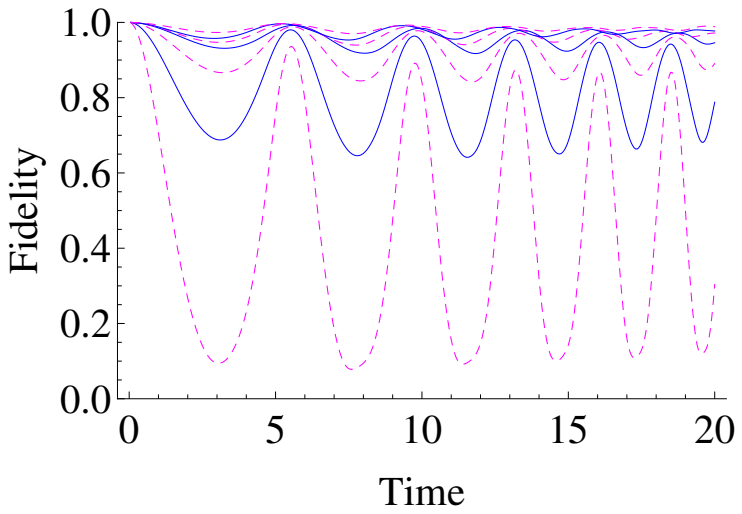

Figure 2.6: Evolution of the fidelity under $\hat{H}_0(t)$, for the simulations described in Table 2.1. The lowermost (dashed magenta) curve corresponds to $\hbar = 1.0$, the next one up (solid blue) corresponds to $\hbar = 2.0$, and so forth up to $\hbar = 7.0$, which is the magenta curve that remains closest to unity.

energy levels increases with $\hbar$. Let us picture a classical process in which initial conditions are sampled from a single energy shell, and trajectories evolve from these initial conditions under the Hamiltonian $H_0(q, p, t)$. The final distribution of energies then provides a crude estimate of the final energy distribution in the corresponding quantum process, in which the system begins in an energy eigenstate. For a fixed final distribution of energies, the distribution of final quantum numbers decreases with increasing $\hbar$, simply because of the decreasing density of energy levels. As a result, excitations out of the initial energy level are inhibited.

Fig.2.6 shows $\mathcal{F}(t)$ for the seven simulations of evolution under $\hat{H}_0(t)$ that are represented in the rightmost column of Table 2.1. These plots confirm that the fidelity improves with increasing $\hbar$ (in the absence of the counterdiabatic term), and they display similar oscillatory behavior, with peaks and valleys occurring at nearly the same times for the seven curves. These observations are consistent with the interpretation that the frequency of the oscillations reflect the corresponding classical evolution, while the magnitude is governed by the quantum energy spacing.

2.7 Summary

We have studied a model system undergoing non-scale-invariant driving: the one-dimensional tilted piston described by the Hamiltonian $H_0(q, p; \boldsymbol{\lambda}(t))$ (Eq. 2.11). We derived exact, closed-form expressions for the classical counterdiabatic Hamiltonian $H_{CD}(q, p, t)$, which we quantized to obtain a Hermitian operator $\hat{H}_{CD}(t)$. In numerical simulations of the time dependent Schrödinger equation, we compared

evolution under $\hat{H}_0$ to that under $\hat{\mathcal{H}} = \hat{H}_0 + \hat{H}_{CD}$, with the system initialized in an energy eigenstate. The simulations reveal that $\hat{H}_{CD}$ very effectively suppresses non-adiabatic transitions: when evolving under $\hat{\mathcal{H}}$, the system remains in an eigenstate of $\hat{H}_0$ with nearly perfect fidelity. These results establish a proof of principle – beyond the regime of scale-invariant driving [32,34] – that quantum counterdiabatic Hamiltonians can successfully be constructed from their classical counterparts.

For most Hamiltonians $H_0(z; \boldsymbol{\lambda}(t))$ of interest, a closed-form expression for $H_{CD}(z,t)$ will not be available. Even for the quite simple system we have studied, the expression for H_{CD} is somewhat involved, and the final result for the operator $\hat{H}_{CD} = \dot{\boldsymbol{\lambda}} \cdot \hat{\xi}_{SC}$ – while given in terms of $\hat{q}$ and $\hat{p}$ (Eq. 2.29) rather than as a spectral sum (Eq. 1.12) – would certainly be difficult to implement in a laboratory setting.

The difficulty in realizing $\hat{H}_{CD}$ experimentally arises not just because it is given by a complicated expression, but because it is *non-local*, i.e. because it depends on the momentum operator, $\hat{p}$. This is also true for the much simpler counterdiabatic Hamiltonians that have been derived for scale-invariant driving (Eq. 2.3), including the harmonic oscillator (Eq. 2.1) as a particular example. In the scale-invariant case, an appropriate canonical (or unitary) transformation of $H_{CD}(q,p,t)$ gives a *local* counterdiabatic potential $U_{FF}(q,t)$; in effect, the non-locality can be "gauged away" to construct a *local* shortcut to adiabaticity equivalent to the fast-forward method, as described in Ref. [34]. Whether a transformation of this sort could be applied to our counterdiabatic Hamiltonian $\hat{H}_{CD}$ (Eq. 2.29) is an open question.

Chapter 3: Quantum shortcuts using flow-fields

3.1 Overview

In the previous chapter, we have seen that even for the simple example of a tilted piston, the method prescribed in Ref. [25] yields a complicated expression for the counterdiabatic Hamiltonian H_{CD}, which is difficult to implement experimentally not only due to its complicated nature but also due to its non-locality, i.e., the momentum dependence of H_{CD}. Note that the H_{CD} from Chap. 2 is same regardless of the choice of the initial state. In this chapter, we find that by trying to develop H_{CD} that depends on the choice of initial state, we get much simpler expressions.

We introduce a new framework for constructing the desired auxiliary Hamiltonian, which consists of three steps. First, we identify the *adiabatic evolution* as the evolution that the system of interest would undergo if the process were performed adiabatically. We then define velocity and acceleration *flow fields* $v(q,t)$ and $a(q,t)$ that characterize the adiabatic evolution, as illustrated in Fig. 3.1 for a quantum system. Finally, from these fields we immediately construct auxiliary terms that provide both counterdiabatic (Eqs. 3.11) and fast-forward (Eqs. 3.14) shortcuts.

This chapter is structured as follows. In Sec. 3.2 we recapituate the salient featues of counterdiabatic driving developed in Ref. [24] and the fast-forward method

developed in Ref. [26]. After deriving the main results of this chapter, Eqs. 3.11 and 3.14, in Sec. 3.3, we compare them with previously obtained shortcuts in Sec. 3.4. In Sec. 3.5, we show how our approach provides insight into the singularities that may arise in the fast-forward approach. We analyze the special case of scale invariant dynamics in Sec. 3.6 and illustrate our approach with numerical simulations in Sec. 3.7. We briefly discuss generalizations to three degrees of freedom in Sec. 3.8 and summarize the results of this chapter in Sec. 3.9.

3.2 Review of quantum shortcuts

Transitionless quantum driving, due to Demirplak and Rice [22] and Berry [24], involves the counterdiabatic Hamiltonian in Eq. 1.9. If a wavefunction evolves under $\hat{H}_0 + \hat{H}_{CD}$ from an initial state $|n(0)\rangle$, then it remains in the n'th instantaneous eigenstate of $\hat{H}_0(t)$ at all times, as the term $\hat{H}_{CD}(t)$ suppresses excitations to other eigenstates [22, 24]. Note that the counterdiabatic term (Eq. 1.9) does not depend on the choice of n.

The fast-forward approach, due to Masuda and Nakamura [26], pertains to a Hamiltonian of the form

$$\hat{H}_0(t) = \frac{\hat{\mathbf{p}}^2}{2m} + U_0(\hat{\mathbf{q}}, t)\,. \tag{3.1}$$

For a given time interval $0 \leq t \leq \tau$, and a particular quantum number n, a fast-forward potential $U_{FF}(\hat{\mathbf{q}}, t)$ is constructed with the following property: if a wavefunction evolves under $\hat{H}_0 + \hat{U}_{FF}$ from the initial state $|n(0)\rangle$, then it will arrive in the eigenstate $|n(\tau)\rangle$ (up to an overall phase) at $t = \tau$. For intermediate times $0 < t < \tau$,

the wavefunction is in a superposition of eigenstates of $\hat{H}_0(t)$, as illustrated in Fig. 1.1 and Fig. 3.3 below. The fast-forward potential depends on the chosen quantum number n. Moreover, $U_{FF}(\mathbf{q}, t)$ typically (though not always) becomes singular at nodes of the instantaneous eigenstate, that is, where $\phi_n(\mathbf{q}, t) \equiv \langle \mathbf{q}|n(t)\rangle = 0$. Hence the applicability of the fast-forward method is generally restricted to the ground state, $n = 0$, although there are exceptions to this statement. We will return to this point later in our discussion.

Both $\hat{H}_{CD}$ and $\hat{U}_{FF}$ are auxiliary Hamiltonians that are tailored to achieve the desired acceleration of adiabatic dynamics. We will use the term counterdiabatic to refer to methods in which the auxiliary term causes the system to follow the adiabatic evolution – at an accelerated pace – for the duration of the process. This is the case with transitionless quantum driving: the wavefunction remains in a given eigenstate of $\hat{H}_0(t)$ at all times, when evolving under $\hat{H}_0 + \hat{H}_{CD}$. The term *fast-forward* (or FF) will refer to methods in which the system strays from the adiabatic evolution at intermediate times, but returns to the adiabatic state at the final time $t = \tau$, as in the Masuda-Nakamura method. As illustrated by the previous paragraphs, auxiliary terms in the fast-forward approach are *local*, in the sense that they are explicit functions of $\hat{\mathbf{q}}$ and t. By contrast, counterdiabatic driving generally requires *non-local* auxiliary terms, given either by spectral sums (as with Eq. 1.9) or by expressions involving both coordinates and momenta (see Refs. [25, 34, 54], or Eq. 3.11 below). Thus, fast-forward auxiliary terms may generically be easier to implement experimentally, than counterdiabatic terms.

In what follows, we bridge the two approaches. We consider a Hamiltonian of

interest

$$\hat{H}_0(t) = \frac{\hat{p}^2}{2m} + U_0(\hat{q}, t) \tag{3.2}$$

in one degree of freedom. We assume that $\hat{H}_0$ varies with time only during the interval $0 \leq t \leq \tau$, and that this time-dependence is turned on and off smoothly – specifically, $\hat{H}_0$, $\partial\hat{H}_0/\partial t$ and $\partial^2\hat{H}_0/\partial t^2$ are continuous functions of time for all t, and $\partial\hat{H}_0/\partial t = 0$ for $t \notin (0, \tau)$. For a given choice of quantum number n, we will define velocity and acceleration flow fields $v(q,t)$ and $a(q,t)$, that characterize how the eigenstate probability distribution $|\langle q|n(t)\rangle|^2$ deforms with t. From these flow fields we will construct simple expressions for both a counterdiabatic Hamiltonian $\hat{H}_{CD}(\hat{q}, \hat{p}, t)$ (Eq. 3.11), and a local fast-forward potential $\hat{U}_{FF}(\hat{q}, t)$ (Eq. 3.14).

3.3 Setup and derivation of main results

Let the real-valued wavefunction $\phi(q,t) = \langle q|n(t)\rangle$ denote the n'th eigenstate of $\hat{H}_0(t)$, with eigenenergy $E(t)$:

$$\hat{H}_0(t)\phi(q,t) = \left[-\frac{\hbar^2}{2m}\frac{\partial^2}{\partial q^2} + U_0(q,t)\right]\phi(q,t) = E(t)\phi(q,t). \tag{3.3}$$

For convenience we omit the subscript n on ϕ and E. The *adiabatic evolution* is identified as follows: [1]

$$\psi_{ad}(q,t) = \phi(q,t)\, e^{i\alpha(t)} \quad , \quad \alpha(t) = -\frac{1}{\hbar}\int_0^t E(t')\, dt' \tag{3.4}$$

[1] The dynamical phase α is generically accompanied by a geometric phase [67], but the latter vanishes for a kinetic-plus-potential Hamiltonian in one degree of freedom.

When the time-dependence of $\hat{H}_0(t)$ is quasi-static, ψ_{ad} is a solution of the Schrödinger equation, $i\hbar\,\partial_t\psi_{ad} = \hat{H}_0\psi_{ad}$ [1,2]. When the time-dependence is arbitrary, ψ_{ad} obeys

$$i\hbar\frac{\partial\psi_{ad}}{\partial t} = (\hat{H}_0 + \hat{H}_{CD})\psi_{ad} \tag{3.5}$$

for the counterdiabatic term given by Eq. 1.9 [22,24]. Thus the addition of the term $\hat{H}_{CD}$ causes the system to follow the adiabatic evolution, ψ_{ad}, when $\hat{H}_0$ is varied rapidly.

In what follows we construct a counterdiabatic term given as an explicit function of $\hat{q}$ and $\hat{p}$ (Eq. 3.11), which accomplishes the same result for a given choice of n. Before proceeding further, let us first focus on the results from scale invariant driving. Under scale invariant driving, if $\psi^0(q)$ is an eigenfunction of the Hamiltonian $\hat{H}_0(\gamma = 1)$, then $\psi(q,\gamma) = \psi^0(q/\gamma)/\sqrt{\gamma}$ is the eigenfunction of $\hat{H}_0(\gamma)$, where γ represents the expansion co-efficient [34]. Then, from Eqs. 1.10 and 1.15, it follows that $\hat{H}_{CD} \propto \hat{p}\hat{q} + \hat{q}\hat{p}$ drives the system along the desired adiabatic path by *stretching* the wavefunction appropriately [20,25,34,61]. The Hamiltonian $(\hat{p}\hat{q} + \hat{q}\hat{p})$ can therefore be viewed as a *linear stretching operator*, as it is linear in p and q. This result suggests that the simplest form of $\hat{H}_{CD}$ for an arbitrarily driven system should be linear in p and non-linear in q so that $\hat{H}_{CD} \propto \hat{p}\hat{v} + \hat{v}\hat{p}$, where $\hat{v} = v(\hat{q},t)$. We choose to retain the linear dependence on momentum instead of position because $\hat{p}$ is a non-local operator while $\hat{q}$ is a local operator. Therefore, higher order terms in $\hat{q}$ are more practical and relatively easier to implement experimentally compared to higher order terms in $\hat{p}$. We describe a method of obtaining $v(\hat{q},t)$ for a general

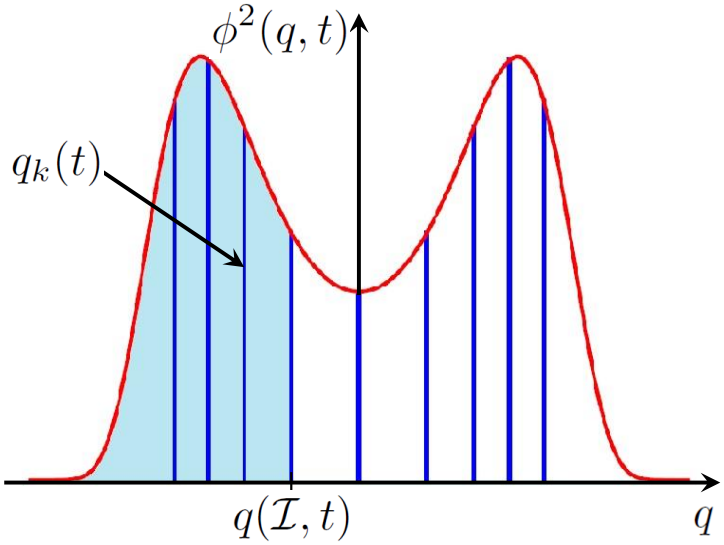

Figure 3.1: The red curve $\phi^2(q,t)$ depicts the probability distribution associated with an energy eigenstate of $\hat{H}_0(t)$. The blue vertical lines divide the area under $\phi^2(q,t)$ into $K \gg 1$ strips of equal area. $q(\mathcal{I},t)$ is the right boundary of the shaded region, which has area $\mathcal{I}$. The positions of the vertical lines vary parametrically with t, and this "motion" is described in terms of velocity and acceleration fields $v(q,t)$ and $a(q,t)$, as given by Eq. 3.8.

system below.

Let us define the integrated probability density function,

$$\mathcal{I}(q,t) \equiv \int_{-\infty}^{q} \phi^2(q',t)dq'. \tag{3.6}$$

and let us invert this function to obtain $q(\mathcal{I},t)$. We then define a velocity flow field [2]

$$v(q,t) = \frac{\partial}{\partial t}q(\mathcal{I},t) = -\frac{\partial_t \mathcal{I}}{\partial_q \mathcal{I}}, \tag{3.7}$$

This flow field can be pictured by dividing the area under $\phi^2(q,t)$ into $K \gg 1$ strips of equal area, delimited by vertical lines at locations $q_1(t), q_2(t), \ldots, q_{K-1}(t)$, so that

[2]The quantity $-v(q,t)$ was identified as a "hydrodynamic velocity" in Ref. [30], Eq. (6).

$\mathcal{I}(q_k(t), t) = k/K$; see Fig. 3.1. The locations $\{q_k(t)\}$ evolve parametrically with t, according to

$$\frac{dq_k}{dt} = v(q_k, t) \tag{3.8a}$$

Note that Eq. 3.8a does not reflect the unitary dynamics generated by $\hat{H}_0(t)$, but rather the variation of the eigenstate probability density $\phi^2(q, t)$ with t. We similarly introduce an acceleration flow field,

$$\frac{d^2q_k}{dt^2} = a(q_k, t) \tag{3.8b}$$

By Eq. 3.8a this field satisfies

$$a(q, t) = v'v + \dot{v} \tag{3.9}$$

where the prime and dot denote ∂_q and ∂_t, respectively. Both flow fields vanish outside the interval $0 < t < \tau$:

$$v(q, t) = 0 = a(q, t) \quad \text{for } t \notin (0, \tau) \tag{3.10}$$

as follows from the assumptions spelled out after Eq. 3.2. We will now use these flow fields to construct counterdiabatic and fast-forward shortcuts, given by Eqs. 3.11 and 3.14 below.

We begin by defining the counterdiabatic Hamiltonian,

$$\hat{H}_{CD}(t) = \frac{\hat{p}\hat{v} + \hat{v}\hat{p}}{2} \quad , \quad \hat{v}(t) = v(\hat{q}, t) \tag{3.11}$$

We claim that the adiabatic wavefunction ψ_{ad} (Eq. 3.4) satisfies Eq. 3.5 for arbitrary time-dependence of $\hat{H}_0(t)$, with $\hat{H}_{CD}$ now given by Eq.3.11. To show this, we first rearrange Eq. 3.7 as $\partial_t \mathcal{I} + v\partial_q \mathcal{I} = 0$. Differentiating both sides with respect to q leads to the continuity equation $\partial_t \phi^2 + \partial_q(v\phi^2) = 0$, equivalently,

$$\dot{\phi} + v\phi' + \frac{1}{2}v'\phi = 0. \tag{3.12}$$

We now use Eqs. 3.3, 3.4 and 3.12 to evaluate the right side of Eq. 3.5:

$$\begin{aligned}
(\hat{H}_0 + \hat{H}_{CD})\psi_{ad} &= \left[\hat{H}_0\phi - \frac{i\hbar}{2}\partial_q(v\phi) - \frac{i\hbar}{2}v(\partial_q\phi)\right] e^{i\alpha} \\
&= \left[E\phi - i\hbar\left(v\phi' + \frac{1}{2}v'\phi\right)\right] e^{i\alpha} \\
&= \left(E\phi + i\hbar\,\dot{\phi}\right) e^{i\alpha} = i\hbar\,\frac{\partial \psi_{ad}}{\partial t}
\end{aligned} \tag{3.13}$$

which establishes that $\psi_{ad}(q, t)$ is a solution of Eq. 3.5. Thus if a wavefunction evolves under $\hat{H}_0 + \hat{H}_{CD}$ from an initial state $\psi(q, 0) = \langle q|n(0)\rangle$, then it remains in the n'th instantaneous eigenstate of $\hat{H}_0(t)$ during the entire process, just as in the case of transitionless quantum driving [22, 24].

Turning our attention to the fast-forward approach, we construct a potential

$U_{FF}(q,t)$ and a companion function $S(q,t)$ as follows:

$$-\partial_q U_{FF} = ma(q,t) \tag{3.14}$$

$$\partial_q S = mv(q,t) \tag{3.15}$$

By Eq. 3.9, these functions satisfy

$$\partial_q \left[\partial_t S + \frac{1}{2m}(\partial_q S)^2 + U_{FF} \right] = 0 \tag{3.16}$$

Eqs. 3.14 and 3.15 specify U_{FF} and S only up to arbitrary functions of time. We use this freedom, along with Eqs. 3.10 and 3.16, to impose the conditions

$$U_{FF}(q,t) = 0 \quad \text{for } t \notin (0,\tau) \tag{3.17}$$

and

$$\partial_t S + \frac{1}{2m}(\partial_q S)^2 + U_{FF} = 0 \tag{3.18}$$

Eq. 3.10 further implies that

$$S(q,0) = S_- \quad , \quad S(q,\tau) = S_+ \tag{3.19}$$

where $S_\pm$ are constants (i.e. independent of q).

We now show that the ansatz

$$\bar{\psi}(q,t) = \psi_{ad}(q,t) \exp\left[i\frac{S(q,t)}{\hbar}\right] = \phi\, e^{i\alpha} e^{iS/\hbar} \tag{3.20}$$

is a solution of the Schrödinger equation

$$i\hbar\frac{\partial\bar{\psi}}{\partial t} = (\hat{H}_0 + \hat{U}_{FF})\bar{\psi} \tag{3.21}$$

Evaluating the right side with the help of Eqs. 3.3, 3.12, 3.15 and 3.18, we obtain

$$\begin{aligned}
& \left(-\frac{\hbar^2}{2m}\frac{\partial^2}{\partial q^2} + U_0 + U_{FF}\right)\phi(q,t)\, e^{i\alpha}\, e^{iS/\hbar} \\
= & \left[-\frac{\hbar^2}{2m}\phi'' - \frac{i\hbar}{m}\phi' S' - \frac{i\hbar}{2m}\phi S'' + \frac{1}{2m}\phi (S')^2 + U_0\phi + U_{FF}\phi\right] e^{i\alpha}\, e^{iS/\hbar} \\
= & \left[E\phi + \frac{1}{2m}(S')^2\phi + U_{FF}\phi - i\hbar\left(v\phi' + \frac{1}{2}v'\phi\right)\right] e^{i\alpha}\, e^{iS/\hbar} \\
= & \left(i\hbar\dot{\phi} + E\phi - \dot{S}\phi\right) e^{i\alpha}\, e^{iS/\hbar} = i\hbar\frac{\partial\bar{\psi}}{\partial t}
\end{aligned} \tag{3.22}$$

which is the desired result. By Eq. 3.19, the wave function $\bar{\psi}(q,t)$ begins in the n'th energy eigenstate at $t \leq 0$ and ends in the n'th energy eigenstate at $t \geq \tau$, which establishes that $\hat{U}_{FF}$ produces fast-forward evolution.

Note that we introduced the function $S(q,t)$ (Eq. 3.15) only to facilitate the derivation of our fast-forward approach. This function need not be evaluated if one simply wishes to construct the potential $U_{FF}(q,t)$. That potential can be determined directly from the acceleration field $a(q,t)$, by Eq. 3.14.

Also, we imposed Eq. 3.17 so as to obtain an auxiliary potential that is turned

on at $t = 0$ and off at $t = \tau$, but this condition is not necessary. Any U_{FF} satisfying Eq. 3.14 will provide a shortcut that transports the n'th eigenstate of $\hat{H}_0(0)$ to the n'th eigenstate of $\hat{H}_0(\tau)$. The addition of an arbitrary function $f(t)$ to $U_{FF}(q,t)$ affects only the overall phase of the evolving wavefunction.

3.4 Comparison with previous results

Eqs. 3.11 and 3.14 are recipes for constructing shortcuts directly from the flow fields $v(q,t)$ and $a(q,t)$. Let us compare these results with previously published counterdiabatic and fast-forward shortcuts.

Our result for $\hat{H}_{CD}$ (Eq. 3.11) is given explicitly in terms of the operators $\hat{q}$ and $\hat{p}$. This appealing feature comes with a cost: in general, a different counterdiabatic term is required for each eigenstate n, since $v(q,t)$ depends on the choice of n. By contrast the Demirplak-Rice-Berry [22, 24] counterdiabatic term (Eq. 1.9) is independent of n, as noted earlier. We conclude that Eqs. 1.9 and 3.11 are not equivalent, although the two counterdiabatic terms produce the same effect when they act on the chosen adiabatic eigenstate:

$$\hat{H}_{CD}^{\text{Eq.1.9}} \neq \hat{H}_{CD}^{\text{Eq.3.11}} \quad \text{but} \quad \hat{H}_{CD}^{\text{Eq.1.9}}|n\rangle = \hat{H}_{CD}^{\text{Eq.3.11}}|n\rangle \tag{3.23}$$

Using the identity $\langle m|\partial_t m\rangle = 0$, which holds for $\hat{H}_0$ given by Eq. 3.2, we rewrite the equality in Eq. 3.23 as follows:

$$i\hbar\frac{\partial}{\partial t}|n\rangle = \frac{\hat{p}\hat{v} + \hat{v}\hat{p}}{2}|n\rangle \tag{3.24}$$

In other words, the operator $\hat{D} \equiv (\hat{p}\hat{v} + \hat{v}\hat{p})/2$ acts as the generator of adiabatic transport (see Eq. 1.15) for the state $|n\rangle$ that was used to construct $v(q,t)$:

$$e^{-i\delta t\hat{D}/\hbar}|n(t)\rangle = |n(t+\delta t)\rangle \tag{3.25}$$

for infinitesimal δt.

Substituting Eq. 3.15 into Eq. 3.12 yields

$$\dot{\phi} + \frac{1}{m}\phi' S' + \frac{1}{2m}\phi S'' = 0. \tag{3.26}$$

Eqs. 3.18 and 3.26 are essentially equivalent to Eqs. 5 and 6 of Torrontegui *et al* [28], to Eqs. 17 and 15 of Takahashi [35], and to Eqs. 4 and 3 of Martínez-Garaot *et al* [30]. In Refs. [28, 30, 35] these equations were used to provide streamlined derivations of the fast-forward approach pioneered by Masuda and Nakamura [26]. (Our Eq. 3.26 is also equivalent to Eq. 2.18 of Ref. [26], and our Eq. 3.15 appears as Eq. 5 in Ref. [30].) Thus our fast-forward potential $\hat{U}_{FF}$ is equivalent to that derived by previous authors [26, 28, 30, 35].

The observation that the quantum counterdiabatic and fast-forward approaches are closely related is not surprising, as previous authors have argued that $\hat{U}_{FF}$ can be constructed from $\hat{H}_{CD}$ by appropriate unitary [31–35] or gauge [36] transformations. The novelty of our approach is that we obtain both $\hat{H}_{CD}$ and $\hat{U}_{FF}$ directly from the velocity and acceleration fields that describe the time-dependence of $\phi^2(q,t)$ (Fig. 3.1). Our results are given by compact, intuitive expressions (Eqs. 3.11, 3.14).

This approach highlights the connection between counterdiabatic and fast-forward shortcuts, and – as we shall see – it provides insight into the divergences that often plague the fast-forward method when it is applied to excited states. Moreover, the construction of $\hat{H}_{CD}$ and $\hat{U}_{FF}$ from v and a is mirrored in classical shortcuts to adiabaticity, as will be discussed in Chap. 4.

Finally, we note that Eq. 3.18 is a Hamilton-Jacobi equation for the Hamiltonian $p^2/2m + U_{FF}$. Okuyama and Takahashi [55] have recently used the Hamilton-Jacobi formalism to explore the correspondence between quantum and classical shortcuts to adiabaticity. It would be interesting to explore the relationship between their approach and ours.

3.5 Divergences and a "no-flux" criterion

By Eq. 3.7, $v(q,t)$ generically diverges at nodes of the wavefunction, where $\partial_q \mathcal{I} = \phi^2$ vanishes; this in turn leads to divergences in $a(q,t)$, and in $\hat{H}_{CD}$ and $\hat{U}_{FF}$. These observations suggest that our method is in general restricted to ground state wavefunctions ($n = 0$), which have no nodes.

While nodes in $\phi(q,t)$ *typically* spoil the applicability of our method, this need not always be the case: the numerator and denominator in Eq. 3.7 might vanish simultaneously in a way that prevents the ratio $v = -\partial_t \mathcal{I}/\partial_q \mathcal{I}$ from blowing up at a node. Here we propose a simple criterion for determining whether our approach (and by extension the fast-forward approach [26, 28, 30, 35]) is applicable when an eigenstate $\phi(q,t)$ has one or more nodes.

Let $q_\nu(t)$ denote the location, and $u_\nu(t) \equiv dq_\nu/dt$ the velocity, of the ν'th node of $\phi(q,t)$. We assume $|u_\nu| < \infty$, as will generally be the case when the potential $U_0(q,t)$ is well-behaved. As t varies parametrically, the flux of probability across this node, from the region $q < q_\nu$ to the region $q > q_\nu$, is given by

$$\Phi_\nu(t) = -\frac{d}{dt}\mathcal{I}(q_\nu,t) = [v(q_\nu,t) - u_\nu(t)]\,\phi^2(q_\nu,t) \tag{3.27}$$

using Eqs. 3.6 and 3.7. This result has the familiar interpretation of "flux equals velocity times density", in the node's co-moving frame of reference. Eq. 3.27 implies that if $v(q,t)$ does not blow up at a given node, then the probability flux $\Phi_\nu(t)$ across that node must be zero. This suggests a simple criterion: if the time-dependence of $\phi^2(q,t)$ is such that there is no flux of probability across any node, i.e. if $\Phi_\nu = 0$ for all ν, then the velocity field $v(q,t)$ will not diverge at the nodes and our method will remain valid and applicable [3]. Generalizing the term "nodes" to include the boundaries at $q = \pm\infty$, the no-flux criterion can alternatively be stated as follows: if the probability between all pairs of adjacent nodes remains independent of t [i.e. if $(d/dt)\int_{q_\nu}^{q_{\nu+1}} \phi^2 dq = 0$ for all ν], then $v(q,t)$ will be free of divergences and $U_{FF}(q,t)$ will be well-behaved.

This "no-flux" criterion is *not* generically satisfied for $\hat{H}_0(t)$ given by Eq. 3.2. However, in Sec. 3.6 we consider a particular class of time-dependent Hamiltonians for which this criterion is satisfied for every eigenstate, due to *scale-invariance* (Eq. 3.28). In agreement with the arguments presented above, our method provides

[3] In fact, if $\Phi_\nu(t) = 0$ then $v(q_\nu,t) = u_\nu(t)$, although we will not make use of this result here.

non-singular counterdiabatic and fast-forward shortcuts for all energy eigenstates, for this class of Hamiltonians. In Sec. 3.7 we present the results of numerical simulations for a *non*-scale-invariant Hamiltonian, for which the no-flux criterion is satisfied for the first excited state; again, our method successfully provides a non-singular shortcut for this situation.

Divergences associated with eigenstate nodes are problematic not only for our approach, but also for those of Refs. [26, 28, 30, 35], since all these approaches lead to equivalent expressions for U_{FF}. This problem has not received much attention in the literature, although Martínez-Garaot *et al* [30] consider it in a slightly different context. In Sec. III.D of their paper, they develop a fast-forward strategy to drive a wavefunction from a ground state ϕ_0 to a first excited state ϕ_1. In their approach the fast-forward potential becomes singular due to the node in ϕ_1, but they demonstrate that *ad hoc* truncation of the singularity produces a well-behaved potential that achieves near-perfect fidelity. It would be interesting to test whether such truncation is also useful in the context of our method, when the no-flux criterion is not satisfied.

3.6 Scale-invariant dynamics

In the special case of *scale-invariant driving*, $U_0(q,t)$ undergoes expansions, contractions and translations. As shown in Ref. [34] (and anticipated in Refs. [25, 32, 52, 61, 68–70]), simple expressions for counterdiabatic and fast-forward shortcuts can be obtained when a system is driven in a scale-invariant manner. In this section we show that these shortcuts are obtained naturally within our framework.

The Hamiltonian for scale-invariant driving takes the form [34]

$$\hat{H}_0(t) = \hat{H}_0(\gamma, f) = \frac{\hat{p}^2}{2m} + \frac{1}{\gamma^2} U_0 \left(\frac{\hat{q} - f}{\gamma} \right), \tag{3.28}$$

where $\gamma(t)$ and $f(t)$ are parameters that describe expansions/contractions, and translations, respectively. If we let $\tilde{\phi}(q)$ denote the n'th eigenstate of $\hat{H}_0(\gamma = 1, f = 0)$, then the n'th eigenstate for a general choice of (γ, f) is given by [34]

$$\phi(q) = \frac{1}{\sqrt{\gamma}} \tilde{\phi} \left(\frac{q - f}{\gamma} \right) \tag{3.29}$$

This scaling result immediately reveals how the "picket fence" of lines $\{q_k\}$ depicted in Fig. 3.1 behaves when γ and f are varied with time. Variations in f result in translations of the entire picket fence, and variations in γ cause the picket fence to expand or contract linearly. These considerations give us

$$v(q, t) = \frac{\dot{\gamma}}{\gamma}(q - f) + \dot{f}, \tag{3.30}$$

and therefore (by Eq. 3.9)

$$a(q, t) = \frac{\ddot{\gamma}}{\gamma}(q - f) + \ddot{f}. \tag{3.31}$$

Eq. 3.30 also follows from Eq. 3.7, $v = -\partial_t \mathcal{I} / \partial_q \mathcal{I}$, since $\partial_q \mathcal{I} = \phi^2$ and (making use

of Eq. 3.29)

$$\begin{aligned}
\partial_t \mathcal{I} &= \left(\dot{\gamma}\,\partial_\gamma + \dot{f}\,\partial_f\right) \int_{-\infty}^{q} \frac{1}{\gamma}\tilde{\phi}^2 \left(\frac{q'-f}{\gamma}\right) dq' \\
&= \dot{\gamma} \int_{-\infty}^{q} -\frac{1}{\gamma^2}\left[\tilde{\phi}^2 + 2(q'-f)\tilde{\phi}(\partial_{q'}\tilde{\phi})\right] dq' + \dot{f}\int_{-\infty}^{q} -\frac{2\tilde{\phi}(\partial_{q'}\tilde{\phi})}{\gamma} dq' \\
&= -\frac{\dot{\gamma}}{\gamma}\int_{-\infty}^{q}\left[\phi^2 + (q'-f)\partial_{q'}(\phi^2)\right] dq' - \dot{f}\int_{-\infty}^{q}\partial_{q'}(\phi^2) dq' \\
&= \left[-\frac{\dot{\gamma}}{\gamma}(q-f) - \dot{f}\right]\phi^2 \qquad (3.32)
\end{aligned}$$

Combining Eqs. 3.30 and 3.31 with Eqs. 3.11 and 3.14, we obtain

$$\hat{H}_{CD} = \frac{\dot{\gamma}}{2\gamma}\left[(\hat{q}-f)\hat{p} + \hat{p}(\hat{q}-f)\right] + \dot{f}\hat{p} \qquad (3.33a)$$

$$\hat{U}_{FF} = -\frac{m}{2}\frac{\ddot{\gamma}}{\gamma}(\hat{q}-f)^2 - m\ddot{f}\hat{q} \qquad (3.33b)$$

in agreement with Eqs. 9 and 30 of Ref. [34]. Thus the shortcuts obtained previously for scale-invariant driving emerge naturally within our framework, from the flow fields v and a (Eqs. 3.30, 3.31).

We end this section by highlighting two exceptional features of scale-invariant Hamiltonians, both of which are due to the fact that all of the eigenstates of $\hat{H}_0$ satisfy the same scaling property, Eq. 3.29. First, although $\phi(q) = \langle q|n\rangle$ denotes a specific energy eigenstate in the above calculations, the resulting flow fields and shortcuts (Eq. 3.33) are independent of the choice of n. This suggests that $\hat{H}_{CD}^{\text{Eq.1.9}} = \hat{H}_{CD}^{\text{Eq.3.11}}$ for scale-invariant driving, in contrast with the general situation discussed in Sec. 3.4. Indeed, it has been shown elsewhere that Eq. 3.33a – which we derived from Eq. 3.11 – follows directly from Eq. 1.9 [34]. Secondly, the shortcuts given by

Eq. 3.33 do not suffer from divergences at the nodes of excited energy eigenstates. This is easy to understand in terms of the no-flux criterion of Sec. 3.5: because variations in γ merely cause the eigenstate ϕ to expand or contract linearly, and variations in f induce simple translations of ϕ, the probability between adjacent nodes of the wavefunction is independent of t.

3.7 Numerical illustration of fast-forward driving

The parameter-dependent potential

$$U_0(q;\xi) = \frac{\xi^2}{16}\left[\cosh(4q) - 1\right] - \frac{3\xi}{2}\cosh(2q), \tag{3.34}$$

belongs to a class of potentials studied by Razavy [71], for which convenient analytical expressions for low-lying eigenstates can be obtained. Here and below, we have set the quantities β, m and $\hbar$ (appearing in Ref. [71]) to unity, so as to work with an effectively dimensionless Hamiltonian. As illustrated in Fig. 3.2, $U_0(q;\xi)$ changes from a broad double well to a narrow single well as ξ is increased from 0.1 to 6.0.

Now consider

$$\hat{H}_0(t) = \frac{\hat{p}^2}{2} + U_0(\hat{q};\xi(t)) \tag{3.35}$$

where $\xi(t)$ varies monotonically from 0.5 to 8.5 over the interval $0 \leq t \leq \tau$, according to

$$\xi(t) = 4.5 + \cos\left(\frac{\pi t}{\tau}\right)\left[\cos\left(\frac{2\pi t}{\tau}\right) - 5\right], \tag{3.36}$$

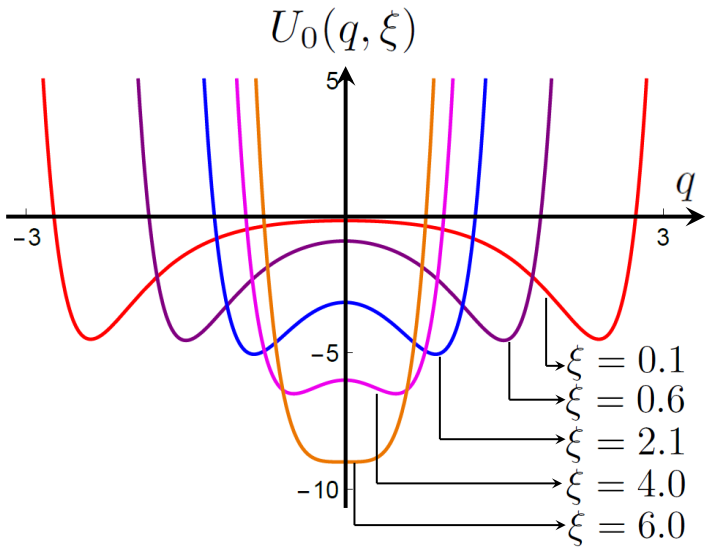

Figure 3.2: $U_0(q,\xi)$ is plotted for five values of ξ.

and $\xi(t)$ remains constant outside this interval. Note that $\dot{\xi}(0) = \dot{\xi}(\tau) = 0$ and $\ddot{\xi}(0) = \ddot{\xi}(\tau) = 0$, hence $\hat{H}_0(t)$ satisfies the continuity conditions described after Eq. 3.2.

The wavefunction for the first excited state of $\hat{H}_0(t)$ is given by [71]

$$\phi(q,t) = \kappa(t)\sinh(2q)\exp\left[-\frac{1}{4}\xi(t)\cosh(2q)\right] \tag{3.37}$$

where $\kappa(t)$ is set by normalization. The corresponding eigenenergy is $E(t) = -2$. Although this eigenstate has a node at the origin, the no-flux criterion of Sec. 3.5 is satisfied by the anti-symmetry of the wavefunction: $\phi(-q,t) = -\phi(q,t)$, hence $\mathcal{I}(0,t) = 1/2$ for all t. Thus we expect our approach to apply despite the presence of the node.

Using the above expressions and setting $\tau = 0.2$, we numerically computed the function $\mathcal{I}(q,t)$ (Eq. 3.6), from which we constructed the flow fields v and a and

the fast-forward potential U_{FF} (Eq. 3.14). As $\xi(t)$ increases from 0.5 to 8.5, $U_0(q,t)$ becomes increasingly narrow (Fig. 3.2), as does the eigenstate $\phi(t)$; this is reflected in the fields v and a, which describe the flow of probability toward the origin. $U_{FF}(q,t)$ initially develops into a potential well that resembles a parabola (though it is not precisely quadratic) – this brings about the acceleration of probability flow toward the origin.

We performed two numerical simulations of evolution under the time-dependent Schrödinger equation

$$i\hbar\frac{\partial\psi}{\partial t} = \hat{H}(t)\psi \tag{3.38}$$

using $\hat{H} = \hat{H}_0$ in the first simulation and $\hat{H} = \hat{H}_0 + \hat{U}_{FF}$ in the second; we will use the notation ψ^0 and ψ^{FF} to distinguish between the two simulations. In both cases the wavefunction was initialized in the state $\psi(q,0) = \phi(q,0)$. The time evolution was performed using the split-time propagation scheme [72, 73], which involves the repeated application of the fast Fourier transform to toggle between the position and momentum representations.

Fig. 3.3 shows snapshots of $\psi(q,t)e^{-i\alpha(t)}$ (solid curves) and $\phi(q,t)$ (dashed curves) for both simulations. Note that $\psi e^{-i\alpha} = \phi$ in the adiabatic limit (Eq. 3.4) – this is our motivation for plotting $\psi e^{-i\alpha}$ rather than ψ, though in the following paragraphs we largely will stop writing the factor $e^{-i\alpha}$, for convenience.

The left panel of Fig. 3.3 shows the evolution of $\psi^0(q,t)$. Due to the nonadiabatic time-dependence of $\hat{H}_0$, the wavefunction ψ^0 "lags" behind the instantaneous eigenstate ϕ. This is particularly evident in Fig. 3.3(b), where the probability associated

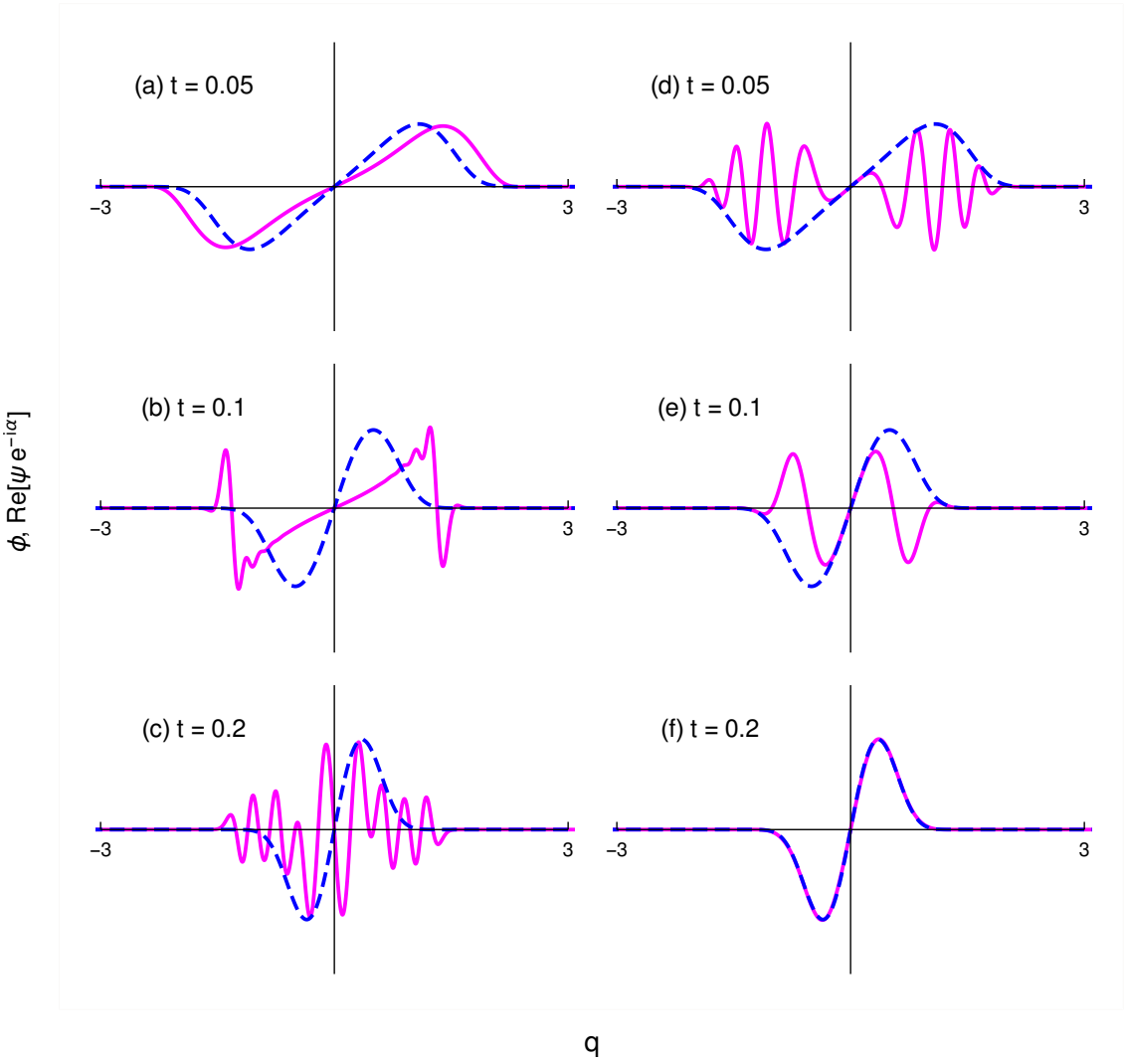

Figure 3.3: Evolution under $\hat{H}_0$ (left panel) and $\hat{H}_0 + \hat{U}_{FF}$ (right panel). The solid magenta curves show $\mathrm{Re}(\psi e^{-i\alpha})$, and the dashed blue curves show the eigenstate ϕ. Snapshots are shown at $t = 0.05$, at $t = 0.1$, and at the end of the process, $t = 0.2$.

with ϕ has shifted substantially toward the origin, while ψ^0 remains somewhat behind. This lag leads to shock waves, which are nascent in Fig. 3.3(b). These shocks propagate inward, and ψ^0 ends in a superposition of excited states [Fig. 3.3(c)].

The right panel shows the evolution of $\psi^{FF}(q,t)$. Here the wavefunction develops excitations at short times [Fig. 3.3(d)], in response to large forces generated by $\hat{U}_{FF}(t)$. These forces eliminate the lag that is observed in the left panel, by "squeezing" the wavefunction and causing probability to accelerate toward the origin. At later times this flow is decelerated – again, due to $\hat{U}_{FF}(t)$ – and the excitations subside [Fig. 3.3(e)]. The wavefunction gently arrives at the desired energy eigenstate at the final time [Fig. 3.3(f)].

In the present context Eq. 3.20 can be written as

$$\psi^{FF} e^{-i\alpha} = \phi\, e^{iS/\hbar} \tag{3.39}$$

which implies that the probability densities $|\psi^{FF}|^2 = |\phi|^2$ at all times, despite the excitations that develop in $\psi^{FF}(q,t)$. We have verified this result in our simulations (data not shown). Eq. 3.39 further implies that $\mathrm{Re}(\psi^{FF} e^{-i\alpha}) = \phi(q,t)\cos[S(q,t)/\hbar]$, which is illustrated in Fig. 3.3(d), where the dashed line is manifestly the envelope of the solid line.

The variation of the potential $U_0(q,t)$ and $U_{FF}(q,t)$ is plotted in Fig. 3.4. While $U_0(q,t)$ follows Eq. 3.34 and ξ is varied according to Eq. 3.36, $U_{FF}(q,t)$ is numerically evaluated using Eq. 3.14. For $\tau = 0.2$, snapshots are presented at $t = 0, 0.04, 0.055, 0.08, 0.12$ and 0.2. The solid magenta curves represent $U_0(q,t)$ while

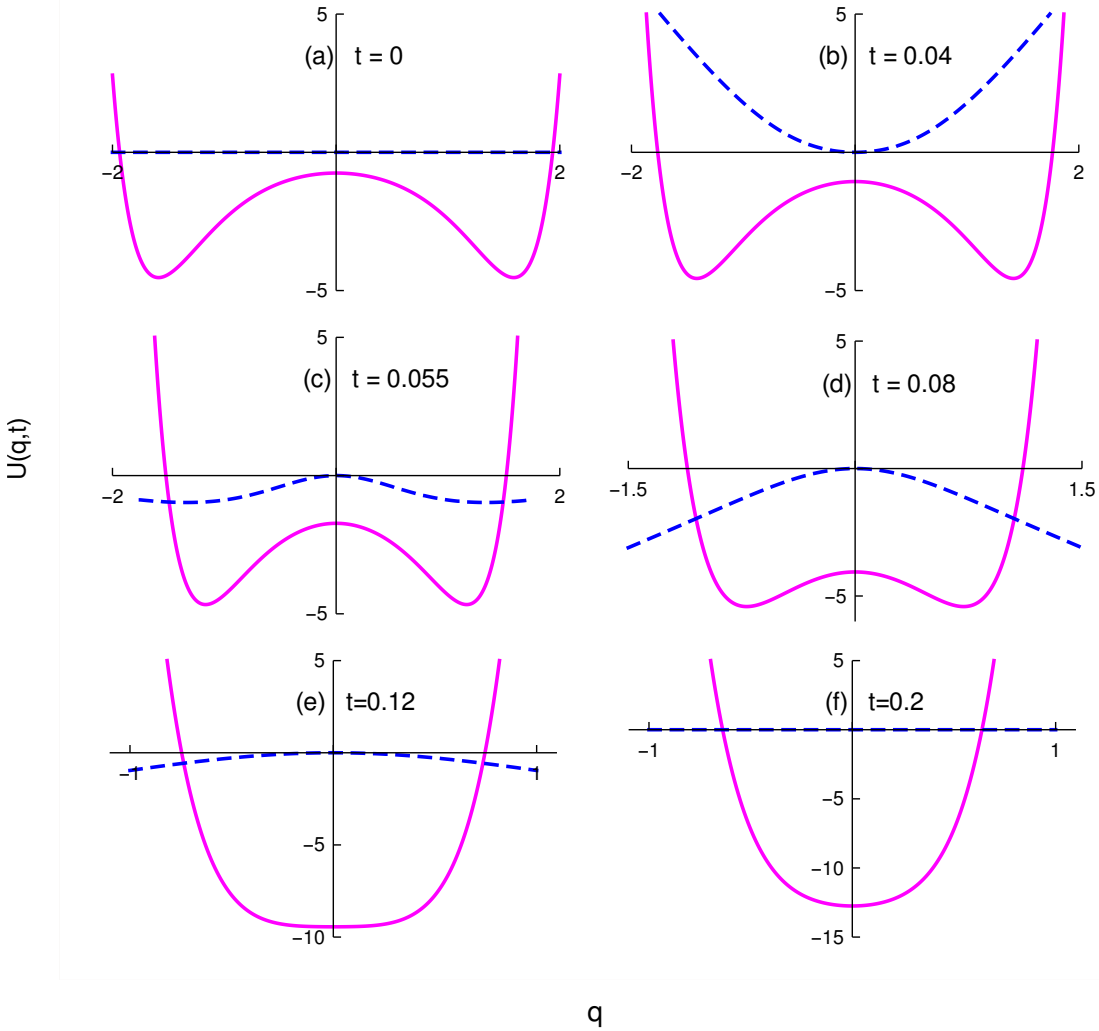

Figure 3.4: The variation of $U_0(q,t)$ and $U_{FF}(q,t)$ is plotted. The solid magenta curves show $U_0(q,t)$ and the dashed blue curves show $U_{FF}(q,t)$ at $t = 0, 0.04, 0.055, 0.08, 0.12$ and 0.2. $U_0(q,t)$ is initially a double well potential, but as it evolves, the wells comes closer to the origin and eventually $U_0(q,t)$ transforms to a single attractive well potential. $U_{FF}(q,t)$ smoothly increases from zero and quickly becomes an attractive well, which then becomes a repulsive well that finally transforms smoothly to zero at $t = \tau$.

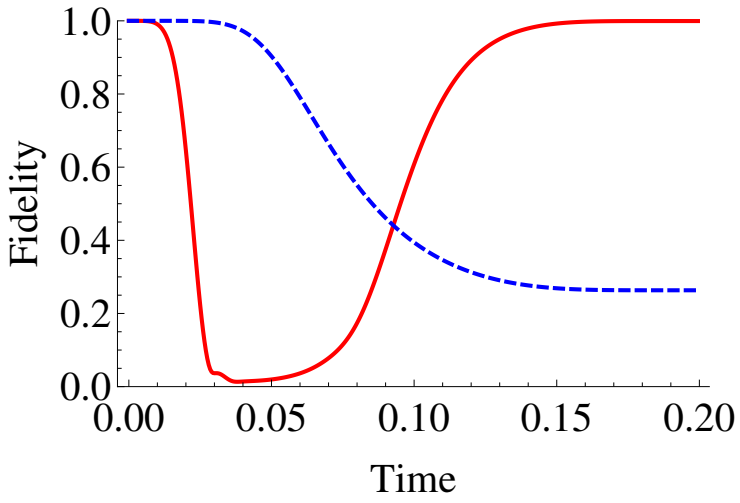

Figure 3.5: The blue dashed curve shows the fidelity $|\langle\phi|\psi^0\rangle|^2$, quantifying the limited extent to which $\psi^0(q,t)$, evolving under $\hat{H}_0$, keeps pace with the energy eigenstate $\phi(q,t)$. The solid red curve shows $|\langle\phi|\psi^{FF}\rangle|^2$, which is the fidelity that is achieved when $\hat{U}_{FF}$ is added to the Hamiltonian.

the blue dashed curves represent $U_{FF}(q,t)$. As shown, $U_{FF}(q,t)$ slowly increases from zero and becomes an attractive well potential. This property of $U_{FF}(q,t)$ squeezes the wavefunction appropriately such that its envelope aligns with the adiabatic path. As a result, excitations are developed in the evolving wavefunction. After a while, the attractive nature of $U_{FF}(q,t)$ becomes repulsive and the well gets inverted as shown. This ensures that the excitations start to die down. The inverted well smoothly becomes zero at the final time τ and a perfect fast-forward driving is achived by $U_{FF}(q,t)$ as supported by Fig. 3.3.

Finally, for both simulations we computed the fidelity $F(t) = |\langle\phi|\psi\rangle|^2$, that is the degree of overlap between the evolving wavefunction and the energy eigenstate. Fig. 3.5 shows the results. In the absence of the auxiliary term, the fidelity $|\langle\phi|\psi^0\rangle|^2$ decays monotonically to $F \approx 0.3$. When $\hat{U}_{FF}$ is included in the Hamiltonian, the fidelity $|\langle\phi|\psi^{FF}\rangle|^2$ at first drops rapidly to nearly zero – due to the excitations that

develop in ψ^{FF} – but then it claws its way back to unity, illustrating the effectiveness of the fast-forward potential obtained from the acceleration flow field $a(q,t)$.

3.8 Extension to three degrees of freedom

Although the focus in this paper is on systems with one degree of freedom, here we briefly discuss how the results of Sec. 3.3 might be extended to three dimensions. We will use boldface to denote vector quantities.

For a given choice of quantum number n, let $\phi(\mathbf{q},t)$ and $E(t)$ denote the n'th eigenstate and eigenenergy, respectively, of the Hamiltonian $\hat{H}_0(t)$ given by Eq. 3.1. Let us define a vector field $\mathbf{v}(\mathbf{q},t)$ by the equation

$$\partial_t \phi^2 + \nabla \cdot (\mathbf{v}\phi^2) = 0 \tag{3.40}$$

which describes how the eigenstate probability density $\phi^2(\mathbf{q},t)$ varies parametrically with t. We assume that $\hat{H}_0(t)$ and its first two time derivatives vanish outside the interval $0 < t < \tau$ (as in the one-dimensional case), therefore $\mathbf{v}$ can be constructed to vanish outside this interval as well: $\mathbf{v} = \mathbf{0}$ for $t \notin (0,\tau)$. [4]

Since Eq. 3.40 is a continuity equation, it can be interpreted as describing an ensemble of independent trajectories, each evolving according to $\dot{\mathbf{q}} = \mathbf{v}(\mathbf{q},t)$. The acceleration of these trajectories is described by a field $\mathbf{a}(\mathbf{q},t)$ whose i'th component

[4] Eq. 3.40 defines $\mathbf{v}(\mathbf{q},t)$ only up to gauge-like transformations of the form $\mathbf{v} \to \mathbf{v} + (\nabla \times \mathbf{B})/\phi^2$, where $\mathbf{B}(\mathbf{q},t)$ is an arbitrary, well-behaved vector field. Hence we have some freedom in constructing $\mathbf{v}$. This freedom was not present in Sec. 3.3, where the $v(q,t)$ was defined using the construction shown in Fig. 3.1, rather than from the continuity equation.

satisfies

$$a_i = \ddot{q}_i = \frac{\partial v_i}{\partial t} + \sum_j \frac{\partial v_i}{\partial q_j}\frac{dq_j}{dt} \tag{3.41}$$

We now define a counterdiabatic Hamiltonian

$$\hat{H}_{CD}(t) = \frac{\hat{\mathbf{p}}\cdot\hat{\mathbf{v}} + \hat{\mathbf{v}}\cdot\hat{\mathbf{p}}}{2} \quad , \quad \hat{\mathbf{v}}(t) = \mathbf{v}(\hat{\mathbf{q}}, t) \tag{3.42}$$

Using $\dot{\phi} + (1/2)(\nabla\cdot\mathbf{v})\phi + \mathbf{v}\cdot\nabla\phi = 0$ (which follows from Eq. 3.40), it is readily verified that the wavefunction

$$\psi_{ad}(\mathbf{q}, t) = \phi(\mathbf{q}, t)\, e^{i\alpha(t)} \quad , \quad \alpha(t) = -\frac{1}{\hbar}\int_0^t E(t')\, dt' \tag{3.43}$$

is a solution of the Schrödinger equation $i\hbar\,\partial_t\psi_{ad} = (\hat{H}_0 + \hat{H}_{CD})\psi_{ad}$.

Now let us suppose that the field $\mathbf{v}(\mathbf{q}, t)$ can be chosen to be curl-free:

$$\nabla\times\mathbf{v} = \mathbf{0} \tag{3.44}$$

We can then introduce a function $S(\mathbf{q}, t)$ that satisfies

$$\nabla S = m\mathbf{v} \tag{3.45}$$

which allows us to rewrite Eq. 3.41 as

$$a_i(\mathbf{q}, t) = \frac{1}{m}\frac{\partial}{\partial q_i}\left[\frac{\partial S}{\partial t} + \frac{(\nabla S)^2}{2m}\right] \tag{3.46}$$

We have used both Eqs. 3.44 and 3.45 in going from Eq. 3.41 to Eq. 3.46. If we now define $U_{FF}(\mathbf{q}, t)$ by the equation

$$\partial_t S + \frac{(\nabla S)^2}{2m} + U_{FF} = 0 \tag{3.47}$$

then Eq. 3.46 implies $-\nabla U_{FF} = m\mathbf{a}$ (compare with Eq. 3.14). It is now a matter of algebra to verify that $\bar{\psi} \equiv \phi e^{i\alpha} e^{iS/\hbar}$ obeys the Schrödinger equation $i\hbar\,\partial_t \bar{\psi} = (\hat{H}_0 + \hat{U}_{FF})\bar{\psi}$. Since $S(\mathbf{q}, t)$ is a constant outside the interval $0 < t < \tau$, we see that the addition of the fast-forward potential U_{FF} causes the chosen eigenstate of the initial Hamiltonian to evolve to the corresponding eigenstate of the final Hamiltonian.

As in the one-dimensional case, divergences in $\mathbf{v}(\mathbf{q}, t)$ may arise whenever $\phi(\mathbf{q}, t) = 0$, potentially causing the method to break down for excited eigenstates. This issue deserves further exploration.

3.9 Summary

We have developed a framework for constructing counterdiabatic and fast-forward shortcuts for quantum systems. This framework is organized around velocity and acceleration flow fields $v(q, t)$ and $a(q, t)$, which describe the time-dependence of the desired adiabatic evolution. Once the flow fields have been determined, the shortcuts are given by simple expressions involving these fields (Eqs. 3.11, 3.14). The flow-fields can be pictured in terms of the evolution of a "picket fence" of lines (Figs. 3.1) that glide around as time is varied parametrically. The fields v and a are

constructed from integrated function $\mathcal{I}$ that define the picket fence.

As noted in Sec. 3.5, the nodes of excited energy eigenstates $\phi(q,t)$ generically pose a problem for our method, as they do for the fast-forward approach in general. The divergences in $v(q,t)$ that result from these nodes can be understood intuitively by considering Eq. 3.27, which gives the probability flux across the ν'th node: $\Phi_\nu = (v-u_\nu)\phi^2$. The two factors on the right represent the flow velocity relative to the motion of the node, $v-u_\nu$, and the local density, ϕ^2. If we momentarily imagine that ϕ^2 is very small but non-zero at q_ν, then we see that $v-u_\nu$ must be very large in order to "push through" a fixed probability flux – an apt analogy is water flowing through a pipe that becomes narrow at a certain point. Thus $v-u_\nu$ diverges as $\phi^2 \to 0$: an infinite velocity is required to achieve a finite flux, at vanishing probability density.

When the time-dependence of $\phi^2(q,t)$ is such that there is no flux of probability across nodes, i.e. when the probability between neighboring nodes remains constant even as the eigenstate deforms, then the flow fields v and a are non-singular and we expect our method (and more generally the fast-forward approach [26]) to work well. This no-flux criterion is satisfied for scale-invariant driving, as well as for the model system studied numerically in Sec. 3.7. In the latter case the criterion is satisfied because the potential $U_0(q,t)$ (Eq. 3.34) is symmetric about the origin. It would be useful to identify a more generic (i.e. non-symmetric) potential and eigenstate for which the no-flux criterion is satisfied, and to test whether our method continues to work in that situation. This would provide a more stringent test of the no-flux criterion than the one studied in Sec. 3.7.

Our framework connects the counterdiabatic and fast-forward approaches for

quantum systems. The fields $v(q,t)$ and $a(q,t)$ provide two mathematical descriptions the for same flow of probability. The former defines the counterdiabatic Hamiltonian $\hat{H}_{CD}$, while the latter (together with the mass, m) determines the fast-forward potential $\hat{U}_{FF}$. It is remarkable that no other input is required to construct these shortcuts. For the moment we lack a deeper or intuitive understanding of why this should be the case.

This chapter presents an open problem in the development of fast-forward shortcuts for excited states of quantum systems, when the no-flux criterion is not satisfied. Our next goal is to probe into this problem. We first study an analogous classical problem on shortcuts in the next chapter, and we extend the flow-fields based method to classical systems. In a subsequent chapter, we will investigate if the intuitions from classical shortcuts may help in constructing exact or approximate quantum shortcuts for excited states when the no-flux criterion is not satisfied, at least in the semiclassical limit.

Chapter 4: Classical shortcuts using flow-fields

4.1 Overview

For a classical system in one degree of freedom, the action variable $I = \oint p \cdot \mathrm{d}q$ is an adiabatic invariant [51]. As an example, when the length of a pendulum is slowly varied, both its energy E and frequency of oscillation ω change with time, but their ratio E/ω, which is proportional to the action, remains constant. The adiabatic invariant can be visualized in phase space by imagining a collection of trajectories evolving under a slowly time-dependent Hamiltonian, H_0. If all initial conditions are sampled from a single energy shell (that is, a level curve) of $H_0(q, p, 0)$, then a snapshot of these trajectories at a later time t will find them located on a single energy shell of $H_0(q, p, t)$, with the same action as the initial shell, as shown in Fig. 4.1.

In this chapter, we pose and answer the following question: How can the adiabatic invariant be preserved under nonadiabatic driving conditions? We consider a Hamiltonian $H_0(q, p, t) = p^2/2m + U_0(q, t)$ that varies at an arbitrary rate. Under the evolution generated by this Hamiltonian, the action $I(q, p, t)$ does not remain constant: If at time $t = 0$ we launch a collection of trajectories, each with the same initial action I_0, then at later times their actions will generally differ from one

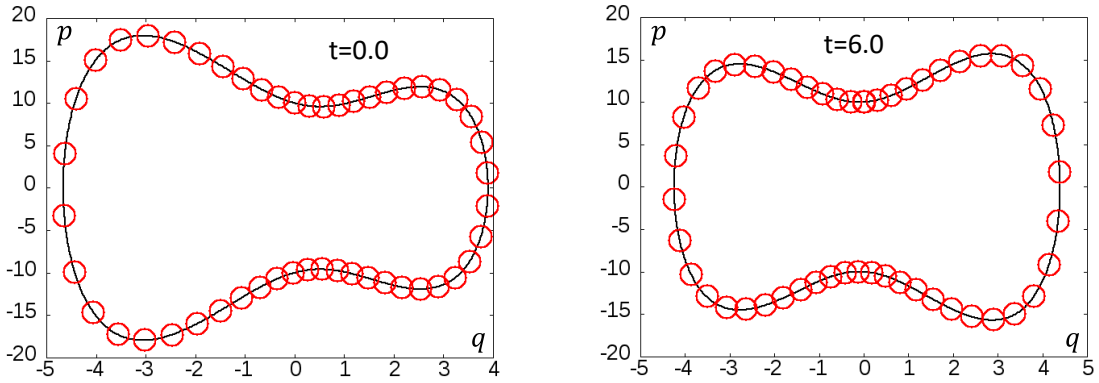

Figure 4.1: Illustration of the classical adiabatic invariant. Fifty trajectories evolving under a slowly varying Hamiltonian are shown at an initial time (on left) and a later time (on right). The closed curves are instantaneous *energy shells* – level curves of H_0 – with identical values of the action $I = \oint p \cdot \mathrm{d}q$. Trajectories were generated using $H(q, p, t)$ given by Eq. 4.21, setting $\tau = 10.0$ to achieve slow driving.

another and from the initial action. Thus under nonadiabatic driving, trajectories wander away from the energy shell associated with the action I_0. But suppose we want these trajectories to "return home" at a specified later time τ, i.e., we demand that the action of each trajectory be equal to I_0 at $t = \tau$, given that its action had this value at $t = 0$. In this chapter we solve for the additional forces that are required to steer the trajectories back to the action I_0 at $t = \tau$. More precisely, we show how to construct an auxiliary fast-forward potential $U_{FF}(q, t)$ with the following property. Under the dynamics generated by the Hamiltonian $H_0 + U_{FF}$, *all trajectories that begin with action* I_0 *at* $t = 0$ *will end with the same action,* I_0*, at* $t = \tau$. Throughout this chapter, the action $I(q, p, t)$ is defined with respect to the original Hamiltonian $H_0(q, p, t)$.

The motivation behind this work comes from the fact that quantum shortcuts derived in Chap. 3 can not be applied to excited states in general. We investigate

a classical analogous problem in shortcuts hoping that it might provide useful insights for designing quantum shortcuts for excited states in the semiclassical limit. However, in this chapter, we focus on solving a self-contained problem of general theoretical interest in elementary classical dynamics, for which we obtain a simple and appealing solution (Eq. 4.11). In Sec. 4.2, we set up the classical problem and define the flow-field velocity and acceleration. We state the expressions for counterdiabatic Hamiltonian and fast-forward potential in Sec. 4.3, and show that these auxiliary fields achieve counterdiabatic and fast-forward driving respectively. We illustrate our results in Sec. 4.4 by solving a model double well Hamiltonian numerically, and conclude in Sec. 4.5. We defer the discussion on the applicability of the results from this chapter to quantum systems in the next chapter.

4.2 Setup and definition of flow-field parameters

Consider a classical system in one degree of freedom, described by a kinetic-plus-potential Hamiltonian

$$H_0(z,t) = \frac{p^2}{2m} + U_0(q,t) \quad , \quad z = (q,p) \tag{4.1}$$

H_0 varies with time during the interval $0 \leq t \leq \tau$, but is constant outside this interval. We assume that H_0 is twice continuously differentiable with respect to time [74], and hence both $\partial H_0/\partial t$ and $\partial^2 H_0/\partial t^2$ vanish at $t = 0$ and $t = \tau$. In Appendix B, we discuss how this assumption can be relaxed.

The term *energy shell* will denote a level curve of $H_0(z,t)$; that is, the set of all

points where H_0 takes on a particular value, E, at time t. We will assume that each energy shell forms a simple, closed loop in phase space. The function

$$\Omega(E,t) = \int \mathrm{d}z\, \theta\left[E - H_0(z,t)\right] = \oint_E p \cdot \mathrm{d}q \tag{4.2}$$

is the volume of phase space enclosed by the energy shell E of $H_0(z,t)$, and the *action*,

$$I(z,t) = \Omega(H_0(z,t),t), \tag{4.3}$$

is the volume enclosed by the energy shell that contains the point z. Eq. 4.3 implies

$$\{I, H_0\} \equiv \frac{\partial I}{\partial q}\frac{\partial H_0}{\partial p} - \frac{\partial I}{\partial p}\frac{\partial H_0}{\partial q} = 0, \tag{4.4}$$

which will prove useful.

Let us choose an arbitrary action value $I_0 > 0$, and define the *adiabatic energy* $\bar{E}(t)$ by the condition

$$\Omega(\bar{E}(t),t) = \oint_{\bar{E}(t)} p'\, dq' = I_0. \tag{4.5}$$

The *adiabatic energy shell* $\mathcal{E}(t) = \{z | H_0(z,t) = \bar{E}(t)\}$ is the level curve of $H_0(z,t)$ with the value $\bar{E}(t)$, enclosing a phase space volume I_0. Hence $I(z,t) = I_0$ for all $z \in \mathcal{E}(t)$. The action value I_0 and the adiabatic energy $\bar{E}(t)$ are classical analogues of the quantum number n and eigenenergy $E_n(t)$.

At $t = 0$, the adiabatic energy shell $\mathcal{E}(0)$ defines a set of initial conditions that form a closed loop in phase space. As trajectories evolve under $H_0(z,t)$ from these

initial conditions, this loop evolves in time,

$$\mathcal{L}(t) = \{z = z_t(z_0) | z_0 \in \mathcal{E}(0)\}, \tag{4.6}$$

where $z_t(z_0)$ indicates the trajectory that evolves under $H_0(z,t)$ from initial conditions z_0. If H_0 varies slowly with time, then these trajectories remain close to the adiabatic energy shell, but under more general conditions the loop $\mathcal{L}(t)$ strays away from $\mathcal{E}(t)$ for $t > 0$.

We now assume that H_0 varies at an arbitrary – i.e. non-adiabatic – rate, but we continue to use the term adiabatic energy to refer to $\bar{E}(t)$ defined by Eq. 4.5, for chosen value of action, I_0. For a trajectory with initial action I_0, we wish to construct a counterdiabatic Hamiltonian $H_{CD}(q,p,t)$ and a fast-forward potential $U_{FF}(q,t)$ such that: (1) if the trajectory evolves under $H_0 + H_{CD}$, it remains on the adiabatic energy shell at all times, that is, $I(t) = I_0$; and (2) if the trajectory evolves under $H_0 + U_{FF}$, it returns to the adiabatic energy shell at the final time: $I(\tau) = I(0) = I_0$. Here and below, $I(t) = I(q(t), p(t), t)$ denotes the value of the action function along the trajectory.

To construct these shortcuts for a given choice of I_0, let

$$\bar{p}(q,t) = [2m(\bar{E} - U_0)]^{1/2} \tag{4.7}$$

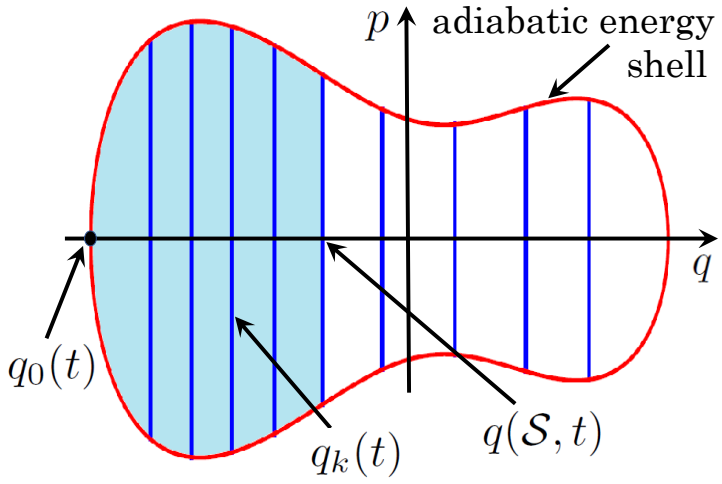

Figure 4.2: The closed red curve, with upper and lower branches $\pm\bar{p}(q,t)$ (Eq. 4.7), depicts the adiabatic energy shell $\bar{E}(t)$ in phase space. The blue vertical lines divide $\bar{E}(t)$ into $K \gg 1$ strips of equal phase space volume. $q(\mathcal{S},t)$ is the right boundary of the shaded region, of phase space volume $\mathcal{S}$. The parametric motion of the vertical lines defines the velocity and acceleration fields $v(q,t)$ and $a(q,t)$.

specify the upper branch of the adiabatic energy shell, and let

$$\mathcal{S}(q,t) = 2\int_{q_0(t)}^{q} \bar{p}(q',t)dq' \tag{4.8}$$

denote the volume of phase space enclosed by the adiabatic energy shell $\bar{E}(t)$ between the left turning point $q_0(t)$ and a point q. The function $\mathcal{S}(q,t)$ can be inverted to obtain $q(\mathcal{S},t)$, which in turn is used to define flow fields

$$v(q,t) = \frac{\partial}{\partial t}q(\mathcal{S},t) = -\frac{\partial_t \mathcal{S}}{\partial_q \mathcal{S}} \tag{4.9a}$$

$$a(q,t) = \frac{\partial^2}{\partial t^2}q(\mathcal{S},t) = v'v + \dot{v} \tag{4.9b}$$

These flow fields are pictured by dividing the adiabatic energy shell into $K \gg 1$

strips enclosing equal phase space volume, delimited by lines drawn at locations $\{q_k(t)\}$; see Fig. 4.2. The fields v and a describe the motion of these lines as the parameter t is varied: $\dot{q}_k = v(q_k, t)$ and $\ddot{q}_k = a(q_k, t)$. Since $\partial H_0/\partial t = \partial^2 H_0/\partial t^2 = 0$ at $t = 0$ and $t = \tau$ (see comments following Eq. 4.1) we have

$$v(q, 0) = v(q, \tau) = 0 \quad , \quad a(q, 0) = a(q, \tau) = 0. \tag{4.10}$$

4.3 Counterdiabatic and fast-forward driving

Using the flow fields parameters defined in Eq. 4.9, we now define a counterdiabatic Hamiltonian

$$H_{CD}(q, p, t) = pv(q, t), \tag{4.11a}$$

and a fast-forward potential U_{FF} that satisfies

$$-\partial_q U_{FF}(q, t) = ma(q, t), \tag{4.11b}$$

both of which vanish for $t \notin (0, \tau)$. We will now demonstrate that Eqs. 4.11a and 4.11b achieves classical counterdiabatic and fast-forward driving.

Consider a point in phase space, $(q_n(t), p_n(t))$, attached to the top of the nth line segment: $p_n = \bar{p}(q_n, t)$ (see Fig. 4.2). As the shape of the energy shell and the locations of the line segments vary parametrically with time, this point (q_n, p_n) moves in phase space, surfing the upper branch of the energy shell. This motion is

described by the equations

$$\dot{q}_n = v(q_n, t) \qquad , \qquad \dot{p}_n = -p_n v'(q_n, t) \tag{4.12}$$

where the equation for $\dot{p}_n$ is obtained by demanding that the phase space volume of the strip between neighboring vertical lines, $\delta S_n \equiv 2p_n(q_{n+1} - q_n)$, remain constant. In Eq. 4.12 and throughout this chapter, dots and primes denote derivatives with respect to t and q respectively. Eq. 4.12 also describes the motion of a point attached to the bottom of one of the vertical lines. We easily verify that Eq. 4.12 is generated by the Hamiltonian H_{CD} of Eq. 4.11a. If we start with initial conditions distributed over the energy shell $\mathcal{E}(0)$, and we evolve trajectories from these initial conditions under the Hamiltonian $H_{CD}(q, p, t)$, then these trajectories cling to the evolving adiabatic energy shell, with each trajectory attached to the upper or lower end of one of the vertical line segments. Hence the flow generated by H_{CD} *preserves the adiabatic energy shell*, in the following sense: for each time step δt, this flow maps points on $\mathcal{E}(t)$ to points on $\mathcal{E}(t + \delta t)$. Equivalently, the action $I(z, t)$ is conserved under this flow, for those trajectories with action I_0. Therefore we have

$$0 = \frac{\partial I}{\partial t} + \frac{\partial I}{\partial q}\dot{q} + \frac{\partial I}{\partial p}\dot{p} = \frac{\partial I}{\partial t} + \{I, H_{CD}\} \qquad \forall\, z \in \mathcal{E}(t) \tag{4.13}$$

Next, we consider the full Hamiltonian $H_0 + H_{CD}$, which generates equations of motion

$$\dot{q} = \frac{p}{m} + v(q, t) \quad , \quad \dot{p} = -U_0'(q, t) - pv'(q, t) \tag{4.14}$$

Along a trajectory $z(t)$ obeying these dynamics,

$$\dot{I} = \frac{\mathrm{d}}{\mathrm{d}t} I(z(t), t) = \frac{\partial I}{\partial t} + \{I, H_0\} + \{I, H_{CD}\} \tag{4.15}$$

Eqs. 4.4, 4.13 and 4.15 imply that $\dot{I} = 0$ for all $z \in \mathcal{E}(t)$. Thus the flow generated by $H_0 + H_{CD}$ preserves the adiabatic energy shell and generates counterdiabatic driving. This is easily understood: with each time step δt, the term $H_{CD}(z, t)$ generates a flow that maps $\mathcal{E}(t)$ onto $\mathcal{E}(t + \delta t)$ while the term $H_0(z, t)$ generates flow parallel to the adiabatic energy shell. As a consistency check, we can verify directly from Hamilton's equations that the flow generated by H_{CD} preserves the adiabatic energy shell (see Appendix C).

To this point, we have constructed a Hamiltonian $H_0 + H_{CD}$ that generates trajectories which cling to the adiabatic energy shell $\mathcal{E}(t)$. Along these trajectories, $I(z, t)$ remains constant. We now introduce a change of variables that effectively transforms $H_{CD}(q, p, t)$ into the fast-forward potential $U_{FF}(q, t)$.

Consider the evolution of the observables

$$Q(q, p, t) = q \qquad , \qquad P(q, p, t) = p + mv(q, t) \tag{4.16}$$

along a trajectory that evolves under Eq. 4.14. By direct substitution we get

$$\frac{\mathrm{d}Q}{\mathrm{d}t} = \frac{P}{m} \qquad , \qquad \frac{\mathrm{d}P}{\mathrm{d}t} = -U_0'(Q, t) + ma(Q, t) \tag{4.17}$$

using Eq. 4.9. Eq. 4.17 is generated by the Hamiltonian

$$H_{\mathrm{FF}}(Z,t) = H_0(Z,t) + U_{FF}(Q,t) \tag{4.18}$$

where $Z = (Q,P)$ and U_{FF} satisfies Eq. 4.11b. Thus Eq. 4.16 defines a time-dependent transformation $\mathcal{M}_t : z \to Z$, which maps any trajectory $z(t)$ evolving under $H_0 + H_{CD}$ to a counterpart trajectory $Z(t)$ evolving under $H_{\mathrm{FF}}(Z,t)$. Now consider specifically a trajectory $z(t)$ that evolves, under $H_0 + H_{CD}$, from initial conditions on the adiabatic energy shell $\mathcal{E}(0)$. As we have already seen, this trajectory remains on the adiabatic energy shell $\mathcal{E}(t)$ for all times $t \in [0,\tau]$. Under the mapping $\mathcal{M}_t$, its image $Z(t)$ (which evolves under H_{FF}) is displaced along the momentum axis by an amount $mv(q,t)$ (Eq. 4.16). By Eq. 4.10, $Z(t)$ begins and ends on the adiabatic energy shell: $Z(0) \in \mathcal{E}(0)$, $Z(\tau) \in \mathcal{E}(\tau)$. This is precisely the fast-forward driving, which concludes our proof.

Consider the loop

$$\mathcal{L}_{\mathrm{FF}}(t) = \{z = z_t^{\mathrm{FF}}(z_0) | z_0 \in \mathcal{E}(0)\} \tag{4.19}$$

which evolves in phase space under H_{FF}. The results of the previous paragraph can be written compactly as follows:

$$\mathcal{M}_t : \mathcal{E}(t) \to \mathcal{L}_{\mathrm{FF}}(t). \tag{4.20}$$

At any time t, $\mathcal{L}_{\mathrm{FF}}(t)$ is the image of $\mathcal{E}(t)$ under the transformation defined by

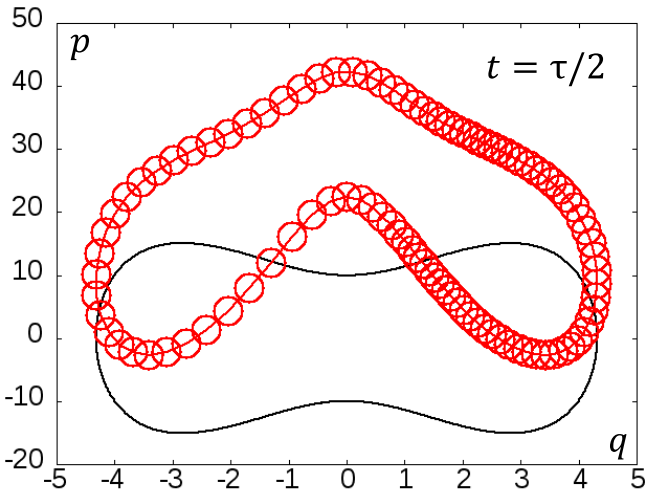

Figure 4.3: A snapshot, at $t = \tau/2$, of 100 trajectories evolving under $H_{\rm FF}(z,t)$ using a rapid protocol, with $\tau = 0.2$ (see text). The closed black loop is the adiabatic energy shell $\mathcal{E}(t)$, and the red loop above it is constructed by displacing each point on the lower loop by an amount $mv(q,t)$ along the p-axis. As predicted by Eq. 4.20, the trajectories coincide with the red loop.

Eq. 4.16 (see Fig. 4.3). This result implies that the function $J(q,p,t) \equiv I(q, p - mv(q,t), t)$ is a *local dynamical invariant*. That is, if a trajectory $z(t)$ is launched from the energy shell $\mathcal{E}(0)$ and then evolves under $H_{\rm FF}$, then the value of J is conserved along this trajectory: $J(z(t),t) = I_0$. For consistency, we can verify directly from Hamilton's equations that $\mathrm{d}J/\mathrm{d}t = 0$ for any point $z \in \mathcal{L}_{\rm FF}$ (see Appendix D).

4.4 Numerical example

To illustrate our results, we chose the dimensionless Hamiltonian

$$H(z,t) = \frac{p^2}{2} + q^4 - 16q^2 + \lambda(t)q \tag{4.21a}$$

with

$$\lambda(t) = 4\cos(\pi t/\tau)[5 - \cos(2\pi t/\tau)] \tag{4.21b}$$

This Hamiltonian describes a particle in a double-well potential, with a linear contribution whose slope $\lambda(t)$ evolves from $+16$ at $t = 0$, to -16 at $t = \tau$, with $\dot{\lambda} = \ddot{\lambda} = 0$ at initial and final times. As illustrated in Fig. 4.1, when $\tau = 10.0$ the driving is sufficiently slow for the adiabatic invariant to be conserved with high accuracy. For the simulations described in the following paragraph, we set $\tau = 1.0$ to obtain non-adiabatic driving.

We considered an initial adiabatic energy shell $\mathcal{E}(0)$ with energy $\bar{E}(0) = 50.0$, which corresponds to $I_0 = 214.035$. We numerically determined the fields $v(q,t)$ and $a(q,t)$ and constructed $U_{\rm FF}(q,t)$ according to Eq. 4.11b. We then generated fifty initial conditions on the energy shell $\mathcal{E}(0)$, shown in Fig. 4.4(a), and we performed two sets of simulations. In the first set, trajectories were evolved from these initial conditions under $H(z,t)$. In the second set, trajectories were evolved from the same initial conditions under the Hamiltonian $H_{\rm FF} = H + U_{\rm FF}$. In the absence of the fast-forward potential $U_{\rm FF}$, the trajectories belonging to the first set have final actions $I(z,\tau)$ that span a range of values, as seen in Fig. 4.4(b). By contrast, the addition of $U_{\rm FF}$ guides the second set of trajectories back to the adiabatic energy shell $\mathcal{E}(\tau)$, where each trajectory ends with $I(z,\tau) = I_0$; see Fig. 4.4(c). Note, however, that while the initial conditions in Fig. 4.4(a) are spaced uniformly with respect to the microcanonical measure, this is not the case for the final conditions in Fig. 4.4(c). As discussed in the Appendix E, this non-uniformity is due to the fact that $U_{\rm FF}(q,t)$

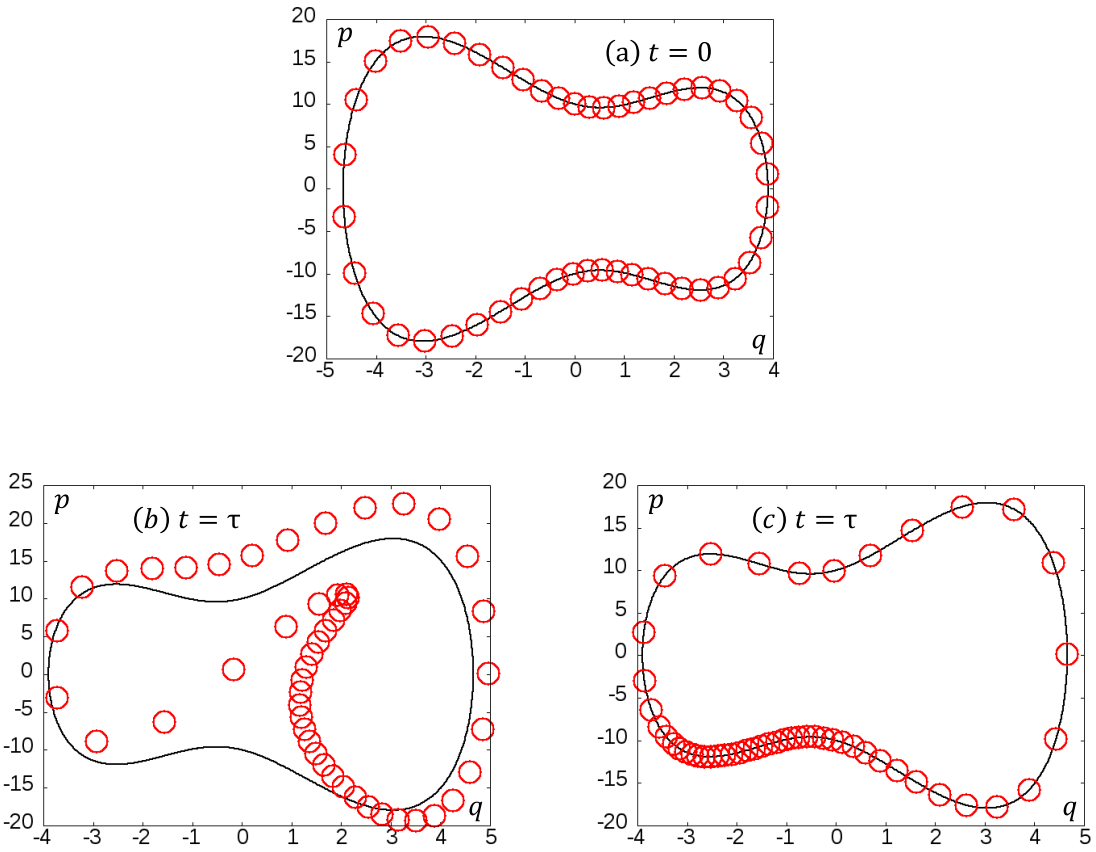

Figure 4.4: Initial (a) and final (b,c) conditions for trajectories launched from a single energy shell $\mathcal{E}(0)$. The trajectories in panel (b) evolved under $H(z,t)$ (Eq. 4.21), while those in panel (c) evolved under $H_{\rm FF} = H + U_{\rm FF}$, with $\tau = 1.0$. The solid black curves show the adiabatic energy shell $\mathcal{E}(t)$ at initial and final times.

depends on the choice of I_0. The variation of $U(q,t)$ and $U_{FF}(q,t)$ with q is shown in Fig. 4.5 with solid magenta curves and dashed blue curves respectively for times $t = 0.2, 0.5$ and 0.8.

We also performed simulations with a shorter duration, $\tau = 0.2$. After constructing $U_{\rm FF}(q,t)$ for this faster protocol, we simulated fifty trajectories evolving under $H_{\rm FF} = H + U_{\rm FF}$, using the initial conditions in Fig. 4.4(a). Fig. 4.3 depicts a snapshot of these trajectories at $t = \tau/2$. The two closed curves show the adiabatic energy shell $\mathcal{E}(t)$ and its image under the mapping $p \to p + v(q,t)$ (see Eq. 4.16).

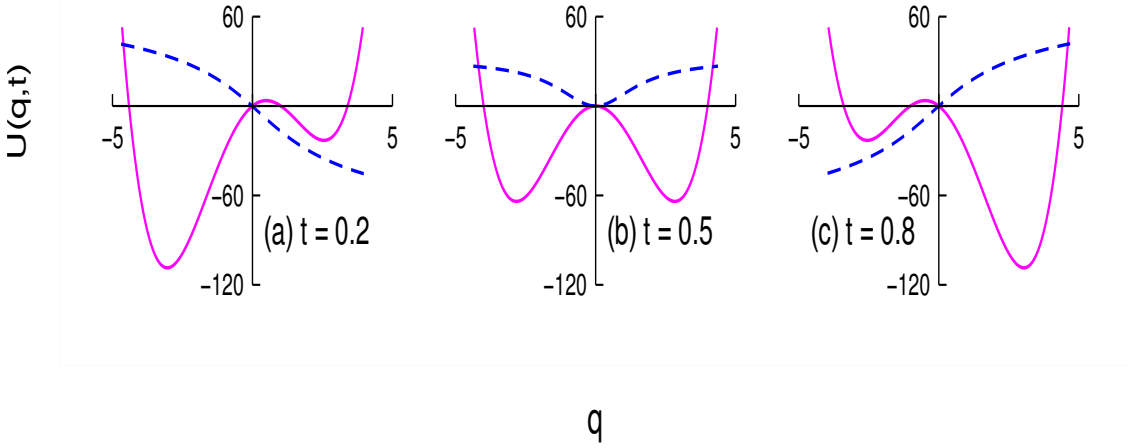

Figure 4.5: A plot of $U_0(q,t)$ and $U_{FF}(q,t)$ is shown in sold magenta and dashed blue curves respectively. $U_{FF}(q,t)$ is non-zero only in the interval $0 \leq t \leq \tau$. Shortly after $t = 0$, $U_{FF}(q,t)$ has a positive value to the left of origin and a negative value to the right of origin, which ensures that the particles from the left well are appropriately pushed towards the right well. Thereafter, the value of $U_{FF}(q,t)$ to the right of the origin begins to increase such that at $t = \tau/2 = 0.5$, an attractive well is formed. Beyond $t = 0.5$, $U_{FF}(q,t)$ starts to decrease to the left of the origin, and finally it monotonically goes to zero at $t = \tau$.

This figure confirms Eq. 4.20: the trajectories evolving under $H_{\rm FF} = H + U_{\rm FF}$ are located on a loop $\mathcal{L}_{\rm FF}(t)$ that is obtained by "shearing" the instantaneous energy shell $\mathcal{E}(t)$ along the momentum axis, by an amount $mv(q,t)$.

For scale invariant driving [34], we consider the classical analogus Hamiltonian from Eq. 3.28. The flow-field velocity is given by Eq. 3.30, and subsequently the fast-forward potential is the classical analogue of Eq. 3.33b which does not depend on I_0 [34]. In this rather special case, every trajectory evolving under $H_{\rm FF}$ returns to its adiabatic energy shell at $t = \tau$, $J(z,t)$ is a *global* dynamical invariant – it is the Lewis-Riesenfeld invariant [75, 76] – and microcanonical initial distributions are mapped to microcanonical final distributions.

4.5 Summary

Adiabatic invariants enjoy a distinguished history in quantum and classical mechanics [77], but the problem of how to achieve adiabatic invariance under non-adiabatic conditions has gained attention only recently. Here we have shown how to construct a potential $U_{\rm FF}(q,t)$ that guides trajectories launched from a given energy shell of an initial Hamiltonian to the corresponding energy shell of the final Hamiltonian, so that the initial and final values of action are identical for every trajectory.

The results presented in this chapter effectively extend the flow-fields based method introduced in Chap. 3 to classical systems. The numerical illustrations show that trajectories distributed uniformly over an initial energy shell, under fast-forward driving, end up on the final energy shell which preserves the action. However the initial uniform distribution is not preserved. These results may offer an alternative approach to solve for quantum shortcuts to adiabaticity, which could overcome the problem that arises due to nodes discussed in Sec. 3.5. The classical fast-forward potential evaluated in this chapter, when quantized, may lead to the quantum fast-forward potential. The classical potential is free from singularities, and for large n the Correspondence Principle suggests that evolution under $\hat{H}+\hat{U}_{\rm FF}^{(n)}$ will cause the initial eigenstate $\phi_n(q,0)$ to evolve to the final eigenstate $\phi_n(q,\tau)$. This will be investigated in the next chapter.

The counterdiabatic Hamiltonian Eq. 4.11a generated by the flow-fields approach can be compared to the approaches in Refs. [25, 52, 54]. In both cases, the

classical action $I(z,t)$ is preserved along the entire trajectory. However, a crucial difference lies in the fact that the counterdiabatic Hamiltonians from the previous approaches are independent of the initial energy of the system, but the counterdiabatic Hamiltonian obtained from the flow-fields method depends on the choice of the initial energy shell (except for scale invariant driving). The quantum counterpart of the classical Hamiltonian obtained in this chapter can be compared to the previous results from Refs. [22, 24], where the quantum eigenstate $|n(t)\rangle$ is preserved along the entire trajectory. We will discuss this in the next chapter.

It is natural to ask whether our results can be applied to systems with $d > 1$ degrees of freedom. In certain situations of experimental relevance, such as ultracold gases in optical lattices, a separation of variables reduces a three-dimensional problem to an effectively one-dimensional one [11,78], providing a potential platform to test our predictions. More generally, the distinction between integrable, chaotic, and mixed phase space systems becomes crucial for d-dimensional systems [79]. For integrable systems, the transformation to action-angle variables [51] may provide a useful first step to extending our results, but for chaotic or mixed systems the task is likely to be more challenging.

Chapter 5: Quantum shortcuts for excited states

5.1 Overview

We now focus on obtaining shortcuts – that is deriving a counterdiabatic Hamiltonian and a fast-forward potential – for a quantum system initialized in an excited energy state. We particularly study the case of an arbitrary driving protocol where the no-flux criterion is not satisfied, and therefore Eqs. 3.11 and 3.14 cannot yield exact shortcuts due to the divergences associated with eigenstate, see Sec. 3.5. In this chapter, we analyze the semiclassical limit of a quantum excited state, and investigate whether classical shortcuts from Chap. 4 provide useful insights for obtaining quantum shortcuts for excited states.

We start this chapter by making a comparison of the flow-fields method for quantum and classical systems – as discussed in Chapters 3 and 4 – in Sec. 5.2. We find that the classical and quantum flow-fields do not match in the semi-classical limit. Therefore, the quantum counterpart of a classical shortcut is not the exact quantum shortcut. In Sec. 5.3, we carry out a semiclassical analysis of an energy eigenfunction. Following our analysis, we hypothesize that the classical auxiliary fields – both the counterdiabatic Hamiltonian and the fast-forward potential – from Chap. 4 should be able to produce a quantum shortcut to a very good approxi-

mation. We test this hypothesis numerically for a model system in Sec. 5.4. We numerically solve the time-dependent Schrödinger equation for a quantum system which is evolving under $\hat{U}_{FF}$ – the quantum counterpart of Eq. 4.1, and test the accuracy with which the quantum counterpart of the classical fast-forward potential of Eq. 4.11b achieves quantum fast-forward driving. In Sec. 5.5, we analyze the final distribution on the classical energy shell and combine it with the numerical results of Sec. 5.4 to quantitatively establish the relationship between the classical and quantum shortcut. In Sec. 5.6, we analytically argue that the accuracy of the quantum fast-forward driving illustrated in Sec. 5.4 will be reflected in the counterdiabatic driving as well, i.e., the quantum counterpart of the classical counterdiabatic Hamiltonian (Eq. 4.11a) will make an excited state track its adiabatic path to a very good approximation. We present concluding remarks in Sec. 5.7.

5.2 Comparison of quantum and classical flow-fields

As proposed in Ref. [25] and illustrated in Chap. 2, a classical counterdiabatic Hamiltonian emerges when the right side of Eq. 1.9 is evaluated in the semiclassical limit. Similarly, it is natural to speculate that the classical shortcuts of Chap. 4 are the semiclassical limit of the quantum shortcuts of Chap. 3. In that case the close similarity between Eqs. 4.11a, 4.11b and Eqs. 3.11, 3.14 would simply reflect the Correspondence Principle. In the following paragraph we address this issue by asking whether the flow fields $v(q,t)$ and $a(q,t)$ defined in Chap. 4 emerge from those of Chap. 3 in the semiclassical limit ($\hbar \to 0$). We will temporarily use the

superscript Q (for "quantum") to denote certain quantities defined in Chap. 3, SC to denote their semiclassical limits, and C to denote quantities defined in Chap. 4.

When we consider the semiclassical limit of the field $v^Q(q,t)$ (Eq.3.7), we immediately run into a difficulty: the divergences discussed in Sec. 3.5 proliferate in this limit, as the number of nodes of ϕ becomes large. This proliferation of divergences (nodes) arises from the rapid spatial oscillations of high-lying eigenstates $\phi(q,t)$. To obtain a non-singular velocity field, we replace the oscillatory probability density ϕ^2 (used to construct v^Q) by a locally averaged counterpart, $\overline{\phi^2}$, that smooths over these oscillations. The semiclassical limit of $\overline{\phi^2}$ is the microcanonical probability distribution, projected from phase space onto the coordinate axis [2]:

$$\lim_{\hbar\to 0}\overline{\phi^2}(q,t) = \mu(q,t) \propto \int dp\, \delta(\bar{E} - H_0) \propto \frac{1}{\bar{p}(q,t)} \tag{5.1}$$

with $\bar{p}$ given by Eq. 4.7. Using μ in place of $\bar{\phi}^2$ in Eq. 3.6 we obtain

$$\mathcal{I}^{SC}(q,t) = \int_{-\infty}^{q} \mu(q',t)\, dq'. \tag{5.2}$$

We use this function to define $v^{SC} = -\partial_t \mathcal{I}^{SC}/\partial_q \mathcal{I}^{SC}$, which is free of divergences and can be viewed as the semiclassical limit of $v^Q = -\partial_t \mathcal{I}^Q/\partial_q \mathcal{I}^Q$ (Eq. 3.7). Comparing $v^{SC}(q,t)$ with the field $v^C(q,t)$ defined by Eq. 4.9a, we see that while one is constructed from the integrated microcanonical distribution $\mathcal{I}^{SC} = \int^q \mu\, dq'$, the other is constructed in terms of the phase space enclosed by the energy shell, $\mathcal{S} = \int^q \bar{p}\, dq'$. Therefore, in general, the two fields differ: $v^{SC} \neq v^C$. We conclude that Eq. 4.11a

should not be viewed as the semiclassical limit of Eq. 3.11. Similar comments apply to the acceleration field $a(q,t)$.

We summarize the situation as follows: while the flow fields v and a are defined similarly in the quantum and classical cases (compare Figs. 3.1 and 4.2), and while the construction of counterdiabatic and fast-forward terms from the flow fields is essentially identical in the two cases, the Correspondence Principle does not provide an adequate explanation for this striking similarity. We also note that scale-invariant driving (Eq. 3.28) provides an exception to this general conclusion: in that case the quantum and classical flow fields are in fact identical [34, 56].

As a final item of semiclassical comparison, let us consider trajectories evolving under the classical Hamiltonian $H_0 + U_{FF}$, with initial conditions sampled from the adiabatic energy shell (Fig. 4.4). It was shown in Ref. [56] that the function

$$J(q,p,t) = I(q, p - mv(q,t), t) \tag{5.3}$$

remains constant along these trajectories: $J(t) = I_0$ for all t. This is illustrated in Fig. 4.3, where the thick red curve is obtained by "boosting" the thin black curve – the adiabatic energy shell – by an amount $mv(q,t)$ along the momentum direction. Now consider the fast-forward wavefunction $\bar{\psi} = \phi\, e^{i\alpha}\, e^{iS/\hbar}$ (Eq. 3.20) evolving under $\hat{H}_0 + \hat{U}_{FF}$. Let us approximate the eigenstate $\phi(q,t)$ by the semiclassical form [2]

$$\phi = A_+ e^{+(i/\hbar)\int^q \bar{p}\, dq'} + A_- e^{-(i/\hbar)\int^q \bar{p}\, dq'} \tag{5.4}$$

where $|A_\pm(q,t)| \propto \sqrt{1/\bar{p}}$. The terms on the right side of Eq. 5.4 represent a right-moving wave train and a left-moving wave train, with local momenta corresponding to the upper and lower branches $\pm\bar{p}$ of the adiabatic energy shell (Fig. 4.2). Then for the fast-forward wavefunction we get

$$\bar{\psi} = \phi\, e^{i\alpha}\, e^{iS/\hbar} = A_+ e^{i\alpha}\, e^{(i/\hbar)\int^q (\bar{p}+mv)\, dq'} + A_- e^{i\alpha}\, e^{(i/\hbar)\int^q (-\bar{p}+mv)\, dq'} \tag{5.5}$$

since $S = \int^q mv\, dq'$ (Eq. 3.15). The terms in Eq. 5.5 are wave trains with local momenta $\pm\bar{p} + mv$. Thus the fast-forward wavefunction $\bar{\psi}$ is represented, in the semiclassical sense, by a "boosted" adiabatic energy shell similar to the one shown as a thick red curve in Fig. 4.3. Although this interpretation provides a neat correspondence between the quantum and classical fast-forward methods, it should not be taken too literally, since the fast-forward method of Chap. 3 generally applies only to the ground state (as discussed earlier), where the semiclassical approximation (Eq. 5.4) is not generally accurate.

5.3 Auxiliary fields for excited states

Motivated by the need to obtain experimentally implementable shortcuts for general, i.e., non scale-invariant systems, we proceed to find $\hat{H}_{CD}(t)$ and $U_{FF}(\hat{q},t)$ for excited states. Note that $\hat{U}_{FF}(t)$ due to its local nature is more practical for experimental purposes compared to $\hat{H}_{CD}(t)$ which has a non-local behaviour. In Chaps. 3 and 4, we have shown that it is straightforward to obtain $\hat{U}_{FF}(t)$ once a counterdiabatic Hamiltonian of the form $\hat{H}_{CD}(t) \propto \hat{p}\hat{v} + \hat{v}\hat{p}$ is obtained. The coun-

terdiabatic Hamiltonian $\hat{H}_{CD}(t)$ produces an appropriate non-linear stretching in an energy eigenfunction in order to drive it through the adiabatic path, as described in Sec. 3.3. However a quantum flow-field velocity $v(\hat{q},t)$ cannot be obtained for excited states due to the presence of nodes, see Sec. 3.5. Therefore we cannot obtain a perfect counterdiabatic Hamiltonian of the form $\hat{H}_{CD}(t) \propto \hat{p}\hat{v} + \hat{v}\hat{p}$ for excited states. Based on the quantum-classical correspondence principle, we anticipate that in the semiclassical limit, the classical velocity $v(q,t)$ may lead to an approximate expression for a quantum velocity $v(\hat{q},t)$ which does not suffer from divergences. As a result we might obtain approximate expressions for $\hat{H}_{CD}(t)$ and $U_{FF}(\hat{q},t)$ in the semiclassical limit.

In the semiclassical limit, an energy eigenfunction of a Hamiltonian $H_0(t)$ be expressed in terms of an amplitude and a phase as shown in Eq. 5.4. The semiclassical eigenfunction has a a natural interpretation in terms of the classical energy shell in phase space whose energy corresponds to the quantum energy eigenvalue as discussed in Sec. 5.2. The phase $\int \bar{p}dq$ is half of $\mathcal{S}(q,t)$ defined in Eq. 4.8 (not to be confused with $S = \int^q mv\, dq'$, (Eq. 3.15)), and the amplitude denotes a microcanonical probability distribution on this energy shell as shown in Eq. 5.1.

Consider the eigenvalue equation, $H_0|\phi\rangle = E|\phi\rangle$, (Eq. 3.3), for a high lying state $|\phi\rangle$. The corresponding adiabatic wavefunction is $\psi_{ad}(q,t) = \langle q|\phi\rangle \exp\left[-i/\hbar(\int_0^t E(t')dt')\right]$, (Eq. 3.4). For an ideal $\hat{H}_{CD}(t) \propto \hat{p}\hat{v} + \hat{v}\hat{p}$ which would carry out perfect counterdia-

batic driving, $\psi_{ad}(q,t)$ satisfies Eq. 3.5. It follows that

$$\begin{aligned}
\left[\hat{H}_0 + \frac{1}{2}(\hat{p}\hat{v} + \hat{v}\hat{p})\right]|\psi_{ad}\rangle &= i\hbar\frac{\partial|\psi_{ad}\rangle}{\partial t} \\
\implies \hat{H}_0|\phi\rangle + \frac{1}{2}(\hat{p}\hat{v} + \hat{v}\hat{p})|\phi\rangle &= E|\phi\rangle + i\hbar\frac{\partial|\phi\rangle}{\partial t} \\
\implies \frac{1}{2}(\hat{p}\hat{v} + \hat{v}\hat{p})|\phi\rangle &= i\hbar\frac{\partial|\phi\rangle}{\partial t}. \qquad (5.6)
\end{aligned}$$

Substituting Eq. 5.4 in Eq. 5.6 and separating the real and the imaginary parts of the equation, we get

$$\partial_t\mathcal{S} + v\partial_q\mathcal{S} = 0, \quad \text{and} \qquad (5.7a)$$

$$\partial_t A_\pm + v\partial_q A_\pm + \frac{1}{2}\partial_q v A_\pm = 0$$

$$\text{or equivalently} \quad \partial_t\rho + \partial_q(v\rho) = 0 \qquad (5.7b)$$

respectively. Note that since we are considering a kinetic plus potential type of Hamiltonian, the energy shell in phase space is symmetric about the q-axis. Defining ρ as $\rho = |A_\pm(q,t)|^2 \propto 1/\bar{p}$, leads to Eq. 5.7b. A perfect velocity $v(q,t)$ must satisfy both the conditions of Eq. 5.7. While Eq. 5.7a describes the deformation of the energy shell, Eq. 5.7b describes the deformation of the microcanonical distribution in space. Except for the special case of scale-invariant driving where the topology of the system is preserved throughout the evolution, there is no reason why a single function $v(q,t)$ should satisfy both the conditions in Eqs. 5.7 simultaneously. This means that for a generic system, we cannot find a perfect $v(q,t)$. This deduction derived from a semiclassical analysis of $|\psi_{ad}\rangle$ aligns with the deduction made in

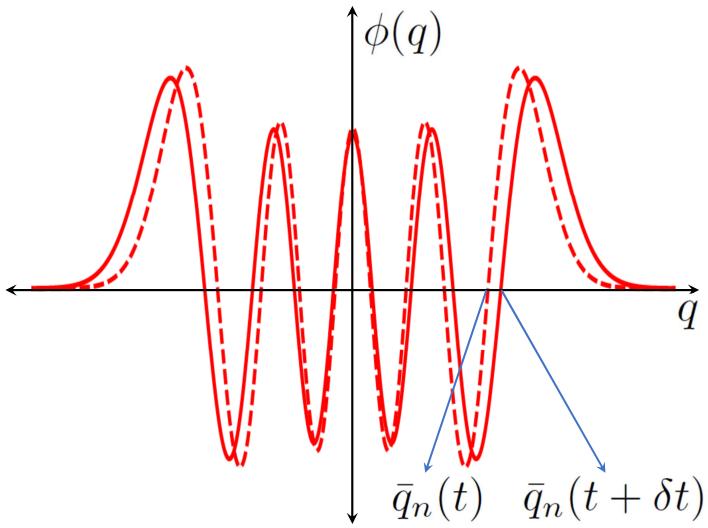

Figure 5.1: A schematic plot of $\phi(q)$ vs. q is presented at times t and $t+\delta t$, represented by dashed and solid curves respectively. The n'th node $\bar{q}_n$ is shown at times t and $t+\delta t$. The wavefunction $\psi(q,t)$ evolving under $\hat{H}_0+\hat{H}_{CD}$ should be guided by the auxiliary term in a way that $\psi(\bar{q}_n,t)=\phi(\bar{q}_n,t)$ is satisfied for every node at every instant, i.e., the nodes of $\phi(q,t)$ and $\psi(q,t)$ should align at every instant.

Sec. 3.5, although the analysis carried out to reach the deduction are different. We now focus on deriving a function $v(q,t)$ which satisfies at least one of the conditions of Eq. 5.7. Since the quantum number is the quantum adiabatic invariant, Eq. 5.7a, which is an equation dependent on the energy shell (instead of the distribution on the shell), gains priority and we focus on obtaining a $v(q,t)$ that satisfies Eq. 5.7a. We expect that $v(q,t)$, should be able to move the nodes of the wavefunction $\psi(q,t)$ evolving under $\hat{H}_0+\hat{H}_{CD}$ appropriately such that they align with the nodes of the instantaneous eigenfunction $\phi(q,t)$. If $\bar{q}_n(t)$ denotes the position of the n'th node of $\phi(q,t)$, then the relation $\psi(\bar{q}_n,t)=\phi(\bar{q}_n,t)$ is desired at every instant for all the nodes. Since the $v(q,t)$ we look for need not satisfy Eq. 5.7b, we anticipate that the amplitude of $\psi(q,t)$ need not overlap with the amplitude of $\psi_{ad}(q,t)$. A close

inspection of Eq. 5.7a indicates that it is identical to Eq. 4.9a which defines the classical flow-field velocity $v(q,t)$. We therefore hypothesize that the classical flow-field velocity and the resulting classical auxiliary fields, upon quantization, will lead to counterdiabatic and fast-forward driving to a very good approximation.

We can also arrive at the hypothesis stated above by carrying out a slightly different analysis of the semiclassical eigenfunction. As the quantum number of the semiclassical wavefunction is related more closely with the equivalent classical energy shell than with the distribution on it, we look for $\hat{H}_{CD}$, or equivalently a $v(q,t)$ which drives the phase appropriately. Driving the phase of the evolving wavefunction $|\psi(t)\rangle$ in conjunction with the phase of $|\phi(t)\rangle$ is equivalent to driving $|\psi\rangle$ in such a way that at every instant its nodes move appropriately and coincide with the nodes of $|\phi\rangle$. The auxiliary fields should therefore preserve the following relation for every set of consecutive nodes, see Fig. 5.1:

$$\bar{p}(q_{\bar{n}})(q_{n+1} - q_n) = \bar{p}(q_{\bar{n}})\delta q \simeq \pi\hbar. \tag{5.8}$$

This condition is similar to the Bohr-Sommerfeld quantization condition. The quantity $\pi\hbar$ on the right side was obtained from Eq. 5.4 upon using $|A_{\pm}| \propto \sqrt{1/\bar{p}}$, and combining the two terms to obtain a cosine term. Eq. 5.8 equivalent to demanding that the action of the classical energy shell, whose energy corresponds to the energy of the quantum eigenstate should be preserved. The problem of preserving the classical action has been addressed in Chap. 4 and Eqs. 4.11 provide the solution. We therefore arrive at the same hypothesis that the classical flow-field

velocity and the resulting classical auxiliary fields, upon quantization, should lead to counterdiabatic and fast-forward driving to a very good approximation. We test this hypothesis numerically in the next section.

5.4 Numerical illustration

We now test the hypothesis proposed in the previous section by using the example of a model double-well Hamiltonian. We use the quantized counterpart $\hat{H}_0(t)$ of the classical model Hamiltonian $H_0(t)$, defined in Eq. 4.21. Unless specified otherwise, the mass of the particle m and Planck's reduced constant $\hbar$ are set to unity. In this section, we initialize the system in an energy eigenstate of $\hat{H}_0(t)$ and compare the final states obtained numerically after subjectng it to the following two evolutions governed by time-dependent Schrödinger equation – one under the bare Hamiltonian $\hat{H}_0(t)$, and the other under the full Hamiltonian $\hat{H}_0(t) + U_{FF}(\hat{q}, t)$. The quantum fast-forward potential $U_{FF}(\hat{q}, t)$ was obtained by quantizing the classical fast-forward potential $U_{FF}(q, t)$, which was in turn numerically obtained upon implementing Eq. 4.11b.

We start by describing how to obtain the n'th energy eigenstate $|\phi_n\rangle$ numerically. We first rewrite $\hat{H}_0(t)$ as a sum of a harmonic-oscillator Hamiltonian $\hat{H}_{HO}(t)$ and a

potential $U(\hat{q},t)$ as shown below:

$$\begin{aligned}\hat{H}_0(t) &= \frac{\hat{p}^2}{2} + \hat{q}^4 - 16\hat{q}^2 + \lambda(t)\hat{q} \\ &= \left[\frac{\hat{p}^2}{2} + \frac{1}{2}\omega^2\hat{q}^2\right] + \left[\hat{q}^4 - \left(16 + \frac{1}{2}\omega^2\right)\hat{q}^2 + \lambda(t)\hat{q}\right] \\ &= \hat{H}_{HO}(t) + U(\hat{q},t). \end{aligned} \tag{5.9}$$

We drop the time argument in the remainder of the paragraph as we are only interested in the eigenfunction $\phi_n(q,t)$ at the initial time $t = 0$. We choose $\omega = 2$ for our analysis. Let the eigenstates of $\hat{H}_{HO}$ be represented by Greek letters, such as $|\alpha\rangle$, $|\beta\rangle$, etc. The matrix representation of $\hat{H}_0$ in the basis of $\hat{H}_{HO}$ can be obtained by making use of the following set of equations:

$$H_{SO,\alpha\beta} = \begin{cases} \left(\beta + \frac{1}{2}\right)\hbar\omega & \alpha = \beta \\ 0 & \text{otherwise} \end{cases}, \tag{5.10}$$

$$\lambda q_{\alpha\beta} = \lambda\sqrt{\frac{\hbar}{2m\omega}} \begin{cases} \sqrt{\beta} & \alpha = \beta - 1 \\ 0 & \text{otherwise} \end{cases}, \tag{5.11}$$

$$q^4_{\alpha\beta} = \left(\frac{\hbar}{2m\omega}\right)^2 \begin{cases} 6\beta^2 + 6\beta + 3 & \alpha = \beta \\ \sqrt{\beta(\beta-1)(\beta-2)(\beta-3)} & \alpha = \beta - 2 \\ (4\beta - 2)\sqrt{\beta(\beta-1)} & \alpha = \beta - 4 \\ 0 & \text{otherwise} \end{cases}, \tag{5.12}$$

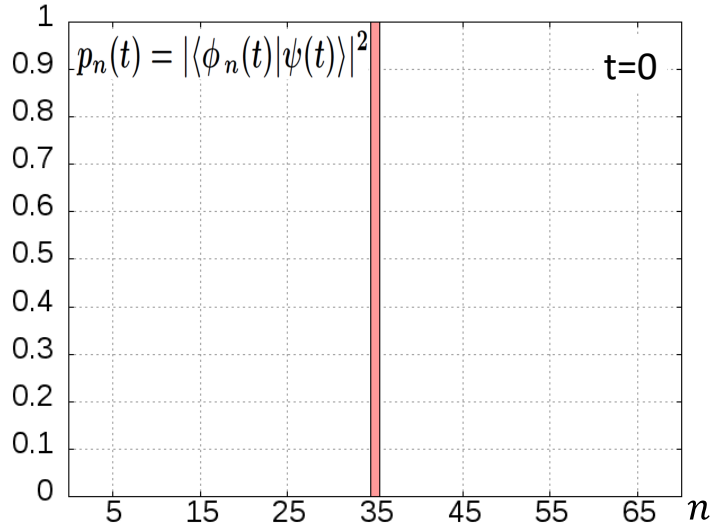

Figure 5.2: A plot of $p_n(t) = |\langle\phi_n(t)|\psi(t)\rangle|^2$ vs. n is presented at the initial time $t = 0$. The system is initialized in the 35^{th} energy eigenstate, which is depicted by the single peak at $n = 35$ with $p_{35}(t = 0) = 1.0$.

$$\eta q^2_{\alpha\beta} \;=\; \eta\left(\frac{\hbar}{2m\omega}\right)\begin{cases} 2\beta+1 & \alpha=\beta \\ \sqrt{\beta(\beta-1)} & \alpha=\beta-2\ , \\ 0 & \text{otherwise} \end{cases} \tag{5.13}$$

where $\eta = 16+\omega^2/2$. In the equations above, we have assumed $\alpha \leq \beta$ and obtained the upper triangular elements. Since $\hat{H}_0$ is Hermitian, the relation $H_{0,\alpha\beta} = H_{0,\beta\alpha}$ enables us to obtain the remaining elements. The Hamiltonian matrix can then be diagonalized to obtain eigenvectors. The n'th energy eigenfunction $|\phi_n\rangle$ of $\hat{H}_0$ can be expressed as

$$|\phi_n\rangle = \sum_\alpha c_{n,\alpha}|\alpha\rangle, \tag{5.14}$$

where the coefficients $c_{n,\alpha}$ are the elements of the n'th eigenvector.

The results below are presented for the 35'th energy eigenstate, corresponding

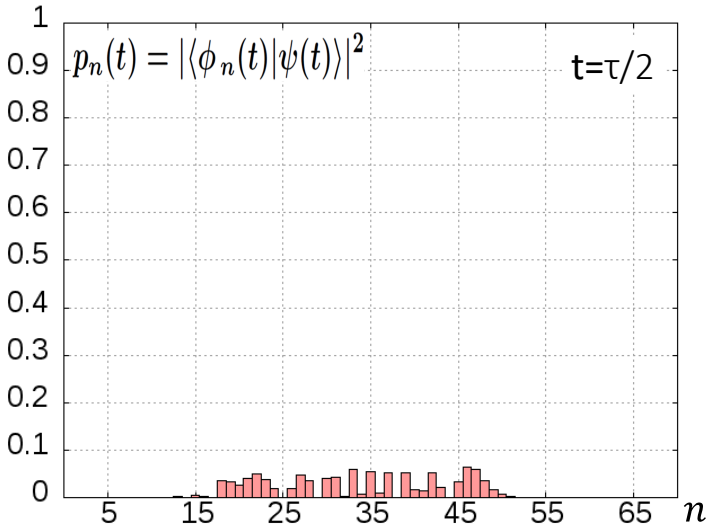

(a) Plot of $p_n(t) = |\langle \phi_n(t)|\psi(t)\rangle|^2$ vs. n at time $t = \tau/2$ for evolution under $\hat{H}_0(t)$.

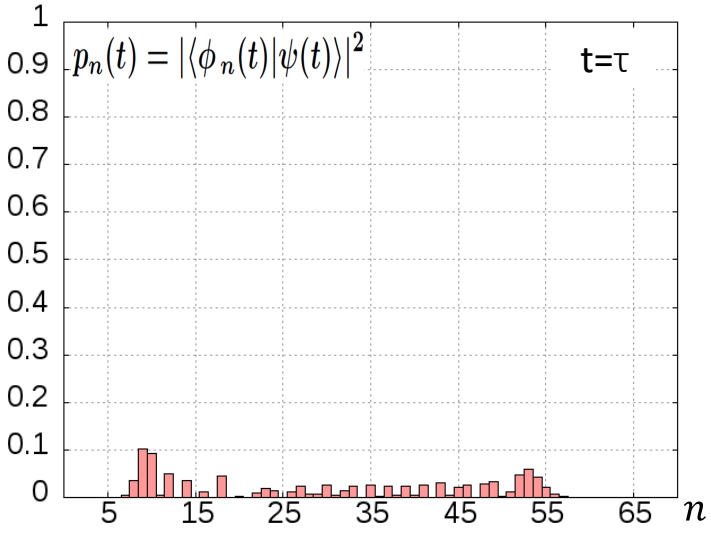

(b) Plot of $p_n(t) = |\langle \phi_n(t)|\psi(t)\rangle|^2$ vs. n at the final time $t = \tau$ for evolution under $\hat{H}_0(t)$.

Figure 5.3: The plots above depict the overlap between the wavefunction $|\psi(t)\rangle$ as it evolves under $\hat{H}_0(t)$ (defined in Eq. 5.9), and the instantaneous energy eigenfunctions $|\phi_n(t)\rangle$ for $0 \leq n \leq 70$. The system is initialized in the 35'th eigenstate, $|\psi(0)\rangle \equiv |\phi_n(t)\rangle$. The system is in a superposition of instantaneous eigenstates at an intermediate time as well as at the final time. The system has developed excitations during the evolution and is unable to reach the final adiabatic state at $t = \tau$. This final state is analogous to the classical final state where the trajectories do not end on the desired energy shell, see Fig. 4.4(b).

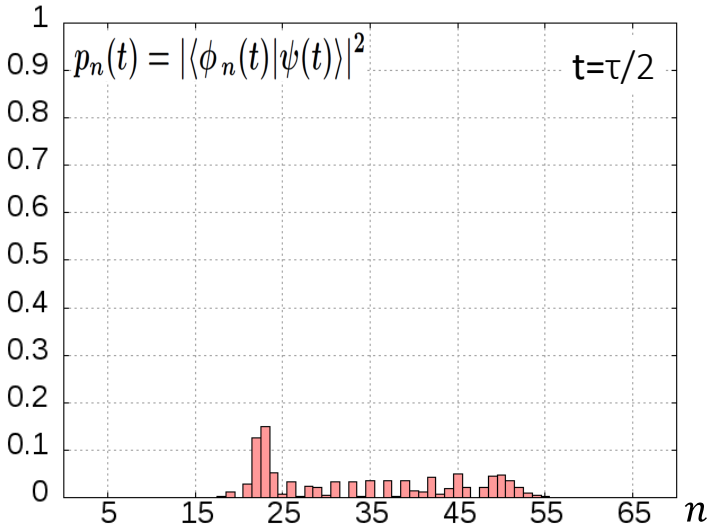

(a) Plot of $p_n(t) = |\langle \phi_n(t)|\psi(t)\rangle|^2$ vs. n at time $t = \tau/2$ for evolution under $\hat{H}_0(t) + U_{FF}(\hat{q}, t)$.

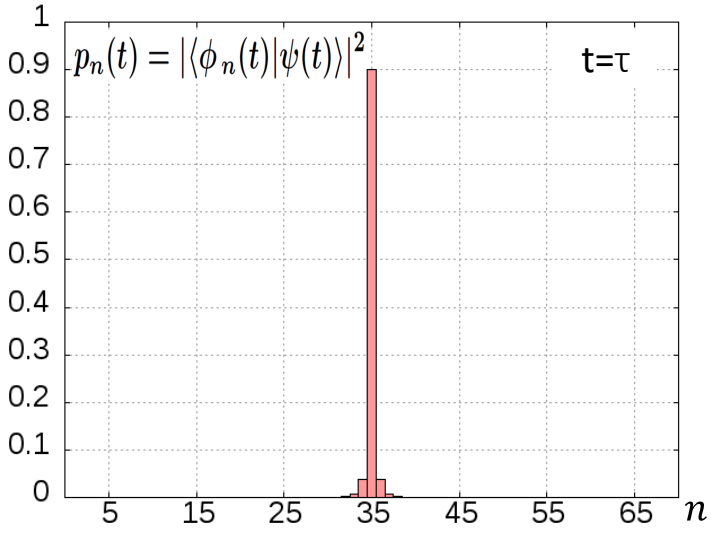

(b) Plot of $p_n(t) = |\langle \phi_n(t)|\psi(t)\rangle|^2$ vs. n at the final time $t = \tau$ for evolution under $\hat{H}_0(t) + U_{FF}(\hat{q}, t)$.

Figure 5.4: Same as Fig. 5.3, except that the system evolves under $\hat{H}_0(t)+U_{FF}(\hat{q}, t)$, where $U_{FF}(\hat{q}, t)$ is the quantized counterpart of the classical fast-forward potential $U_{FF}(q, t)$ which is obtained numerically from Eq. 4.11b. The system is in a superposition of instantaneous eigenstates at an intermediate time, but it reaches the desired final state at $t = \tau$ with high accuracy. At the final time, $|\psi(\tau)\rangle$ has a 90% overlap with $|\phi_{35}(\tau)\rangle$, i.e., $p_{35} = 0.90$. The combined probability $p_{34} + p_{35} + p_{36} = 0.98$. Fig. 5.4(b) is analogous to the classical final state where the trajectories end on the desired energy shell but the initial uniform distribution is not preserved, see Fig. 4.4(c).

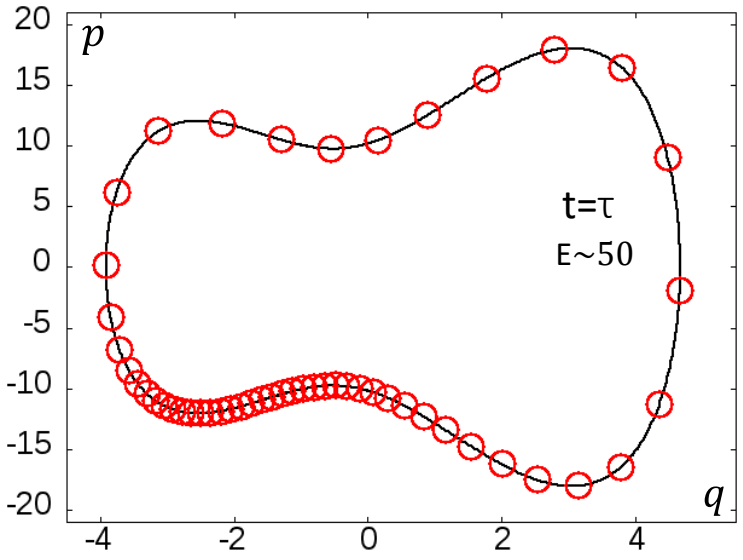

(a) Plot of the final distribution of classical trajectories on the energy shell for $E = 51.76$, when fifty uniformly distributed initial trajectories evolve under the analogous classical Hamiltonian $H_0(t) + U_{FF}(q,t)$.

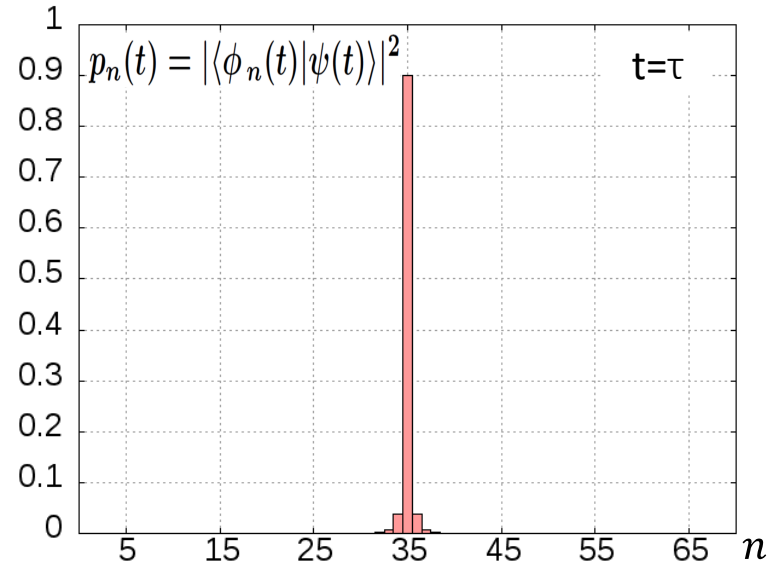

(b) Plot of $p_n(t) = |\langle\phi_n(t)|\psi(t)\rangle|^2$ vs. n at time $t = \tau$. The system is initialized in $|\psi(0)\rangle \equiv |\phi_{35}(0)\rangle$ and evolves under $\hat{H}_0(t) + U_{FF}(\hat{q},t)$.

Figure 5.5: The final distribution of classical trajectories is non-uniform as depicted in the phase-space plot. This non-uniformity is reflected in the quantum evolution as depicted in the plot of $p_n(\tau) = |\langle\phi_n(\tau)|\psi(\tau)\rangle|^2$ vs. n (same as Fig. 5.4(b)). The peak value is $p_{35}(\tau) = 0.90$.

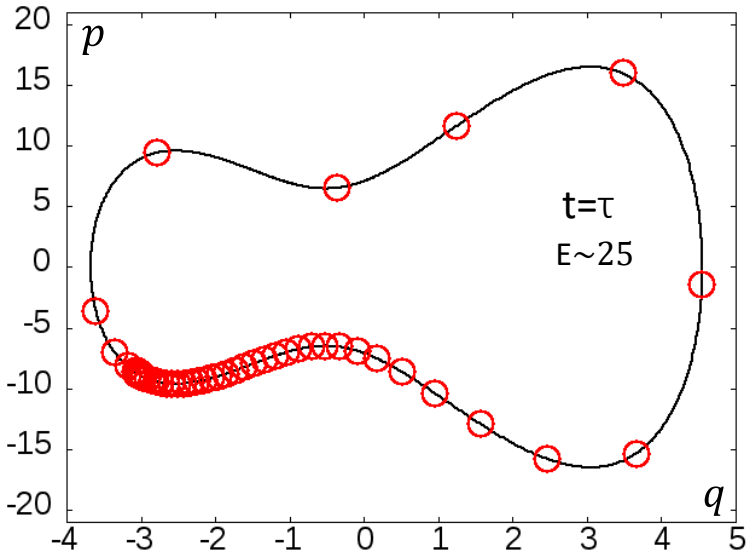

(a) Plot of the final distribution of classical trajectories on the energy shell for $E = 25.08$, when fifty uniformly distributed initial trajectories evolve under the analogous classical Hamiltonian $H_0(t) + U_{FF}(q,t)$.

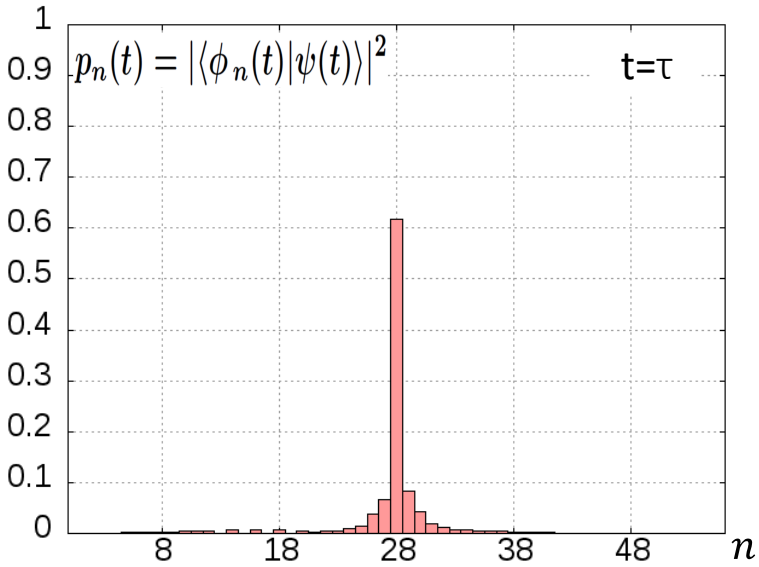

(b) Plot of $p_n(t) = |\langle\phi_n(t)|\psi(t)\rangle|^2$ vs. n at time $t = \tau$. The system is initialized in $|\psi(0)\rangle \equiv |\phi_{28}(0)\rangle$ and evolves under $\hat{H}_0(t) + U_{FF}(\hat{q},t)$.

Figure 5.6: Same as Fig. 5.6, except $E = 25.08$ and $n = 28$. The final classical distribution has a higher degree of non-uniformity compared to Fig. 5.5(a), which is reflected in the quantum evolution. In Fig. 5.6(b), the peak value is $p_{28}(\tau) = 0.62$, and sideband excitations are more prominent compared to Fig. 5.5(b).

to an initial eigenvalue $E = 51.76$. The time-dependent parameter $\lambda(t)$ varied from -16 to $+16$ over a time $\tau = 1.0$ according to Eq. 4.21b, which resulted in a non-adiabatic driving of the Hamiltonian. The initial energy eigenfunction was subjected to two different evolutions – one under time-dependent Schrödinger equation with the bare Hamiltonian $\hat{H}_0(t)$, and the other with $\hat{H}_0(t) + U_{FF}(\hat{q}, t)$. The numerical methods used to evolve the quantum and classical systems are specified in Secs. 4.4 and 3.7 respectively. Figs. 5.2 - 5.4 plot the probability $p_n(t) = |\langle\phi_n(t)|\psi(t)\rangle|^2$, which quantifies the overlap between the evolving wavefunction $|\psi(t)\rangle$ and the instantaneous eigenfunction $|\phi_n(t)\rangle$. At $t = 0$, $\psi(0) \equiv \phi_{35}(0)$ which means $p_n(0) = 1$ for $n = 35$ and vanishes for all other values of n, as illustrated in Fig. 5.2. Figs. 5.3(a) and 5.4(a) plots $p_n(t)$ at an intermediate time $t = \tau/2 = 0.5$. It can be seen that the evolving wavefunction $|\psi(t)\rangle$ is in a superposition of the instantaneous eigenfunctions $|\phi_n(t)\rangle$ for both the evolution protocols. The plots $p_n(t)$ at the final time $t = \tau = 1.0$ are illustrated in Figs. 5.3(b) and 5.4(b). Fig. 5.3(b) indicates that the final state $|\psi(\tau)\rangle$ which evolves under $\hat{H}_0(t)$ is in a superposition of eigenfunctions having undergone excitations during the evolution. On the other hand, as seen in Fig. 5.4(b), the final state $|\psi(\tau)\rangle$ which has evolved under $\hat{H}_0(t) + U_{FF}(\hat{q}, t)$ is very close to the 35'th eigenfunction $\phi_{35}(\tau)$. At the final time, $U_{FF}(\hat{q}, t)$ produces a peak at $n = 35$ with $p_{35}(\tau) = 0.90$ indicating that it achieves fast-forward driving with a high accuracy by supressing excitations. The combined probability of the peak and the immediate sidebands yield $p_{34}(\tau) + p_{35}(\tau) + p_{36}(\tau) = 0.98$.

Several other initial conditions were tested and it was verified that the composite Hamiltonian $\hat{H}_0(t) + U_{FF}(\hat{q}, t)$ always outperformed the bare Hamiltonian $\hat{H}_0(t)$

in supressing excitations. The numerical results support our hypothesis that the quantized counterpart of a classical fast-forward potential can achieve quantum fast-forward driving with a high accuracy. It was also observed that the degree of accuracy achieved by the quantum fast-forward potential $U_{FF}(\hat{q},t)$ is directly related to the degree of uniformity in the final distribution of trajectories achieved by the analogous classical fast-forward potential $U_{FF}(q,t)$. This is illustrated in Figs. 5.5 and 5.6, where the system is initialized in $n = 35$ and $n = 28$ with a corresponding value of $E = 51.76$ and $E = 25.08$ respectively. The evolution protocol is same as specified in the previous paragraph. The degree of non-uniformity of the final distribution of classical trajectories is lower in Fig. 5.5(a) than in Fig. 5.6(a). This is reflected in the quantum evolution as seen in Figs. 5.5(b) and 5.6(b). The sidebands for $n = 28$ are significantly more prominent than for $n = 35$. For the quantum state initialized in $n = 28$, $p_{28}(\tau) = 0.62$ and $p_{27}(\tau) + p_{28}(\tau) + p_{29}(\tau) = 0.77$.

5.5 Semiclassical analysis of quantum peaks and final classical distribution

In this section, we will show that the numerical peaks obtained in the previous section can be determined quantitatively by analyzing the final distribution on the classical energy shell (from Sec. 4.4), and relating it to the semiclassical representation $\psi_{SC,E}(q,\tau)$ of the final state $|\psi(\tau)\rangle$ which has evolved under fast-forward driving. We assume throughout this section that $\psi_{SC,E}(q,t)$ is initialized in the n'th energy eigenstate of $\hat{H}_0$, and evolves under $\hat{H}_0 + \hat{U}_{FF}$ during the interval $0 \leq t \leq \tau$.

Here, $\hat{H}_0$ and $\hat{U}_{FF}$ are obtained by quantizing Eqs. 4.1 and 4.11b respectively. Let $\psi_{SC,k}(q,t)$ denote the semiclassical wavefunction of the k'th energy eigenstate of $\hat{H}_0$. Let $\rho_{MC,k}(q,\tau)$ denote the microcanonical distribution on the final energy shell whose energy corresponds to the k'th quantum level. For a classical system starting initialized in a microcanonical distribution on an energy shell and evolving under $H_0 + U_{FF}$, let $\rho_E(q,\tau)$ denote the final distribution on the classical energy shell. For an initial action I_k we define

$$\bar{\mathcal{S}}_k(q, I_k) = \int^q \bar{p}(q', I_k) dq', \tag{5.15}$$

where the intergral is carried out on an energy shell whose energy is equal to the k'th energy eigenvalue of $\hat{H}_0$. The wavefunctions $\psi_{SC,k}$ and $\psi_{SC,E}$ can be expressed respectively as

$$\psi_{SC,k}(q,t) = A_{MC,k,+} \exp\left(i\frac{\bar{\mathcal{S}}_k}{\hbar}\right) + A_{MC,k,-} \exp\left(i\frac{\bar{\mathcal{S}}_k}{\hbar}\right) \tag{5.16}$$

and

$$\psi_{SC,E}(q,t) = A_{E,+} \exp\left(i\frac{\bar{\mathcal{S}}_n}{\hbar}\right) + A_{E,-} \exp\left(i\frac{\bar{\mathcal{S}}_n}{\hbar}\right), \tag{5.17}$$

where the subscripts '+' and '−' corresponds to the upper and lower branch of the energy shell, the functional dependences have been dropped. The amplitudes are

related to the distribution on the energyshell as

$$A_E \equiv \sqrt{\rho_E} \tag{5.18a}$$

$$A_{MC,k} \equiv \sqrt{\rho_{MC,k}} \tag{5.18b}$$

The overlap between $\psi_{SC,k}(q,\tau)$ and $\psi_{SC,E}(q,\tau)$ can be calculated as shown below. We show the analysis only for the upper branch of a classical energy shell and drop the functional dependences. The analysis for the lower branch follows the exact same behaviour. We have for the uppper branch,

$$\langle \psi_{SC,k} | \psi_{SC,E} \rangle = \int_{q_L}^{q_R} dq' A_{E,+} A_{MC,k,+} \exp\left[\frac{i}{\hbar}(\bar{\mathcal{S}}_n - \bar{\mathcal{S}}_k)\right], \tag{5.19}$$

where q_L and q_R denote the left and right turning points respectively. The Taylor expansion of $\bar{\mathcal{S}}(q, I_n)$ is carried out to obtain

$$\begin{aligned} \bar{\mathcal{S}}(q, I_n) &= \bar{\mathcal{S}}(q, I_k) + \frac{\partial \bar{\mathcal{S}}}{\partial I}(I_n - I_k) + \dots \\ &= \bar{\mathcal{S}}(q, I_k) + (n-k)\hbar\theta + \mathcal{O}(\hbar^2), \end{aligned} \tag{5.20}$$

where $\theta = \partial \bar{\mathcal{S}}/\partial I$ is the *angle* variable and the Bohr-Sommerfeld quantization relation, $I_n = (n + 1/2)\hbar$, has been used for simplication. By applying a change of variables from q to θ, Eq. 5.19 becomes

$$\langle \psi_{SC,k} | \psi_{SC,E} \rangle = \int_0^{\pi} d\theta e^{i(n-k)\theta} \frac{\tilde{A}_{E,+}(\theta)}{\sqrt{2\pi}} \tag{5.21}$$

where $\tilde{A}_{E,+}$ is the representation of $A_{E,+}$ in the angle coordinates and the following transformations have been made:

$$dq \rightarrow d\theta, \tag{5.22a}$$

$$q_L \rightarrow 0, \tag{5.22b}$$

$$q_R \rightarrow \pi, \tag{5.22c}$$

$$A^2_{MC,k,+}dq \rightarrow \frac{1}{2\pi}d\theta \tag{5.22d}$$

$$\text{and} \quad A^2_{E,+}dq \rightarrow \tilde{A}^2_{E,+}d\theta. \tag{5.22e}$$

Note that Eqs. 5.22d and 5.22e are obtained by equating the fractional probability of final trajectories in an infinitesimal region of the energy shell. Note that Eq. 5.21 indicates that the numerical peaks of Sec. 5.4 are related to the Fourier transform of the final classical distribution expressed in the angle coordinates. The quantum superposition $p_n(\tau) = |\langle\phi_n(\tau)|\psi(\tau)\rangle|^2$, of the final state $|\psi(\tau)\rangle$ which has evolved under fast-forward driving, and the energy eigenfunctions $|\phi_n(\tau)\rangle$ is plotted as a bar-graph, while $|\langle\psi_{SC,n}|\psi_{SC,E}\rangle|^2$ (Eq. 5.21) is depicted by blue dots in Fig. 5.7. The blue dots, which are derived from the classical final distribution overlap perfectly with the bars, which result from the quantum fast-forward evolution under time-dependent Schrödinger equation. The semiclassical analysis clearly establishes a relation between the classical and the quantum fast-forward driving.

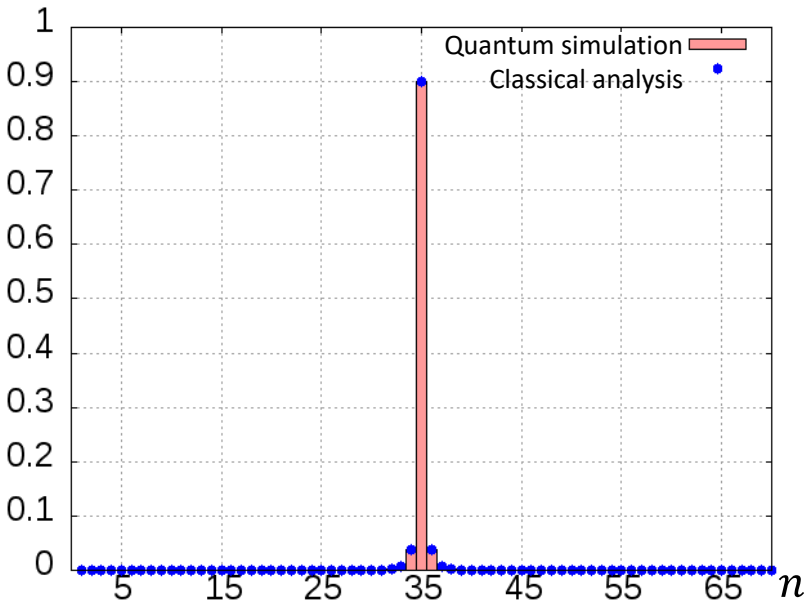

Figure 5.7: A plot of $p_n(t) = |\langle\phi_n(t)|\psi(t)\rangle|^2$ vs. n is presented at the initial time $t = 0$. The system is initialized in the 35^{th} energy eigenstate, which is depicted by the single peak at $n = 35$ with $p_{35}(t = 0) = 1.0$.

5.6 Relating counterdiabatic and fast-forward driving

We have numerically shown in Sec. 5.4 that the quantum counterpart of the classical fast-forward potential (Eq. 4.11b) leads to quantum fast-forward driving with a high accuracy. Given this result, we can analytically show that the quantum counterpart of the classical counterdiabatic Hamiltonian (Eq. 4.11a) leads to quantum counterdiabatic driving with the same level of accuracy. In this section we prove the following statement: If a wavefunction ψ_{FF} satisfies the time-dependent Schrödinger equation

$$\left[\hat{H}_0(t) + U_{FF}(\hat{q}, t)\right] \psi_{FF}(t) = i\hbar \frac{\partial \psi_{FF}(t)}{\partial t}, \tag{5.23}$$

then, the wavefunction ψ_{CD} related to ψ_{FF} as

$$\psi_{CD}(q,t) = \psi_{FF}(q,t) \exp\left[-i\frac{S(q,t)}{\hbar}\right], \tag{5.24}$$

will satisfy the time-dependent Schrödinger equation

$$\left[\hat{H}_0(t) + \hat{H}_{CD}(t)\right] \psi_{CD}(t) = i\hbar\frac{\partial\psi_{CD}(t)}{\partial t}. \tag{5.25}$$

In the statement above $U_{FF}(\hat{q},t)$ is obtained by quantizing Eq. 4.11b and $\hat{H}_{CD}(t)$ is obtained by quantizing Eq. 4.11a to obtain

$$\hat{H}_{CD}(t) = \frac{1}{2}\left(\hat{p}\hat{v} + \hat{v}\hat{p}\right), \tag{5.26}$$

where $\hat{v}$ is the quantum counterpart of Eq. 4.9a. The function $S(q,t)$ (not to be confused with $\mathcal{S}$ of Eq. 4.8) is determined by solving the equation

$$\partial_q S(q,t) = mv(q,t). \tag{5.27}$$

We also provide numerical evidence to show that the wavefunction evolving under $\left[\hat{H}_0(t) + \hat{H}_{CD}(t)\right]$ will follow the adiabatic path with a high accuracy.

To show that Eq. 5.23 implies Eq. 5.25, we start by substituting Eq. 5.24 in Eq. 5.25 and then simplify the left and right sides of the equation. Henceforth, we will drop the arguments of the functions in this section. Firstly note from Eq. 5.24

that

$$\frac{\partial \psi_{CD}^2}{\partial q^2} \cdot \exp\left[i\frac{S(q,t)}{\hbar}\right] = \left[\frac{\partial \psi_{FF}^2}{\partial q^2} - \frac{1}{\hbar^2}\psi_{FF}\left(\frac{\partial S}{\partial q}\right)^2\right] - \frac{i}{\hbar}\left[2\frac{\partial \psi_{FF}}{\partial q}\frac{\partial S}{\partial q} + \psi_{FF}\frac{\partial^2 S}{\partial q^2}\right]. \tag{5.28}$$

Upon using $\hat{p} = -i\hbar\partial_q$ and Eq. 3.1, the left side (LS) of Eq. 5.25 simplifies to

$$\begin{aligned} \text{LS} \cdot \exp\left[i\frac{S(q,t)}{\hbar}\right] &= \left[-\frac{\hbar^2}{2m}\frac{\partial \psi_{FF}^2}{\partial q^2} + U_0\psi_{FF} + \frac{1}{2m}\psi_{FF}\left(\frac{\partial S}{\partial q}\right)^2 - v\psi_{FF}\frac{\partial S}{\partial q}\right] \\ &+ i\hbar\left[\frac{1}{m}\frac{\partial \psi_{FF}}{\partial q}\frac{\partial S}{\partial q} + \frac{1}{2m}\psi_{FF}\frac{\partial^2 S}{\partial q^2} - v\frac{\partial \psi_{FF}}{\partial q} - \frac{1}{2}\partial_q v\psi_{FF}\right], \end{aligned} \tag{5.29a}$$

while the right side (RS) simplifies to

$$\text{RS} \cdot \exp\left[i\frac{S(q,t)}{\hbar}\right] = \frac{\partial \psi_{CD}}{\partial t} \cdot \exp\left[i\frac{S(q,t)}{\hbar}\right] = \frac{\partial \psi_{FF}}{\partial t} + \frac{1}{i\hbar}\frac{\partial S}{\partial t}\psi_{FF} \tag{5.29b}$$

After equating the left and right sides of Eq. 5.29, we separate the real and imaginary parts to obtain

$$\text{Re[LS-RS]} \exp\left[i\frac{S(q,t)}{\hbar}\right] = \left[\frac{1}{2m}\left(\frac{\partial S}{\partial q}\right)^2 - v\frac{\partial S}{\partial q} - \frac{\partial S}{\partial t}\right]\psi_{FF} \tag{5.30}$$

and

$$\text{Im[LS-RS]} \exp\left[i\frac{S(q,t)}{\hbar}\right] = \frac{\hbar}{m}\frac{\partial \psi_{FF}}{\partial q}\left[\frac{\partial S}{\partial q} - mv\right] + \psi_{FF}\frac{\hbar}{2m}\left[\frac{\partial S^2}{\partial q^2} - m\partial_q v\right] \tag{5.31}$$

respectively. The term in the parenthesis of Eq. 5.30 is only a function of time as

shown below. We start from the definition of the flow-field acceleration, Eq. 4.9b and use Eqs. 5.27 and 4.11b for simplication.

$$
\begin{aligned}
& a = v\partial_q v + \partial_t v \\
\Rightarrow \quad & ma = mv\partial_q v + m\partial_t v \\
\Rightarrow \quad & -\partial_q U_{FF} = \frac{m}{2} v\partial_q v + m\partial_t v \\
\Rightarrow \quad & -\partial_q U_{FF} = \frac{1}{2m}\partial_q (mv)^2 + m\partial_t(\partial_q S) \\
\Rightarrow \quad & \partial_q \left[\frac{1}{2m} \left(\frac{\partial S}{\partial q} \right)^2 - v\frac{\partial S}{\partial q} - \frac{\partial S}{\partial t} \right] = 0
\end{aligned}
\tag{5.32}
$$

Since Eq. 5.27 defines S upto an arbitrary function of time, we can exploit this freedom to choose an S such that the the right side of Eq. 5.30 vanishes. Eq. 5.27 also implies that the terms in the parenthesis on the right side of Eq. 5.31 vanish. This concludes our proof.

We have shown that if a wavefunction ψ_{FF} satisfies Eq. 5.23, then a wavefunction ψ_{CD} related to ψ_{FF} by Eq. 5.24 satisfies Eq. 5.25. In other words, once we numerically establish that the fast-forward potential U_{FF} of Eq. 4.11b carries out quantum fast-forward driving with a high accuracy, we can deduce that the counterdiabatic Hamiltonian H_{CD} of Eq. 5.26 will carry out quantum counterdiabatic driving with the same level of accuracy. This claim is supported by the numerical result shown in Fig. 5.8 which plots the probability density $|\phi_{18}(q,t)|^2$ of the instantaneous eigenfunction, and $|\psi(q,t)|^2$, the probability density of the wavefunction evolving under $\hat{H}_0 + \hat{U}_{FF}$. As seen in the figure, the minima of $|\psi(q,t)|^2$ align with

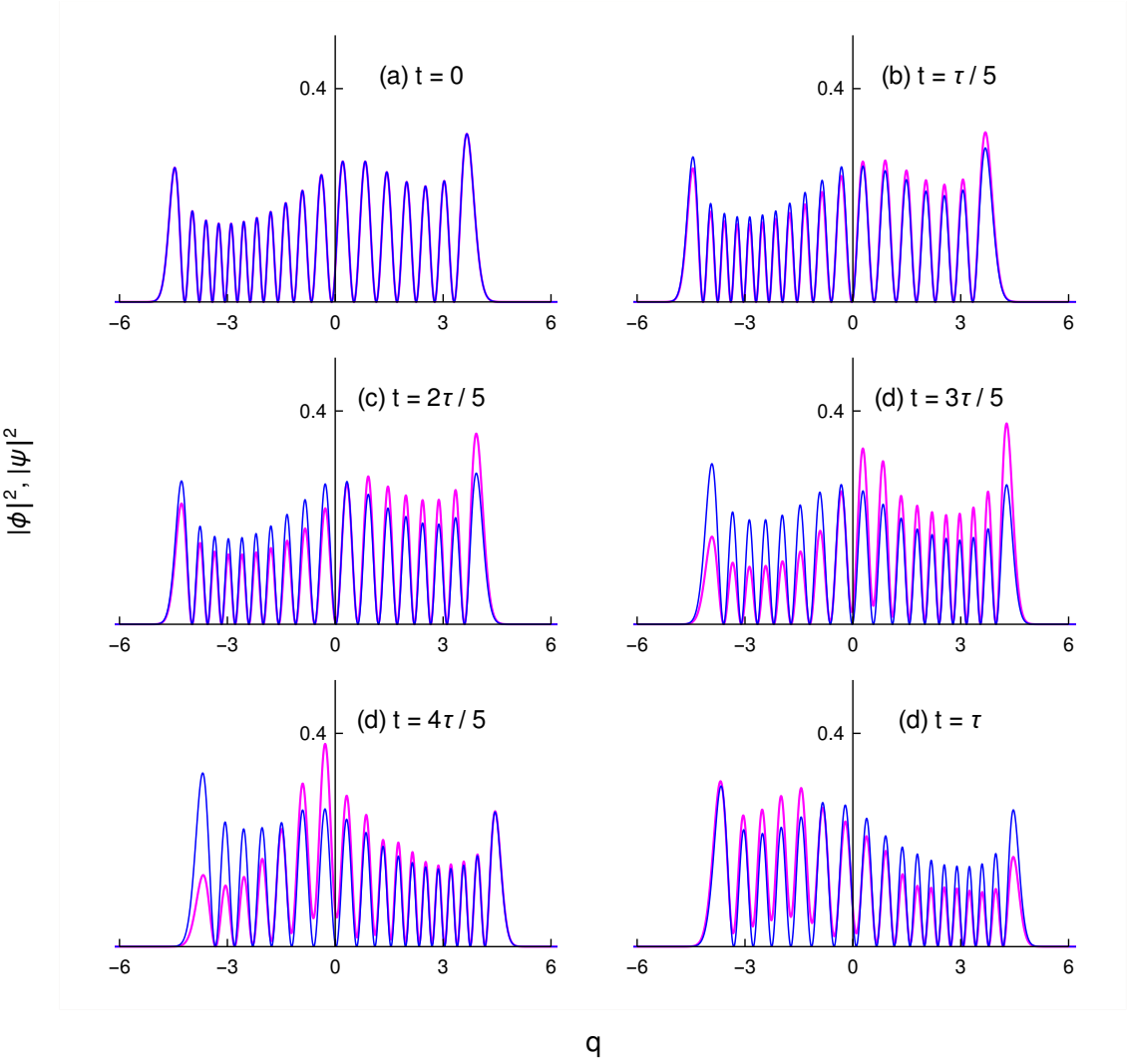

Figure 5.8: The magenta curves depict the instantaneous probability density $|\psi(q,t)|^2$ of the wavefunction $\psi(q,t)$ evolving under $\hat{H}_0 + \hat{U}_{FF}$. $|\psi(q,t)|^2$ is plotted with respect to q for times $t = 0, \tau/5, 2\tau/5, 3\tau/5, 4\tau/5$ and τ, for $\tau = 1.0$. The blue curves correspond to $|\phi_{18}(q,t)|^2$, the probability density of the instantaneous energy eigen state. The other parameters for numerical evolution were chosen as $m = 1$, $\hbar = 2$ and $E = 53.76$, which corresponds to $n = 18$. As seen in the snapshots, the minima of $|\psi(q,t)|^2$ align with the nodes of $|\phi_{18}(q,t)|^2$ at every instant, but the amplitudes do not match.

the nodes of $|\phi_{18}(q,t)|^2$ at every instant, although the amplitudes do not align. For the evolution depicted in Fig. 5.8, $\hbar = 2$ and $E = 53.76$ so that $n = 18$. The final time τ was set to unity. Combining this numerical result with the fact that a wavefunction ψ_{CD} related to ψ_{FF} by Eq. 5.24 satisfies Eq. 5.25, we can deduce that $\hat{H}_{CD}$ obtained from the classical $v(q,t)$ achieves counterdiabatic driving with a high accuracy.

5.7 Summary

In this chapter, we have explored the problem of achieving shortcuts to adiabaticity for excited states which are driven under an arbitrary protocol. We have shown that the flow-fields method for quantum and classical systems, as discussed in Chaps. 3 and 4 respectively, have many similarities but are not equivalent in the semiclassical limit. This led to the study of the semiclassical limit of an energy eigenfunction. We determined that a perfect flow-field velocity must satisfy Eqs. 5.7 in order to produce exact counterdiabatic and fast-forward fields. However, as pointed out in Sec. 3.5, the nodes of the wavefunction make it impossible to obtain a well defined flow-field velocity and therefore the set of Eqs. 5.7 can not be satisfied simultaneously. We then attempt to find a velocity which satisfies at least one of Eqs. 5.7. We prioritized Eq. 5.7a as it preserves the phase of the wavefunction which is directly related to the quantum nummber. Eq. 5.7a is in fact equivalent to the condition that the classical action of a system undergoing analogous classical dynamics be preserved. Following this, we hypothesized that the quantum counterpart

of a classical fast-forward potential should be able to achieve quantum fast-forward driving to a good approximation.

We tested our hypothesis using a model double-well Hamiltonian subjected to a non scale invariant driving. We first obtained the classical fast-forward potential $U_{FF}(q,t)$ for a chosen dynamics. We then quantized this potential to obtain $U_{FF}(\hat{q},t)$, and subjected a quantum system to the analogous quantum driving under time-dependent Schrödinger equation. We compared the evolutions under the bare Hamiltonian $\hat{H}_0(t)$ and the composite Hamiltonian $\hat{H}_0(t) + U_{FF}(\hat{q},t)$. We deduced from Figs. 5.2 - 5.4 that $U_{FF}(\hat{q},t)$ carries out fast-forward driving with a very high accuracy.

The accuracy of $U_{FF}(\hat{q},t)$ was tested for different initial conditions by studying $p_n(t) = |\langle\phi_n(t)|\psi(t)\rangle|^2$ which represents the overlap between the evolved state and the energy eigenstate at time t. It was observed that the non-uniformity in the distribution of the final trajectories on classical energy shell is directly related to the accuracy with which $U_{FF}(\hat{q},t)$ achieves fast-forward driving. Our analysis shows that the higher the quantum number of the initial state, the more accurate is the fast-forward driving. The quantum peaks obtained at the final time after fast-forward driving was infact obtained quantitatively by comparing the semiclassical analysis of the semiclassical wavefunction and the final classical distribution. It was shown that the Fourier transform of the final classical distribution represented in the angle coordinates matches perfectly with the quantum peaks obtained from numerical evolution under time-dependent Schrödinger equation. It was also shown analytically and supported numerically in Fig. 5.8 that the numerical accuracy of the

quantum fast-forward driving will be reflected in quantum counterdiabatic driving as well, where the auxiliary counterdiabatic Hamiltonian is obtained from the quantum counterpart of the classical flow-field velocity, see Eq. 5.26.

This chapter provides a novel approach to solve quantum shortcuts for a system initialized in an excited state and subjected to an arbitrary driving protocol. The importance of the classical auxiliary fields in obtaining quantum auxiliary fields for analogous driving protocols is established. The problem arising due to nodes of an excited wavefunction, as discussed in Sec.3.5, has been overcome to a great extent and highly accurate auxiliary fields have been derived. A crucial point to note about the analysis in this chapter is that the auxiliary fields depend on the choice of the initial state. It remains an open problem to solve for a flow-field velocity which satisfies Eq. 5.7b instead of Eq. 5.7a, and compare the auxiliary fields obtained as a result. Once a solution is obtained, one may try to find an optimal way to combine these auxiliary fields in order to obtain a resulting field which is closest to the ideal auxiliary field which can achieve perfect shortcuts to adiabaticity.

Chapter 6: Stochastic shortcuts using flow-fields

6.1 Overview

In this chapter, we establish the broad applicability of the flow-fields method by extending it to stochastic systems. This work has been motivated by a recent experiment by Martínez *et al*, where swift-equilibration was achieved in a system of overdamped Browninan particles [59]. The experimental setup in Ref. [59] consisted of a microsphere immersed in water, which was trapped by an optical harmonic potential of the form $U(q,t) = \kappa(t)q^2/2$. The power of the trapping laser controlled the stiffness $\kappa(t)$ of the trapping potential. The dynamics of the system was overdamped and described by a Langevin equation. In the experiment, the stiffness $\kappa(t)$ was doubled over a time t_f much shorter than the natural relaxation time τ_{relax} of the system. It was shown that when $\kappa(t)$ was doubled according to the protocol termed *engineered swift equilibration*, the system of Brownian particles reached final equilibrium much faster than the natural relaxation time. In fact the system reached equilibrium at the final time t_f, i.e., as soon $\kappa(t)$ reached its final value.

The experiment in Ref. [59] prompted us to frame a problem on stochastic shortcuts as follows: Given a system of overdamped Browninan particles trapped in a potential $U_0(q,t)$, is it possible to guide the system along the instantaneous

equilibrium state at all times? This problem is equivalent to counterdiabatic driving discussed in previous chapters. We would like to construct an auxiliary trapping potential $U_{CD}(q,t)$, such that when the system evolves under the composite trapping potential $U_0(q,t) + U_{CD}(q,t)$, it tracks the instantaneous equilibrium distribution corresponding to $U_0(q,t)$ at all times. This is the problem for counterdiabatic driving in a stochastic system. Unlike the quantum and classical Hamiltonian systems, it will be shown that for an overdamped stochastic system, counterdiabatic driving can be achieved using a potential (or a local field). This may be attributed to the separation of time-scales between the particles in the system and its surroundings for an overdamped system.

We derive the flow-fields method for stochastic systems in Sec. 6.2, compare our results with previous results from Martínez *et al* (Ref. [59]) in Sec. 6.3 and present a brief summary in Sec. 6.4.

6.2 Derivation of results

Let us consider an overdamped Brownian particle in a time-dependent potential $U_0(q,t)$, which varies smoothly for $0 \leq t \leq \tau$ but is fixed outside this interval. The particle is in contact with a thermal reservoir at temperature T. The interactions with the degrees of freedom of the reservoir give rise to the random and dissipative forces that characterize Brownian dynamics.

We will work in the ensemble picture, in which the dynamics are described by a probability density function $\rho(q,t)$ that evolves according to the Fokker-Planck

equation

$$\partial_t \rho = \frac{1}{\gamma}\partial_q \left[(\partial_q U_0)\rho\right] + D\partial_q^2 \rho \equiv \hat{\mathcal{L}}_0(t)\rho, \tag{6.1}$$

The friction and diffusion coefficients, γ and D, obey the Einstein-Smoluchowski relation, $\gamma D = k_B T \equiv 1/\beta$, where k_B is the Boltzmann constant. The equilibrium distribution associated with the potential $U_0(q,t)$ is given by

$$\rho^{eq}(q,t) = \frac{1}{Z(t)} \exp\left[-\beta U_0(q,t)\right] \tag{6.2}$$

where $Z(t)$ is the partition function. It is straightforward to verify the identity

$$\hat{\mathcal{L}}_0(t)\rho^{eq}(q,t) = 0 \tag{6.3}$$

which confirms that the equilibrium distribution is a stationary solution of the dynamics, when the potential does not vary with time. When $U_0(q,t)$ changes quasi-statically, then the slowly varying $\rho^{eq}(q,t)$ is a solution of Eq. 6.1 (both sides tend toward zero in that limit), as expected for a reversible process. Therefore, the *adiabatic evolution* is identified by the ensemble evolving through the continuous sequence of equilibrium states $\rho^{eq}(q,t)$. [1]

We now consider the case in which the potential $U_0(q,t)$ is varied at an arbitrary rate. To this potential we will add a counterdiabatic term $U_{CD}(q,t)$, so that the

[1] Here we use the term *adiabatic* consistently with its usage in the rest of the paper, namely to denote a slow process. This differs from its usage in thermodynamics, where an adiabatic process is one in which heat is not absorbed or released by a system. The dual meaning of this term is unfortunate.

system evolves under

$$\begin{aligned}\partial_t \rho &= \frac{1}{\gamma}\partial_q \left\{\left[\partial_q (U_0 + U_{CD})\right] \rho\right\} + D\partial_q^2 \rho \\ &= \hat{\mathcal{L}}_0 \rho + \frac{1}{\gamma}\partial_q \left[(\partial_q U_{CD})\rho\right] \end{aligned} \tag{6.4}$$

We wish to design $U_{CD}(q,t)$ so as to achieve adiabatic evolution, i.e. so that $\rho^{eq}(q,t)$ (Eq. 6.2) is an exact solution of Eq. 6.4. We define an integrated distribution

$$\mathcal{F}(q,t) = \int_{-\infty}^{q} \rho^{eq}(q',t) dq' \tag{6.5}$$

similar to $\mathcal{I}(q,t)$ (Eq. 3.6). Inverting this function to obtain $q(\mathcal{F},t)$ (see Fig. 6.1), we construct a velocity flow field

$$v(q,t) = \frac{\partial}{\partial t} q(\mathcal{F},t) = -\frac{\partial_t \mathcal{F}}{\partial_q \mathcal{F}}. \tag{6.6}$$

Rearranging this result as $\partial_t \mathcal{F} + v\partial_q \mathcal{F} = 0$ and differentiating with respect to q produces the continuity equation

$$\partial_t \rho^{eq} + \partial_q (v\rho^{eq}) = 0. \tag{6.7}$$

Since we wish $\rho^{eq}(q,t)$ to be a solution of Eq. 6.4, we use Eqs. 6.3 and 6.7 to rewrite that equation as follows:

$$-\partial_q (v\rho^{eq}) = \frac{1}{\gamma}\partial_q \left[(\partial_q U_{CD})\rho^{eq}\right] \tag{6.8}$$

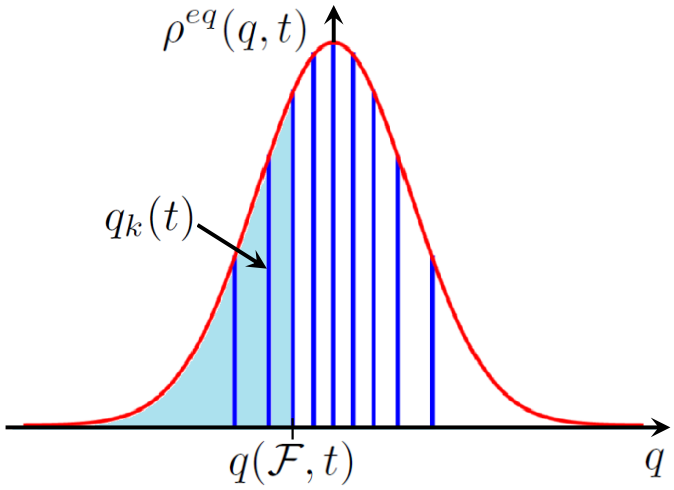

Figure 6.1: The blue lines divide the equilibrium distribution into strips of equal area. $q(\mathcal{F},t)$ is the right boundary of the shaded region, which has area $\mathcal{F}$. The velocity field $v(q,t)$ describes the motion of the vertical lines with t (Eq. 6.6).

Integrating both sides gives

$$-v\rho^{eq} - J(t) = \frac{1}{\gamma}(\partial_q U_{CD})\rho^{eq} \tag{6.9}$$

Here, $J(t)$ is an arbitrary function of time that we set to zero, for convenience, arriving at the result

$$-\partial_q U_{CD}(q,t) = \gamma v(q,t) \tag{6.10}$$

Eq. 6.10 defines $U_{CD}(q,t)$ up to an additive function of time that has no influence on the dynamics, and which can be adjusted so that $U_{CD} = 0$ for $t \notin (0,\tau)$. The potential $U_{CD}(q,t)$ has the desired counterdiabatic property: when the system evolves in the time-dependent potential U_0+U_{CD}, it remains in equilibrium (with respect to U_0) over the entire duration of the process. Our potential U_{CD} is equivalent to the auxiliary potential obtained by Li *et al* [60], as can be seen by differentiating

both sides of Eq. 12 of Ref. [60] with respect to x.

Eq. 6.10 has elements in common with both the counterdiabatic and fast-forward shortcuts of previous chapters. It is counterdiabatic in that the system follows the adiabatic evolution (it remains in the state ρ^{eq}) at all times. Moreover, U_{CD} is given in terms of the velocity field v (compare Eqs. 3.11, 4.11a, and 6.10), rather than the acceleration field a. However, just as with the fast-forward shortcuts described earlier, U_{CD} is *local*, i.e. it is a time-dependent potential (compare Eqs. 3.14, 4.11b, and 6.10). Also, as in Chaps. 3 and 4, Eq. 6.10 defines the auxiliary potential only up to an arbitrary function of time that does not affect the dynamics.

When the Brownian particles evolve under $U_0(q,t)$ alone, the state of the ensemble, $\rho(q,t)$, *lags* behind the instantaneous equilibrium state, $\rho^{eq}(q,t)$, as illustrated in Fig. 1 of Ref. [80]. The addition of the counterdiabatic potential $U_{CD}(q,t)$ eliminates this lag. Lagging distributions are relevant for numerical free-energy estimation methods, where the lag gives rise to poor convergence of the free-energy estimate. Vaikuntanathan and Jarzynski [57] have developed a method in which this lag is reduced or eliminated by the addition of an artificial flow field to the dynamics, although in Ref. [57] this flow field was not related to an auxiliary potential U_{CD}. Comparing Eq. 6.7 above with Eq. 15 of Ref. [57], we see that our field v is equivalent to the *perfect flow field* (u^*) that "escorts" the system faithfully along the equilibrium path.

While our analysis has been restricted to overdamped Brownian motion, Le Cununder and colleagues [81] have recently used a micromechanical cantilever to implement engineered swift equilibration for an underdamped harmonic oscillator.

For underdamped motion in a general one-dimensional, time-dependent potential, Li, Quan and Tu [60] have proposed a momentum-dependent counterdiabatic term that achieves the desired adiabatic evolution. It remains to be seen whether this progress will lead to expressions for a momentum-*independent* counterdiabatic potential that extends the fast-forward method to underdamped Brownian dynamics beyond the harmonic regime.

6.3 Comparision with engineered swift equilibration

As a simple example, which makes a connection to the engineered swift equilibration approach in Ref. [59], we consider a time-dependent harmonic potential,

$$U_0(q,t) = \frac{1}{2}\kappa_0(t)q^2 \tag{6.11}$$

The instantaneous equilibrium distribution is

$$\rho^{eq}(q,t) = \sqrt{\frac{\sigma}{\pi}}\exp(-\sigma q^2) \quad , \quad \sigma(t) \equiv \beta\kappa_0(t)/2. \tag{6.12}$$

Eq. 6.5 then gives

$$\mathcal{F}(q,t) = \frac{1}{2}\left[1 + \mathrm{erf}(\sqrt{\sigma(t)}q)\right], \tag{6.13}$$

where erf$(\cdot)$ is the Gaussian error function. In turn, Eq. 6.6 yields $v(q,t) = -\dot{\sigma}/2\sigma$, and from there we use Eq. 6.10 to obtain

$$U_{CD}(q,t) = \left(\frac{\gamma\dot{\sigma}}{2\sigma}\right)\frac{q^2}{2}. \tag{6.14}$$

Therefore, under a harmonic trap of stiffness

$$\kappa(t) = \kappa_0 + \frac{\gamma\dot{\sigma}}{2\sigma} = \kappa_0 + \frac{\gamma\dot{\kappa_0}}{2\kappa_0} \tag{6.15}$$

the ensemble remains in the equilibrium state ρ^{eq} (Eq. 6.12) at all times.

Rearranging Eq. 6.15 and using $\sigma = \beta\kappa_0/2$, we get

$$\frac{\dot{\sigma}}{\sigma} = \frac{2\kappa}{\gamma} - \frac{4k_BT\sigma}{\gamma}. \tag{6.16}$$

This result is identical to Eq. 6 of Martínez *et al* [59], where the goal was to bring the system rapidly to the final equilibrium state, without concern for the intermediate states visited along the way. Our approach achieves the same result by guiding the system along the equilibrium path during the entire process. Eq. 6.16 was also obtained by Schmiedl and Seifert, in the contexts of optimal finite-time control [82] and stochastic heat engines [83].

6.4 Summary

In this chapter, we have extended the *flow-fields* method – developed in the previous chapters for classical and quantum Hamiltonian systems – to a system of overdamped Brownian particles. We have constructed an auxiliary potential $U_{CD}(q,t)$ in Eq. 6.10 which guides an ensemble of Brownian particles along the instantaneous equilibrium distribution of the trap potential of interest $U_0(q,t)$. We have related $U_{CD}(q,t)$ with the shortcut protocols discussed in the previous chapters.

The results from Chaps. 3, 4 and 6 demonstrate that the flow-fields approach is a unifying framework to obtain shortcuts for quantum, classical as well as stochastic systems. The flow-fields approach also relates the the two distinct shortcut protocols – the counterdiabatic driving and the fast-forward driving.

Appendix A: Derivation of Eq. 2.44

Because the classical function $\eta(q,p) = \text{sign}(p)$ is non-analytic, the matrix representation of its quantal counterpart $\hat{\eta}$ cannot be obtained by a procedure like the one used in Sec. 2.5. Here we instead construct the matrix representation of η by equating its classical and quantum auto-correlation functions.

Consider a quantum particle in a box with a flat base ($s = 0$) and hard walls at $q = 0$ and $q = L$, described by the Hamiltonian $\hat{H}' = \hat{p}^2/2m + \Theta(\hat{q}; 0, L)$. Following Ref. [84], we write the quantum auto-correlation function of $\hat{\eta}$, for the eigenstate $|\alpha\rangle$, as

$$\begin{aligned} C_\alpha(\tau) &= \langle\alpha|\hat{\eta}\exp\left(\frac{i\hat{H}'\tau}{\hbar}\right)\hat{\eta}\exp\left(-\frac{i\hat{H}'\tau}{\hbar}\right)|\alpha\rangle \\ &= \sum_\beta |\tilde{\eta}_{\alpha\beta}|^2 \exp\left[\frac{i(E_\beta - E_\alpha)\tau}{\hbar}\right], \end{aligned} \tag{A.1}$$

where $\tilde{\eta}_{\alpha\beta} = \langle\alpha|\hat{\eta}|\beta\rangle$, and E_α is the energy corresponding to the eigenstate $|\alpha\rangle$. The Fourier transform of the auto-correlation function is

$$\mathbb{C}_\alpha(\omega) = \sum_\beta |\tilde{\eta}_{\alpha\beta}|^2 \delta(\omega - \omega_{\alpha\beta}), \tag{A.2}$$

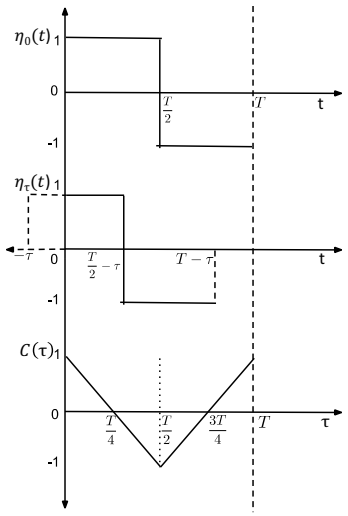

Figure A.1: The function $\eta_0(t)$ plotted over one time period of oscillation is a square wave (top figure). The function $\eta_\tau(t)$ is obtained by shifting this square wave leftward by an amount τ (middle figure). The autocorrelation function $C(\tau)$ is the product of these square wave pulses, integrated over one period, yielding a triangular wave (bottom figure).

where

$$\omega_{\alpha\beta} \equiv \frac{E_\beta - E_\alpha}{\hbar}. \tag{A.3}$$

For a classical particle evolving under the equivalent Hamiltonian, $\eta = \text{sign}(p)$ is a square wave pulse with unit amplitude over a time period around the energy shell. The functions $\eta_0^E(t)$ and $\eta_\tau^E(t)$ describe the dependence of η on time for a particle of energy E that starts from $L = 0$ at times $t = 0$ and $t = -\tau$ respectively, as depicted in Fig.A.1. The classical auto-correlation function, $C_E(\tau) = (1/T)\int_0^T dt\, \eta_0^E(t)\eta_\tau^E(t)$, is a triangular wave given by

$$C_E(\tau) = \begin{cases} \frac{T-4\tau}{T} & , \quad 0 \le \tau \le \frac{T}{2} \\ \frac{4\tau-3T}{T} & , \quad \frac{T}{2} \le \tau \le T \end{cases}, \tag{A.4}$$

shown in Fig.A.1. The Fourier transform of $C_E(\tau)$ is

$$\mathbb{C}_E(\omega) = \sum_{\text{odd}}^{\infty} \sum_{\gamma=-\infty} \frac{4}{\pi^2\gamma^2}\delta(\omega - \omega_\gamma), \tag{A.5}$$

where

$$\omega_\gamma = \frac{2\pi\gamma}{T}. \tag{A.6}$$

The correspondence principle suggests that the functions $\mathbb{C}_\alpha(\omega)$ and $\mathbb{C}_E(\omega)$ ought to be equal, in the semiclassical limit, when $E_\alpha = E$. To compare these functions, we first note that for one dimensional systems, the classical action $J(E) = \oint_E p \cdot dq$ satisfies

$$\frac{dJ}{dE} = T. \tag{A.7}$$

For neighboring energy levels $|\alpha\rangle$ and $|\alpha + 1\rangle$, the energy spacing is

$$dE = E_{\alpha+1} - E_\alpha = \hbar\omega_{\alpha,\alpha+1}, \tag{A.8}$$

and the action spacing is given by the Bohr-Sommerfeld quantization condition:

$$dJ = 2\pi\hbar. \tag{A.9}$$

From Eqs.(A.7) - (A.9) we obtain $\omega_{\alpha,\alpha+1} = 2\pi/T$, which generalizes to

$$\omega_{\alpha\beta} = \frac{2\pi(\beta - \alpha)}{T}, \tag{A.10}$$

provided α and β are not too far apart.

Comparing Eqs.(A.6) and (A.10) we confirm that the delta-functions in Eqs.(A.2) and (A.5) appear at the same frequencies, and by equating the coefficients of these delta-functions we obtain

$$|\tilde{\eta}_{\alpha\beta}| = \begin{cases} \frac{2}{|\alpha-\beta|\pi} & \alpha-\beta = odd \\ 0 & \alpha-\beta = even \end{cases} . \tag{A.11}$$

To ensure that the operator $\hat{\eta}$ is Hermitian (as it represents a physical observable), we impose the condition $\tilde{\eta}_{\alpha\beta} = \tilde{\eta}^*_{\beta\alpha}$, which then implies

$$\tilde{\eta}_{\alpha\beta} = \begin{cases} \pm\frac{2i}{(\alpha-\beta)\pi} & \alpha-\beta = odd \\ 0 & \alpha-\beta = even \end{cases} \tag{A.12}$$

Finally to determine the sign in Eq.(A.12), the ground state eigenfunction of $\hat{H}'(t)$ was boosted by a momentum $p = \pi k/L$, where $k \in \mathbb{Z}$, which results in the wave packet $\psi(q) = \sqrt{\frac{2}{L}}\sin(\frac{\pi q}{L})\exp(\frac{i\pi kq}{L})$. By demanding that $\langle\psi|\hat{\eta}|\psi\rangle \to 1$ for $k \gg 1$ and $\langle\psi|\hat{\eta}|\psi\rangle \to -1$ for $k \ll -1$, a series of straightforward calculations yields

$$\tilde{\eta}_{\alpha\beta} = \begin{cases} \frac{2i}{(\beta-\alpha)\pi} & \alpha-\beta = odd \\ 0 & \alpha-\beta = even \end{cases} \tag{A.13}$$

Appendix B: Continuity conditions on $H_0(z,t)$

In Sec. 4.2, we specified that $H_0(z,t)$ is constant in time for $t < 0$, then varies between $t = 0$ and $t = \tau$, then remains constant in time for $t > \tau$. As a result, H_0 cannot be an entirely smooth function of time: for some $n \geq 0$, the derivative $\partial^n H_0/\partial t^n$ must be discontinuous. We explicitly assumed that this discontinuity occurs at $n \geq 3$, giving us

$$\frac{\partial H_0}{\partial t}(z,0) = \frac{\partial H_0}{\partial t}(z,\tau) = 0 \tag{B.1a}$$

$$\frac{\partial^2 H_0}{\partial t^2}(z,0) = \frac{\partial^2 H_0}{\partial t^2}(z,\tau) = 0 \tag{B.1b}$$

leading to Eq. 4.10.

The assumption that H_0 is twice continuously differentiable was made both for clarity of presentation, and because it arises in proofs of the adiabatic invariance of the action [74]. In our context, however, the assumption is not necessary, therefore in the following we will discuss how Eq. B.1 can be relaxed. We will continue to require that H_0 itself is a continuous function of time. Without loss of generality, we will assume that discontinuities in $\partial H_0/\partial t$ and $\partial^2 H_0/\partial t^2$ occur only at $t = 0$ and $t = \tau$, and not within the time interval $0 < t < \tau$.

We first consider the simpler case, in which the above-mentioned discontinuity occurs at $n = 2$, i.e. Eq. B.1a holds but B.1b is violated. Then $v(q, 0) = v(q, \tau) = 0$, but $a(q, t)$ changes abruptly at $t = 0$ and/or $t = \tau$. In this situation the fast-forward potential will also be discontinuous at these times (see Eq. 4.11b) but otherwise the analysis in the main text remains valid. Thus the violation of Eq. B.1b simply implies that $V_{\mathrm{FF}}(q, t)$ is turned on and/or off suddenly rather than continuously.

Now consider the case in which the discontinuity occurs at $n = 1$, hence Eq. B.1a is violated. Specifically, suppose the time-dependence of the Hamiltonian is turned on abruptly: $\partial H_0/\partial t \neq 0$ at $t = 0^+$, hence

$$v_0(q) \equiv v(q, 0^+) \neq 0 \tag{B.2}$$

The velocity field changes suddenly from $v(q, 0^-) = 0$ to $v(q, 0^+) = v_0(q)$. The term $\partial v/\partial t$ in Eq. 4.10 then leads to a singular term $v_0(q)\delta(t)$ in the acceleration field $a(q, t)$. By Eq. 4.11b, this term leads to a contribution to U_{FF} that is proportional to $\delta(t)$, which produces an impulsive force field at $t = 0$:

$$-\frac{\partial U_{\mathrm{FF}}}{\partial q}(q, t) = m v_0(q)\delta(t) + [\text{other terms}] \tag{B.3}$$

The effect of this impulse is simple to state: a trajectory located at (q, p) at time $t = 0^-$ is instantaneously "boosted" to $(q, p + m v_0(q))$ at time $t = 0^+$ as it evolves under H_{FF}.

Similar comments apply if $\partial H_0/\partial t \neq 0$ at $t = \tau^-$. Then

$$v_\tau(q) \equiv v(q, \tau^-) \neq 0 \tag{B.4}$$

and we get a singular term in $U_{\rm FF}$ that produces an impulsive force

$$-mv_\tau(q)\delta(t-\tau). \tag{B.5}$$

Now consider a collection of trajectories that, for $t < 0$, are found on the adiabatic energy shell $\mathcal{E}(0)$. As in the main text, let the loop $\mathcal{L}_{\rm FF}(t)$ describe the evolution of these trajectories, under $H_{\rm FF}(z,t)$. At $t = 0$, the impulsive force in Eq. B.3 boosts these trajectories from $\mathcal{L}_{\rm FF}(0^-) = \mathcal{E}(0)$ to a loop $\mathcal{L}_{\rm FF}(0^+)$ that is displaced along the momentum axis by an amount $mv_0(q)$. Subsequently, this loop evolves exactly as described in the main text: for $0 < t < \tau$, $\mathcal{L}_{\rm FF}(t)$ is displaced from the adiabatic energy shell $\mathcal{E}(t)$ by an amount $mv(q,t)$ (Eq. 4.20). In particular, at $t = \tau^-$ this loop is displaced from $\mathcal{E}(\tau)$ by $mv_\tau(q)$. The final impulse at $t = \tau$ (Eq. B.5) instantaneously brings the collection of trajectories from $\mathcal{L}_{\rm FF}(\tau^-)$ to $\mathcal{L}_{\rm FF}(\tau^+) = \mathcal{E}(\tau)$.

Thus, non-vanishing derivatives $\partial H_0/\partial t$ at initial and final times can be accommodated by impulse-like terms in $U_{\rm FF}(q,t)$. See Section III.A. of Ref. [34] for an example that illustrates this point in the context of scale-invariant driving.

Appendix C: Flow under $H_0 + H_{CD}$ preserves the adiabatic energy shell

The Hamiltonian $H_0 + H_{CD}$ generates the flow (Eq. 4.14)

$$\dot{q} = \frac{p}{m} + v(q,t) \qquad , \qquad \dot{p} = -\frac{\partial U_0}{\partial q}(q,t) - p\frac{\partial v}{\partial q}(q,t) \tag{C.1}$$

Let $\dot{H}_0(q,p,t)$ denote the instantaneous rate of change of H_0, along a trajectory that passes through the point (q,p) at time t as it evolves under these dynamics:

$$\begin{aligned} \dot{H}_0(q,p,t) &\equiv \frac{\partial H_0}{\partial q}\dot{q} + \frac{\partial H_0}{\partial p}\dot{p} + \frac{\partial H_0}{\partial t} \\ &= \frac{\partial U_0}{\partial q}v - \frac{p^2}{m}\frac{\partial v}{\partial q} + \frac{\partial U_0}{\partial t} \end{aligned} \tag{C.2}$$

To establish that the flow given by Eq. C.1 preserves the adiabatic energy shell, we must show that

$$\dot{H}_0(q,p,t) = \frac{\mathrm{d}}{\mathrm{d}t}\bar{E}(t) \qquad \text{when} \quad (q,p) \in \mathcal{E}(t) \tag{C.3}$$

We evaluate $\dot{H}_0$ at a point $(q,p) \in \mathcal{E}(t)$, by setting $p = \pm\bar{p}(q,t) = \pm\left[2m(\bar{E}-U_0)\right]^{1/2}$:

$$\begin{aligned}
\dot{H}_0(q,\pm\bar{p},t) &= \frac{\partial U_0}{\partial q}v - 2(\bar{E}-U_0)\frac{\partial v}{\partial q} + \frac{\partial U_0}{\partial t} \\
&= -\frac{1}{v}\frac{\partial}{\partial q}\left[(\bar{E}-U_0)v^2\right] + \frac{\partial U_0}{\partial t} \\
&= \frac{\partial_q S}{\partial_t S}\frac{\partial}{\partial q}\left[\frac{\bar{p}^2}{2m}\left(\frac{\partial_t S}{\partial_q S}\right)^2\right] + \frac{\partial U_0}{\partial t} \\
&= \frac{\bar{p}}{2m}\partial_q\partial_t S + \frac{\partial U_0}{\partial t} = \frac{\bar{p}}{m}\frac{\partial\bar{p}}{\partial t} + \frac{\partial U_0}{\partial t} \\
&= \frac{\partial}{\partial t}\left[\frac{\bar{p}^2(q,t)}{2m} + U_0(q,t)\right] = \frac{\mathrm{d}}{\mathrm{d}t}\bar{E}(t) \qquad \text{(C.4)}
\end{aligned}$$

which is the desired result. In obtaining Eq. C.4 we have made repeated use of the identities $\partial_q S = 2\bar{p}$ and $v = -\partial_t S/\partial_q S$ (Eqs. 4.8 and 4.9a).

Appendix D: Local dynamical invariance of $J(q,p,t)$

$H_{\rm FF}(z,t)$ generates the equations of motion

$$\dot{q} = \frac{p}{m} \quad , \quad \dot{p} = -U_0' + ma = -U_0' + mv'v + m\frac{\partial v}{\partial t} \tag{D.1}$$

Consider the quantity

$$J(q,p,t) = I(q, p - mv(q,t), t) \tag{D.2}$$

and let $\dot{J}(z,t)$ denote the instantaneous rate of change of J along a trajectory that passes through the point $z = (q,p)$ at time t. We have, by direct substitution,

$$\begin{aligned} \dot{J}(z,t) &= \frac{\partial I}{\partial q}\dot{q} + \frac{\partial I}{\partial p}\left(\dot{p} - mv'\dot{q} - m\frac{\partial v}{\partial t}\right) + \frac{\partial I}{\partial t} \\ &= \frac{\partial I}{\partial q}\frac{p}{m} - \frac{\partial I}{\partial p}U_0' - \frac{\partial I}{\partial p}v'(p - mv) + \frac{\partial I}{\partial t} \end{aligned} \tag{D.3}$$

where the derivatives of I are evaluated at $(q, p - mv(q,t), t)$.

In general $\dot{J}(z,t) \neq 0$. However, let us now restrict our attention to a point z

that satisfies $J(z,t) = I_0$ at a particular time t. At such a point, we have

$$p = \pm\,\bar{p}(q,t) + mv(q,t) \tag{D.4}$$

with $\bar{p} = \left[2m(\bar{E} - U_0)\right]^{1/2}$. Taking $p = \bar{p} + mv$ for specificity (the case $p = -\bar{p} + mv$ gives the same result) we get

$$\begin{aligned} \dot{J}(z,t) &= \frac{\partial I}{\partial q}\left(\frac{\bar{p}}{m} + v\right) - \frac{\partial I}{\partial p}U_0' - \frac{\partial I}{\partial p}v'\bar{p} + \frac{\partial I}{\partial t} \\ &= \{I, H_0\} + \{I, H_{CD}\} + \frac{\partial I}{\partial t} \end{aligned} \tag{D.5}$$

where all quantities on the right side are evaluated at $(q,\bar{p}) \in \mathcal{E}(t)$. From Eqs. 4.4 and 4.13 we conclude that the right side of the above equation is zero, hence

$$J(z,t) = I_0 \quad \Rightarrow \quad \dot{J}(z,t) = 0 \tag{D.6}$$

where the symbol $\Rightarrow$ is short for "implies that".

Eq. D.6 establishes that $J(z,t)$ is a local dynamical invariant, in the following sense. Along trajectories z_t evolving under $H_{\mathrm{FF}}(z,t)$ from initial conditions $z_0 \in \mathcal{E}(0)$, the value of J remains constant:

$$J(z_t,t) = I_0 \tag{D.7}$$

Appendix E: Evolution of the microcanonical measure under $H_{\rm FF}$

As mentioned in the main text, initial conditions that are sampled from a microcanonical distribution on $\mathcal{E}(0)$ generally evolve (under $H_{\rm FF}$) to final conditions that are *not* distributed microcanonically on $\mathcal{E}(\tau)$, as illustrated in Fig. 4.4(c). To understand this point, let

$$\Phi_{\rm FF} : z_0 \to z_\tau \tag{E.1}$$

denote evolution under $H_{\rm FF}(z,t)$ from $t = 0$ to $t = \tau$. $\Phi_{\rm FF}$ maps initial points $z_0 \in \mathcal{E}(0)$ to final points $z_\tau \in \mathcal{E}(\tau)$. Now consider an initial phase space distribution $\rho(z,0)$ that is uniform in the thin annular region $\mathcal{R}$ between the energy shells $\mathcal{E}(0)$ and

$$\mathcal{E}_{{\rm d}E}(0) \equiv \{z | H(z,0) = \bar{E}(0) + {\rm d}E\} \tag{E.2}$$

and zero elsewhere. In the limit ${\rm d}E \to 0$, this distribution converges to a microcanonical distribution on $\mathcal{E}(0)$.

For finite ${\rm d}E$, $\rho(z,0)$ evolves to a distribution $\rho(z,\tau)$ that is uniform (by Liouville's theorem) in the region $\mathcal{R}' = \Phi_{\rm FF}(\mathcal{R})$ between the *images* of $\mathcal{E}(0)$ and $\mathcal{E}_{{\rm d}E}(0)$ under $\Phi_{\rm FF}$. Although $\Phi_{\rm FF}$ maps $\mathcal{E}(0)$ to $\mathcal{E}(\tau)$, in general it does not map $\mathcal{E}_{{\rm d}E}(0)$ to an energy shell of $H(z,t)$. As a result, in the limit ${\rm d}E \to 0$, $\rho(z,\tau)$ converges to

a distribution on $\mathcal{E}(\tau)$ that is not microcanonical. Thus the clustering of points in Fig. 4.4(c) traces back to the fact that $V_{\mathrm{FF}}(q,t)$ depends on the choice of I_0.

Bibliography

[1] M. Born and V. A. Fock. Beweis des adiabatensatzes. *Zeitschrift für Physik A*, 51:165, 1928.

[2] D. J. Griffiths. *Introduction to Quantum Mechanics*. Pearson Prentice Hall, 2nd edition, 2004.

[3] X. Chen, A. Ruschhaupt, S. Schmidt, A. del Campo, D. Guéry-Odelin, and J. G. Muga. Fast optimal frictionless atom cooling in harmonic traps: Shortcut to adiabaticity. *Phys. Rev. Lett.*, 104:063002, 2010.

[4] M. S. Sarandy, E. I. Duzzioni, and R. M. Serra. Quantum computation in continuous time using dynamic invariants. *Phys. Lett. A*, 375:3343, 2011.

[5] A. C. Santos and M. S. Sarandy. Superadiabatic controlled evolutions and universal quantum computation. *Nat. Sci. Rep.*, 5:15775, 2015.

[6] M. A. Nielsen and I. L. Chuang. *Quantum Computation and Quantum Information*. Cambridge University Press, Cambridge, UK, 2000.

[7] E. Torrontegui, S. Ibáñez, X. Chen, A. Ruschhaupt, D. Guéry-Odelin, and J. G. Muga. Fast atomic transport without vibrational heating. *Phys. Rev. A*, 83:013415, 2011.

[8] R. Bowler, J. Gaebler, Y. Lin, T. R. Tan, D. Hanneke, J. D. Jost, J. P. Home, D. Leibfried, and D. J. Wineland. Coherent diabatic ion transport and separation in a multizone trap array. *Phys. Rev. Lett.*, 109:080502, 2012.

[9] A. del Campo. Frictionless quantum quenches in ultracold gases: A quantum-dynamical microscope. *Phys. Rev. A*, 84:031606(R), 2011.

[10] A. del Campo, M. M. Rams, and W. H. Zurek. Assisted finite-rate adiabatic passage across a quantum critical point: Exact solution for the quantum ising model. *Phys. Rev. Lett.*, 109:115703, 2012.

[11] S. Masuda, K. Nakamura, and A. del Campo. High-fidelity rapid ground-state loading of an ultracold gas into an optical lattice. *Phys. Rev. Lett.*, 113:063003, 2014.

[12] V. Mukherjee, S. Montangero, and R. Fazio. Local shortcut to adiabaticity for quantum many-body systems. *Phys. Rev. A*, 93:062108, 2016.

[13] V. Giovanetti, S. Lloyd, and L. Maccone. Quantum metrology. *Phys. Rev. Lett.*, 96:010401, 2006.

[14] M. G. Bason, M. Viteau, N. Malossi, P. Huillery, E. Arimondo, D. Ciampini, R. Fazio, V. Giovannetti, R. Mannella, and O. Morsch. High-fidelity quantum driving. *Nature Physics*, 8:147, 2011.

[15] A. Trabesinger. Quantum simulation. *Nature Physics*, 8:263, 2012.

[16] P. Salamon, K. H. Hoffmann, Y. Rezek, and R. Kosloff. Maximum work in minimum time from a conservative quantum system. *Phys. Chem. Chem. Phys.*, 11:1027, 2009.

[17] Y. Rezek, P. Salamon, K. H. Hoffman, and R. Kosloff. The quantum refrigerator: The quest for absolute zero. *Euro. Phys. Lett.*, 85:30008, 2009.

[18] P. Skrzypczyk, J. A. Short, and S. Popescu. Work extraction and thermodynamics for individual quantum systems. *Nat. Comm.*, 5:4185, 2014.

[19] E. Torrontegui, S. Ibáñez, S. Martínez-Garaot, M. Modugno, A. del Campo, D. Guéry-Odelin, A. Ruschhaupt, X. Chen, and J. G. Muga. Chapter 2 – shortcuts to adiabaticity. *Adv. At. Mol. Opt. Phys.*, 62:117, 2013.

[20] X. Chen, E. Torrontegui, and J. G. Muga. Lewis-riesenfeld invariants and transitionless quantum driving. *Phys. Rev. A*, 83:062116, 2011.

[21] E. Torrontegui, S. Martínez-Garaot, and J. G. Muga. Hamiltonian engineering via invariants and dynamical algebra. *Phys. Rev. A*, 89:043408, 2014.

[22] M. Demirplak and S. A. Rice. Adiabatic population transfer with control fields. *J. Phys. Chem. A*, 107:9937, 2003.

[23] M. Demirplak and S. A. Rice. Assisted adiabatic passage revisited. *J. Phys. Chem. B*, 109:6838, 2005.

[24] M. V. Berry. Transitionless quantum driving. *J. Phys. A: Math. Theor.*, 42:365303, 2009.

[25] C. Jarzynski. Generating shortcuts to adiabaticity in quantum and classical dynamics. *Phys. Rev. A*, 88:040101(R), 2013.

[26] S. Masuda and K. Nakamura. Fast-forward of adiabatic dynamics in quantum mechanics. *Proc. R. Soc. A*, 466(2116):1135, 2010.

[27] S. Masuda and K. Nakamura. Acceleration of adiabatic quantum dynamics in electromagnetic fields. *Phys. Rev. A*, 84:043434, 2011.

[28] E. Torrontegui, S. Martínez-Garaot, A. Ruschhaupt, and J. G. Muga. Shortcuts to adiabaticity: Fast-forward approach. *Phys. Rev. A*, 86:013601, 2012.

[29] A. Kiely, J. P. L. McGuinness, J. G. Muga, and A. Rauschhaupt. Fast and stable manipulation of a charged particle in a penning trap. *J. Phys. B: At. Mol. Opt. Phys.*, 48:075503, 2015.

[30] S. Martínez-Garaot, M. Palmero, J. G. Muga, and D. Guéry-Odelin. Fast driving between arbitrary states of a quantum particle by trap deformation. *Phys. Rev. A*, 94:063418, 2016.

[31] S. Ibáñez, X. Chen, E. Torrontegui, J. G. Muga, and A. Ruschhaupt. Multiple schrödinger pictures and dynamics in shortcuts to adiabaticity. *Phys. Rev. Lett.*, 109:100403, 2012.

[32] A. del Campo. Shortcuts to adiabaticity by counterdiabatic driving. *Phys. Rev. Lett.*, 111:100502, 2013.

[33] S. Martínez-Garaot, E. Torrontegui, X. Chen, and J. G. Muga. Shortcuts to adiabaticity in three-level systems using lie transforms. *Phys. Rev. A*, 89:053408, 2014.

[34] S. Deffner, C. Jarzynski, and A. del Campo. Classical and quantum shortcuts to adiabaticity for scale-invariant driving. *Phys. Rev. X*, 4:021013, 2014.

[35] K. Takahashi. Unitary deformations of counterdiabatic driving. *Phys. Rev. A*, 91:042115, 2015.

[36] D. Sels and A. Polkovnikov. Minimizing irreversible losses in quantum systems by local counterdiabatic driving. *Proc. Natl. Acad. Sci. USA*, 114:3909, 2017.

[37] S. Ibáñez, S. Martínez-Garaot, X. Chen, E. Torrontegui, and J. G. Muga. Shortcuts to adiabaticity for non-hermitian systems. *Phys. Rev. A*, 84:023415, 2011.

[38] B. T. Torosov, G. D. Valle, and S. Longhi. Non-hermitian shortcut to adiabaticity. *Phys. Rev. A*, 87:052502, 2013.

[39] G. Vacanti, R. Fazio, S. Montangero, G. M. Palma, M. Paternostro, and V. Vedral. Transitionless quantum driving in open quantum systems. *New J. Phys.*, 16:053017, 2014.

[40] J. Song, Z. Zhang, Y. Xia, X. Sun, and Y. Jiang. Fast coherent manipulation of quantum states in open systems. *Opt. Exp.*, 24:21674, 2016.

[41] S. Deffner. Shortcuts to adiabaticity: suppression of pair production in driven dirac dynamics. *New Journal of Physics*, 18:012001, 2016.

[42] J. G. Muga, M. A. Simón, and A. Tobalina. How to drive a dirac system fast and safe. *New. J. Phys.*, 18:021005, 2016.

[43] X. Song, F. Deng, L. Lamata, and J. G. Muga. Robust state preparation in quantum simulations of dirac dynamics. *Phys. Rev. A*, 95:022332, 2017.

[44] J.-F. Schaff, X.-L. Song, P. Vignolo, and G. Labeyrie. Fast optimal transition between two equilibrium states. *Phys. Rev. A*, 82:033430, 2010.

[45] J.-F. Schaff, X.-L. Song, P. Capuzzi, P. Vignolo, and G. Labeyrie. Shortcut to adiabaticity for an interacting Bose-Einstein condensate. *Europhys. Lett.*, 93:23001, 2011.

[46] A. Walther, F. Ziesel, T. Ruster, S. T. Dawkins, K. Ott, M. Hettrich, K. Singer, F. Schmidt-Kaler, and U. Poschinger. Controlling fast transport of cold trapped ions. *Phys. Rev. Lett.*, 109:080501, 2012.

[47] J. Zhang, J. Hyun Shim, I. Niemeyer, T. Taniguchi, T. Teraji, H. Abe, S. Onoda, T. Yamamoto, T. Ohshima, J. Isoya, and D. Suter. Experimental implementation of assisted quantum adiabatic passage in a single spin. *Phys. Rev. Lett.*, 110:240501, 2013.

[48] S. An, D. Lv, A. del Campo, and K. Kim. Shortcuts to adiabaticity by counterdiabatic driving in trapped-ion transport. *Nat. Comm.*, 7:12999, 2016.

[49] S. Deffner and S. Campbell. Trade-off between speed and cost in shortcuts to adiabaticity. *Phys. Rev. Lett.*, 118:100601, 2017.

[50] K. Funo, J.-N. Zhang, C. Chatou, K. Kim, M. Ueda, and A. del Campo. Universal work fluctuations during shortcuts to adiabaticity by counterdiabatic driving. *Phys. Rev. Lett.*, 118:100602, 2017.

[51] H. Goldstein. *Classical Mechanics*. Addison-Wesley, Reading, Massachusetts, 2nd edition, 1980.

[52] J. Deng, Q. Wang, Z. Liu, P. Hänggi, and J. Gong. Boosting work characteristics and overall heat engine performance via accelerated adiabatic control: quantum and classical. *Phys. Rev. E*, 88:062122, 2013.

[53] M. Okuyama and K. Takahashi. From classical nonlinear integrable systems to quantum shortcuts to adiabaticity. *Phys. Rev. Lett.*, 117:070401, 2016.

[54] A. Patra and C. Jarzynski. Classical and quantum shortcuts to adiabaticity in a tilted piston. *J. Phys. Chem. B*, 121:3403, 2017.

[55] M. Okuyama and K. Takahashi. Quantum-classical correspondence of shortcuts to adiabaticity. *J. Phys. Soc. Japan*, 86:043002, 2017.

[56] C. Jarzynski, S. Deffner, A. Patra, and Y. Subasi. Fast forward to the classical adiabatic invariant. *Phys. Rev. E*, 95:032122, 2017.

[57] S. Vaikuntanathan and C. Jarzynski. Escorted free energy simulations: Improving convergence by reducing dissipation. *Phys. Rev. Lett.*, 100:190601, 2008.

[58] Z. C. Tu. Stochastic heat engine with the consideration of inertial effects and shortcuts to adiabaticity. *Phys. Rev. E*, 89:052148, 2014.

[59] I. A. Martínez, A. Petrosyan, D. Guéry-Odelin, E. Trizac, and S. Ciliberto. Engineered swift equilibration of a brownian particle. *Nat. Phys.*, 12:843, 2016.

[60] G. Li, H. T. Quan, and Z. C. Tu. Shortcuts to isothermality and nonequilibrium work relations. *Phys. Rev. E*, 96:012144, 2017.

[61] A. del Campo and M. G. Boshier. Shortcuts to adiabaticity in a time-dependent box. *Sci. Rep.*, 2:648, 2012.

[62] C. Jarzynski. Geometric phases and anholonomy for a class of chaotic classical systems. *Phys. Rev. Lett.*, 74:1732, 1995.

[63] A. Patra and Jarzynski. C. Shortcuts to adiabaticity using flow fields. arXiv:1707.01490, 2017.

[64] M. Demirplak and S. A. Rice. On the consistency, extremal, and global properties of counterdiabatic fields. *J. Chem. Phys.*, 129:154111, 2008.

[65] A. Julg. The complete symmetrization of quantum operators: new thoughts on an old problem. *Theor. Chim. Acta*, 74:323, 1988.

[66] S. Gill. A process for the step-by-step integration of differential equations in an automatic digital computing machine. *Cambridge Philos. Soc.*, 47:96, 1951.

[67] M. V. Berry. Quantal phase factors accompanying adiabatic changes. *Proceedings of the Royal Society A.*, 392:45, 1984.

[68] H. R. Lewis and P. G. Leach. A direct approach to finding exact invariants for onedimensional timedependent classical hamiltonians. *J. Math. Phys.*, 23:2371, 1982.

[69] J. G. Muga, X. Chen, S. Ibáñez, I. Lizuain, and A. Ruschhaupt. Transitionless quantum drivings for the harmonic oscillator. *J. Phys. B: At. Mol. Opt. Phys.*, 43:085509, 2010.

[70] S. Di Martino, F. Anza, P. Facchi, A. Kossakowski, G. Marmo, A. Messina, B. Militello, and S. Pascazio. A quantum particle in a box with moving walls. *J. Phys. A: Math. Theor.*, 46(36):365301, 2013.

[71] M. Razavy. An exactly soluble schrdinger equation with a bistable potential. *Am. J. Phys.*, 48:285, 1980.

[72] M. D. Feit, J. A. Fleck, Jr., and A. Steiger. Solution of the schrödinger equation by a spectral method. *J. Comp. Phys.*, 47:412, 1982.

[73] R. Kosloff. Time-dependent quantum-mechanical methods for molecular dynamics. *J. Phys. Chem.*, 92:2087, 1988.

[74] V. I. Arnold. *Mathematical Methods of Classical Mechanics*. Springer, New York, Reading, Massachusetts, USA, 1978.

[75] H. R. Lewis. Class of exact invariants for classical and quantum timedependent harmonic oscillators. *J. Math. Phys.*, 9:1976, 1968.

[76] H. R. Lewis and W. B. Riesenfeld. An exact quantum theory of the time-dependent harmonic oscillator and of a charged particle in a time-dependent electromagnetic field. *J. Math. Phys.*, 10:1458, 1969.

[77] P. Navarro and E. Pérez. Paul ehrenfest: The genesis of the adiabatic hypothesis, 19111914. *Arch. Hist. Exact Sci.*, 60:209, 2006.

[78] I. Bloch. Ultracold quantum gases in optical lattices. *Nat. Phys.*, 1:23, 2005.

[79] M. Berry. Topics in nonlinear dynamics. *AIP Conference Proceedings No. 46, ed. S. Jorna*, page 16, 1978.

[80] S. Vaikuntanathan and C. Jarzynski. Dissipation and lag in irreversible processes. *Europhys. Lett.*, 87:60005, 2009.

[81] Anne Le Cunander, Ignacio Martínez, Artyom Petroysan, David Guéry-Odelin, Emmanuel Trizac, and Sergio Ciliberto. Fast equilibrium switch of a micro mechanical oscillator. *Appl. Phys. Lett*, 109:113502, 2016.

[82] T. Schmiedl and U. Seifert. Optimal finite-time processes in stochastic thermodynamics. *Phys. Rev. Lett.*, 98:108301, 2007.

[83] T. Schmiedl and U. Seifert. Efficiency at maximum power: An analytically solvable model for stochastic heat engines. *Europhys. Lett.*, 81:20003, 2008.

[84] M. Feingold and A. Peres. Distribution of matrix elements of chaotic systems. *Phys. Rev. A*, 34:591, 1986.